Durham E-Theses

Some properties of ultrafine ferromagnetic particles

Mundell, P.A.

How to cite:

Mundell, P.A. (1976) *Some properties of ultrafine ferromagnetic particles*, Durham theses, Durham University. Available at Durham E-Theses Online: http://etheses.dur.ac.uk/8180/

Use policy

The full-text may be used and/or reproduced, and given to third parties in any format or medium, without prior permission or charge, for personal research or study, educational, or not-for-profit purposes provided that:

- a full bibliographic reference is made to the original source
- a link is made to the metadata record in Durham E-Theses
- the full-text is not changed in any way

The full-text must not be sold in any format or medium without the formal permission of the copyright holders.

Please consult the full Durham E-Theses policy for further details.

Academic Support Office, Durham University, University Office, Old Elvet, Durham DH1 3HP
e-mail: e-theses.admin@dur.ac.uk Tel: +44 0191 334 6107
http://etheses.dur.ac.uk

SOME PROPERTIES OF ULTRAFINE FERROMAGNETIC PARTICLES

by

P.A. MUNDELL, BSc. (DUNELM)

PRESENTED IN CANDIDATURE FOR

DEGREE OF DOCTOR OF PHILOSOPHY

MARCH 1976

DURHAM UNIVERSITY
SCIENCE
- 6 APR 1976
SECTION
LIBRARY

The copyright of this thesis rests with the author. No quotation from it should be published without his prior written consent and information derived from it should be acknowledged.

ABSTRACT

In an attempt to produce hard magnetic material, ultrafine particles of iron-cobalt alloys and nickel have been produced by an evaporation-condensation technique.

To investigate the magnetic properties of these particles, a Faraday Balance Magnetometer was constructed. A Pulsed Field Magnetometer was also employed. These were used to measure magnetization and coercivity, and to produce hysteresis loops for random assemblies of particles. The d.c. static and demagnetization remanences have also been measured.

X-ray diffraction techniques were used to find the structure and lattice parameters of the particles. The morphology was studied with the aid of an electron microscope.

The observed values of magnetization can be explained in terms of a core of ferromagnetic material surrounded by a surface oxide layer. For cobalt this layer is antiferromagnetic and for iron it is ferrimagnetic.

The results of the electron microscopy show that the particles are almost perfectly spherical and their sizes lie within a normal distribution curve. The peak in the distribution falls at approximately 400Å. The particles show a strong tendancy to chain together. This is believed to be due to magnetic attraction.

All the samples show a low remanence to saturation ratio, typically 0.20, and a difficulty to saturate. The resulting hysteresis loops can be explained in terms of fanning, coherent rotation and multidomain mechanisms. It is believed that some of the particles are genuinely single domain, and that their

magnetization reverses coherently. In addition there are particles large enough to contain more than one domain. The remaining reversal mechanism which is fanning, was proposed by Jacobs and Bean for a chain of spheres.

The above model would appear to be further supported by the results of electron microscopy.

ACKNOWLEDGMENTS

I should like to take this opportunity to thank Dr W D Corner most sincerely for his help and guidance throughout the period of my study.

My gratitude also goes to Professor G D Rochester and Professor A W Wolfendale for allowing me the use of the facilities in the Physics Department. I am indebted to Mr G Russell of the Department of Applied Physics for permitting me the use of the electron microscope.

I should also like to express special thanks to all my colleagues and technicians, particularly Mr K Moulson and Mr J Scott for their impeccable assistance.

LIST OF CONTENTS

LIST OF THE MOST IMPORTANT SYMBOLS

A	-	The exchange constant
D_a, D_b, D_c	-	Demagnetizing factors
E_K	-	Magnetocrystalline anisotropy energy density
E_m	-	Magnetoelastic anisotropy energy density
h	-	Reduced field parameter
H	-	Applied field
H_c	-	Coercive force
H_D	-	Demagnetizing field
H_K	-	Anisotropy field
H_n	-	Nucleation field
H_r	-	Remanence coercivity
I	-	Intensity of magnetization
I_r	-	Remanent magnetization
I_s	-	Saturation magnetization
$I_{ar}(H)$	-	Anhysteretic remanence
$I_D(H)$	-	D.C. demagnetization remanence
J	-	Exchange integral

DURHAM UNIVERSITY SCIENCE 6 APR 1976 SECTION LIBRARY

k	-	Boltzmann's constant
K_o, K_1, K_2	-	Magnetocrystalline anisotropy constants
p	-	Packing factor
S	-	Reduced cylinder radius
T	-	Temperature
T'	-	Uniaxial stress
λ_s	-	Saturation magnetostriction constant
ρ	-	Density
σ	-	Specific magnetization
σ_s	-	Specific saturation magnetization at room temperature

CHAPTER 1

INTRODUCTION

Magnetism is an important property of materials, a particularly valuable group of which are those called ferromagnetic. The prefix "ferro" is used because iron is the commonest example of a solid which behaves in this way. For technological applications ferromagnetic substances can be subdivided into hard and soft magnetic materials. Both classes of materials produce magnetic hysteresis effects, the nature of which enables a rough division into the two classes to be made.

Hard magnetic materials are often called permanent magnet materials. These substances are used in the production of permanent magnets and magnetic recording media. Such materials have high coercivity, high remanence and a wide hysteresis loop.

On the other hand, soft magnetic materials which are used for transformers and motors have low coercivity and a narrow hysteresis loop.

The need for materials having the properties of these two classes has therefore led to the production of substances with widely varying ferromagnetic properties. Over the years attention has been turned towards fine particles in order to find improvements on existing permanent magnet characteristics (1, 2). These fine particles, which hereafter may also be referred to as powders, micropowders and microparticles, have been produced by a number of different techniques. These have included the precipitation, evaporation and straightforward

ball milling processes. The size of particles thus produced ranges from 10 Å up to about 10^5 Å. The particles have then been compressed in order to produce permanent particulate magnets or dispersed, and subsequently coated on to plastic tape. This latter has been the basis for producing particulate magnetic recording tapes.

In knowing how such a magnet or tape will behave, it is necessary to know the magnetic properties and mechanisms involved in the magnetization of an assembly of particles.

1.1. Aim of this Work

The evaporation method for producing fine particles takes place in inert gas at low pressure. This gas-evaporation process was first performed by Beeck et al (3) in 1940. The method was subsequently rediscovered by some Japanese workers, Kimoto et al (4, 5, 6, 7), and also I.R.D.* in Newcastle (8, 9, 10).

The Japanese workers initially used this method for producing particles of a variety of metals. Later they developed a greater interest in magnetic metals. Some American workers have actually patented the process (11). At I.R.D. the technique was adopted and developed to produce a dry colloid technique. This is a refinement of the Bitter and Wet Colloid technique which enables the observation of magnetic domain boundaries. The main advantage is that this technique can be used at low temperatures when normal wet colloid would have frozen. This method has been applied to the study of domains in Gd by Al-Bassam et al (12) and in Tb by Al-Bassam et al (13) and Herring et al (14).

The main aim of the present work is to produce powders

* I.R.D. = International Research & Development

by an identical process, and to investigate their magnetic and physical properties. It is believed that the results obtained may shed new light on the magnetic mechanisms involved.

Before dealing with the theory of fine ferromagnetic particles, a short account of magnetism in general will be given.

1.2. Early Magnetism

"At this point I shall set out to explain what law of nature causes iron to be attracted by that stone which the Greeks call from its place of origin magnet, because it occurs in the territory of the Magnesians." These are the words of a Roman poet Lucretius Carus who lived in the 1st century B.C. (15). Actually there is an alternative origin to the word magnet. Pliny (16) attributes the name to its discoverer, a shepherd called Magnes. Evidently the nails in his shoes were attracted by a magnet while he was attending to his sheep.

Whatever the origin, it is believed that the properties of loadstone were known to the Greeks as long ago as 800 B.C. (17). The first 'magnetic' invention was the compass although the date of origin is uncertain. The early Greeks had their own ideas on magnetism which were based more on philosophy than on experiment. The first experimenter in magnetism was Peter Peregrinus (Anglicized), who lived in the latter half of the 13th century. He was the first person to use the term "poles of a magnet". The most famous of the early experimenters was William Gilbert who was born in 1544. He was interested in terrestial magnetism and also discovered that ferromagnetism could be destroyed at high temperatures. Gilbert is sometimes called "the father of magnetism". Even so there was much superstition and mysticism surrounding magnetism at that time.

It was believed that onions and garlic had adverse effects on the attractive powers of loadstone; and also that magnets had magical healing powers.

The first of the modern investigators was Coulomb who produced his law of attraction at the start of the 18th century. There then followed a great number of experiments performed by such people as Oersted, Faraday and Curie.

It was not until the advent of quantum theory, at the beginning of the 20th century, that the theory of magnetism took a form which is recognizable today. Since then a mountain of information about the subject has been accumulated.

1.3. The Origins of Magnetism (18, 19)

Magnetic effects are produced as a result of moving electric charge. Thus the effects of magnetism may be observed when an electric current flows in a conductor or as a result of the inherent motion of electrons in different materials. All matter contains moving electrons therefore all matter is in some sense magnetic. The main types of magnetism observed in materials are ferromagnetism, ferrimagnetism, antiferromagnetism, paramagnetism and diamagnetism. This work is concerned with ferromagnetic substances which can exhibit large magnetic moments even in the absence of an external applied field.

The origin of the magnetic moment in atoms is twofold - the orbital motion and the spin of electrons. How these are affected by the external field or the internal crystal field results in the different forms of magnetism which are observed.

Diamagnetism is a weak magnetism which arises from the orbital motion of the electrons in a magnetic field. The applied field modifies the electron motion causing a precession of the orbit about the field. In accordance with Lenz's law,

the electrons move in such a way that the resulting magnetization opposes the applied field. It is for this reason that diamagnetic materials possess negative susceptibility.

Paramagnetism requires the existence of permanent magnetic dipoles. In ionic paramagnetic materials the moment is associated with the total angular momentum of electrons. This is represented by the vectorial sum of the orbital momentum and the spin momentum. Because of the pairing of antiparallel spins in filled shells, the moment must be due to the unpaired electrons in unfilled shells.

Rare earth ions have unfilled 4f shells which are deep in the atoms, so that the moments are more or less isolated from their magnetic environment. On the other hand, ions of the iron group salts have unfilled 3d shells. These are the outermost and so are exposed to the crystal field. This is an inhomogeneous electric field produced by the neighbouring ions. The result of this is that the spin momentum is unaffected, but the orbital momentum is quenched. Therefore the magnetic moment in iron group salts is due in the first approximation to the spin momentum alone (20).

Due to thermal agitation the moments of an assembly of atoms assume random orientation, and there is no net magnetization (see fig. 1.1.a). The application of a magnetic field produces a slight alignment of the moments in the direction of the field (see fig. 1.1.b). The amount of alignment depends upon the size of field and temperature, since the effect of one is to oppose the other.

Paramagnetism is also observed in metals. In this case the dipole moment is due to the conduction electrons. In the

absence of an external magnetic field, the electrons fill up all the available states that have energies less than the Fermi energy. Half of the electrons have positive spin and half have negative spin. Therefore the net moment is zero. Upon application of an external field, the magnetic moments due to the spins line up either parallell or antiparallel to the field. The effect of the field is to increase the energy of the electrons with antiparallel spins and decrease the energy of those with parallel spins. The situation is unstable, and

FIG. 1.1.

(a)

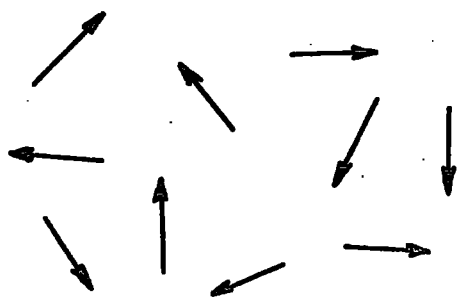

Arrangement of paramagnetic spins
Applied Field = 0

(b)

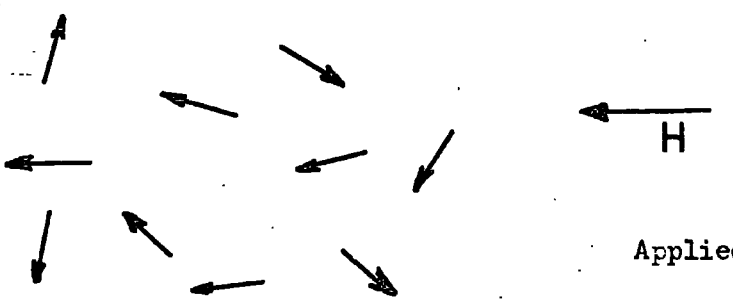

Applied Field >0

results in some of the electrons in the antiparallel states undergoing transitions to the lower energy parallel states. This means that there are now more electrons with parallel moments than with antiparallel moments. Hence the metal in an applied field possesses a net magnetic moment (21). The magnetization due to this effect (Pauli paramagnetism) is weak and is often

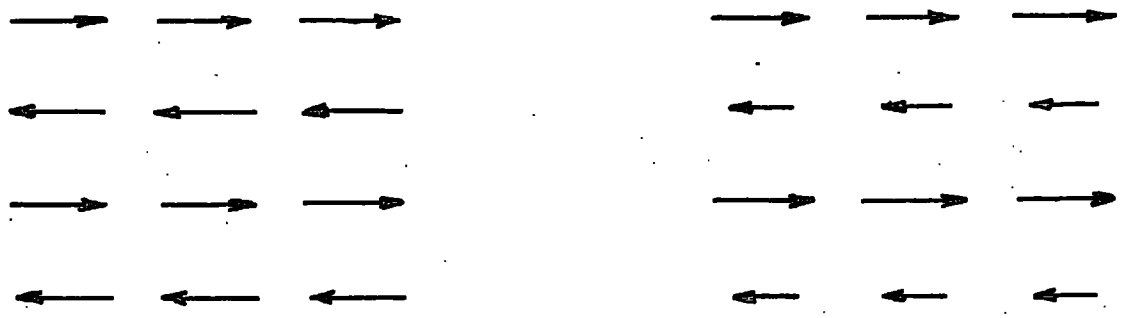

(a) Antiferromagnetic (b) Ferrimagnetic

FIG. 1.2

ARRANGEMENT OF SPINS FOR SIMPLE
ANTIFERROMAGNETIC AND FERRIMAGNETIC SYSTEMS

masked by stronger effects due to the moments of the atomic cores.

In ferromagnetic, antiferromagnetic and ferrimagnetic substances, there is a strong interaction between the magnetic moments of the individual atoms. In simple antiferromagnetic and ferrimagnetic materials, the interaction is negative. This produces an arrangement of antiparallel spins which exactly cancel in the antiferromagnetic case (see fig.1.2 (a)). There is therefore no net magnetization. In the case of a simple

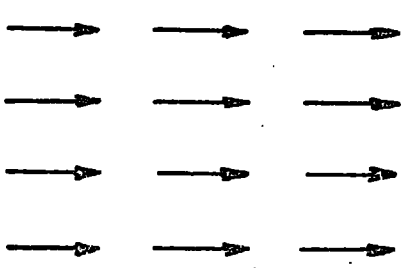

FIG. 1.3

FERROMAGNETIC
ARRANGEMENT OF SPINS
AT $0^{\circ}K$

ferrimagnetic though, the net magnetic moment in one direction is larger than the net magnetic moment in the other. This is due to different ions on different lattice sites having unequal moments or to antiferromagnetic coupling between two sub-lattices containing different numbers of sites. Therefore a resultant magnetization is observed (see fig. 1.2(b)).

These are not the only arrangements of antiferromagnetic and ferrimagnetic systems (22). For example parasitic ferromagnetism, or canted antiferromagnetism as it is sometimes called, occurs in materials which are essentially antiferromagnetic but whose spins can be rotated slightly away from their usual orientation.

In the case of ferromagnetism there is a strong positive interaction between spins which results in parallel alignment. At absolute zero the alignment is perfect (fig. 1.3). As the temperature is raised the arrangement is disturbed due to thermal agitation. Eventually, when high enough temperatures are reached, the alignment is completely destroyed. The orientation is then random and the material behaves like a paramagnet. Upon cooling, the ferromagnetism is recoverable.

It was suggested by Weiss (23) at the beginning of the century that a strong "molecular field" was responsible for the alignment of spins. The origin of this field was unknown to Weiss. Calculations of its magnitude gave values of the order of 10^7Oe. These are much too large to be explained by simple dipole interactions. Heisenberg later showed that the origin of the Weiss molecular field is in fact due to quantum mechanical exchange interactions between spins.

Heisenberg (24) based his theory upon the hydrogen

molecule in which it is assumed that the electrons are localized at the atoms. He showed that an exchange interaction between electrons in different quantum states leads to a minimum in energy provided both the spin quantum numbers are the same, i.e. if the spins are parallel. The strength of the exchange interaction depends upon the interatomic distance. As two atoms are brought together the spins of unpaired electrons align parallel. If the atoms are brought closer still, the exchange forces decrease and finally pass through zero. An antiparallel spin arrangement then becomes energetically favourable. The potential energy between two atoms having spins S_i and S_j is given by

$$V_{ij} = -2JS_i \cdot S_j \qquad \ldots\ldots\ldots\ldots\ldots\ldots \quad (1.1)$$

where J is the exchange integral. If J is positive, the energy is least when S_i is parallel to S_j; and if J is negative, it is least when S_i is antiparallel to S_j. The exchange constant A is defined as

$$A = 2JS_iS_j / a_o$$

where a_o is the lattice parameter.

So far it has been assumed that the electrons are tightly bound to the atoms. This is the case for insulators. However most ferromagnetic materials are metallic, in which case mobile electrons must be taken into account. Attempts have therefore been made to explain ferromagnetism by the band theory of solids (25, 26).

In the iron group series, the 4s shells are filled, and the 3d shells are only partially filled. With the

exception of the 4s electrons, the 3d electrons are the most exposed in the atom. The shells of these can be assumed to be nearly touching or overlapping those of neighbouring atoms. The energy levels are perturbed, giving rise to an energy band. Above the Curie temperature, where ferromagnetism vanishes, the band contains equal populations of electrons with positive and negative spin.

Well below the Curie temperature, the exchange interaction between electrons gives rise to a splitting of the energy band. Electrons with negative spin have their energy increased and those with positive spin have their energy decreased. As in the case of Pauli paramagnetism in metals, the situation is unstable. This results in electrons from the negative spin band spilling over into the positive spin band until equilibrium is reached. There is now a net magnetic moment.

1.4. Macroscopic Ferromagnetism

The previous section dealt with magnetism at the atomic level. For practical purposes however, most magnetic measurements are made on material which actually contains many atoms. It is for this reason that the term 'macroscopic' has been chosen for this section.

A block of ferromagnetic material can have zero net magnetization even though it contains many atoms each of which has a magnetic moment. To account for this, Weiss postulated the presence of small spontaneously magnetized regions. These he called domains. Within each domain, the atomic moments are aligned except for the effects of thermal disordering. The arrangement of the domains within the body may then be such

that the net magnetization of the configuration is small or even zero. Domains are formed so as to minimise the total energy which arises from a number of sources.

It turns out that the magnetization is an anisotropic property of a crystal. That is, it is direction sensitive. There exist certain crystallographic directions in which the magnetization preferentially points. These directions are called easy directions. The directions along which it is most difficult to magnetize the sample are called hard directions. To magnetize a crystal in a direction other than an easy one requires additional energy. This is called the magnetocrystalline anisotropy energy (27).

For a uniaxial crystal it is given by,

$$E_K = K_0 + K_1 \sin^2\phi + K_2 \sin^4\phi \quad \ldots\ldots\ldots\ldots (1.2)$$

where K_0, K_1 and K_2 are constants and ϕ is the angle between the direction of magnetization and the easy axis. Often the expression may be approximated to

$$E_K = K_1 \sin^2\phi \quad \ldots\ldots\ldots\ldots (1.3)$$

For a cubic crystal, the anisotropy energy density is given by

$$E_K = K_0 + K_1(\alpha_1^2\alpha_2^2 + \alpha_2^2\alpha_3^2 + \alpha_3^2\alpha_1^2) + K_2\alpha_1^2\alpha_2^2\alpha_3^2 \quad (1.4)$$

Again K_0, K_1 and K_2 are constants and $\alpha_1, \alpha_2, \alpha_3$ are the direction cosines of the magnetization vector with respect to the cubic axes.

The crystal structure is not the only property which produces anisotropy. Shape can have a similar effect. The anisotropy energy due to the shape of a sample arises from demagnetizing effects. This energy is called the demagnetizing

or magnetostatic energy.

In addition there are exchange energy, magnetoelastic energy, and energy of interaction with an applied field. In the absence of an externally applied field, this last term is zero.

The magnetoelastic energy arises from internally and externally applied stresses. When dealing with ideal crystals, these are often assumed to be zero. Therefore it is normally assumed that there is no magnetoelastic energy.

The formation of domains results in a reduction of the magnetostatic energy because of the decrease in the surface free pole density. However a boundary is produced, between the domains, in which the moments are no longer parallel. This leads to an increase in the other energies; i.e. exchange and magnetocrystalline. The overall energy of the system usually falls until the formation of any extra boundary would require more energy than the corresponding reduction in magnetostatic energy.

The boundaries between domains, mentioned above, are not sharply defined but are spread over a finite thickness. These layers are called domain walls. In these boundaries, the magnetic moments rotate gradually from one domain to the next. The thickness of this layer is governed primarily by competition between the exchange energy which favours thick walls and the anisotropy energy which conversely favours thin walls.

When an increasing magnetic field is applied to a ferromagnetic body, the overall magnetization increases until it reaches some saturation value. This process is generally not

reversible. Therefore hysteresis is observed. The mechanism which produces the magnetization growth is not merely a straightforward rotation of moments into the field direction. Instead the magnetization increases initially as a result of a domain wall displacement process.

If a crystal is placed randomly in a magnetic field, in general the field direction will not be the same as an easy direction, but at some angle to it. Domains which have their moments closest to the field direction grow at the expense of domains whose moments are furthest from this direction. Eventually these domains cover the whole sample. Final saturation is then accomplished by the rotation of the magnetization in the domain. This process is shown for a simple situation in fig. 1.4, and a typical magnetization curve for such a process is shown in fig. 1.5. Along OA the magnetization increases by the reversible movement of domain walls. Between A and B the magnetization increases more quickly. In larger samples this is caused by an irreversible displacement of domain walls. Range BC is due to the reversible rotation of the magnetization vector into the field direction. This results in an assymptotic approach to the saturation value.

When a magnetic field is applied to a ferromagnetic body, the internal field is not usually the same as the external one. This is due to demagnetizing effects (28). An external field H_{ex} induces free poles at both ends of the sample (see fig.1.6). The effect of these poles is to produce an internal field which opposes the external one. This demagnetizing field is given by

$$\bar{H}_D = -D.\bar{I}. \qquad \text{(in c.g.s. units)}$$

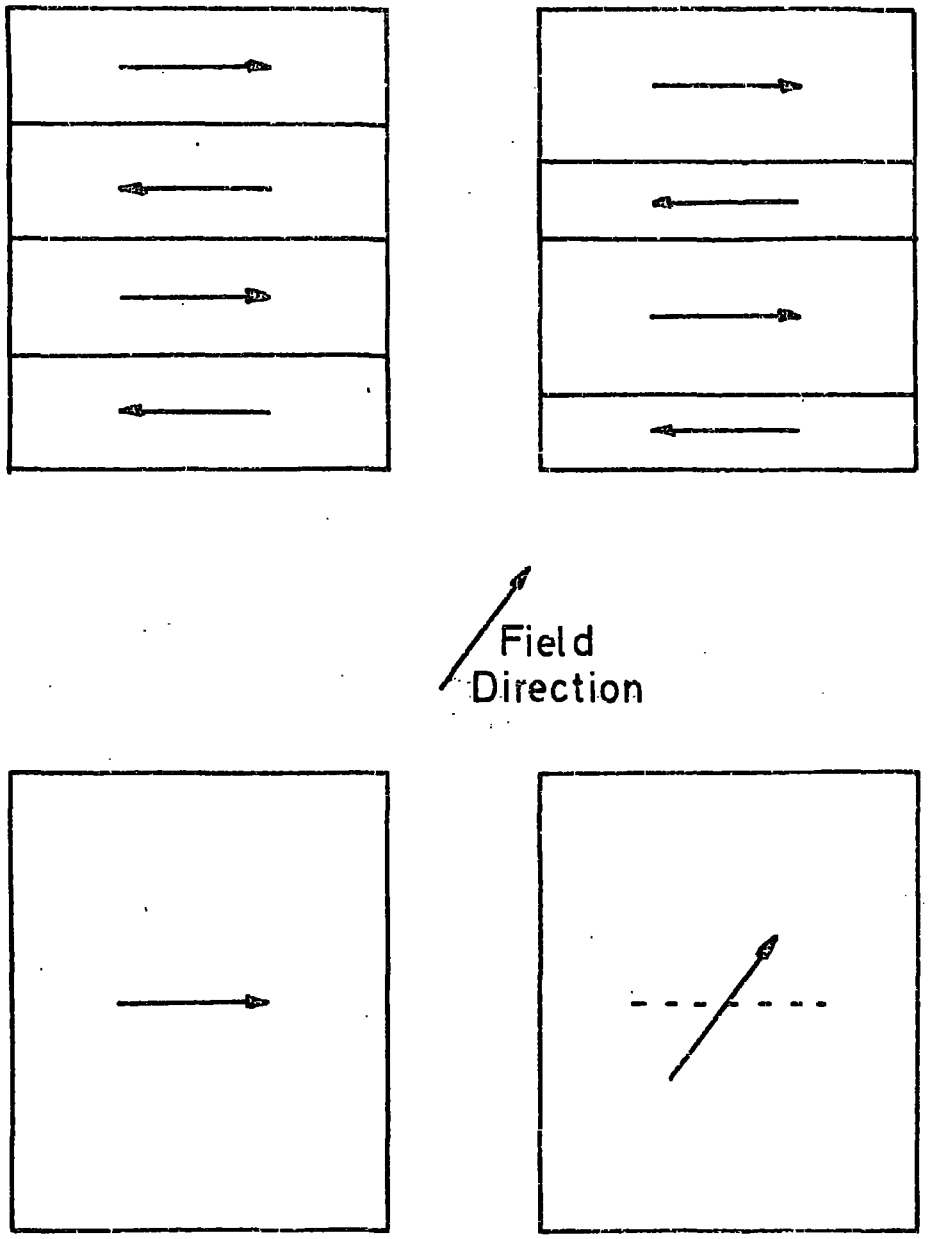

FIG. 1.4

SIMPLIFIED DOMAIN GROWTH
DUE TO THE APPLICATION
OF A MAGNETIC FIELD

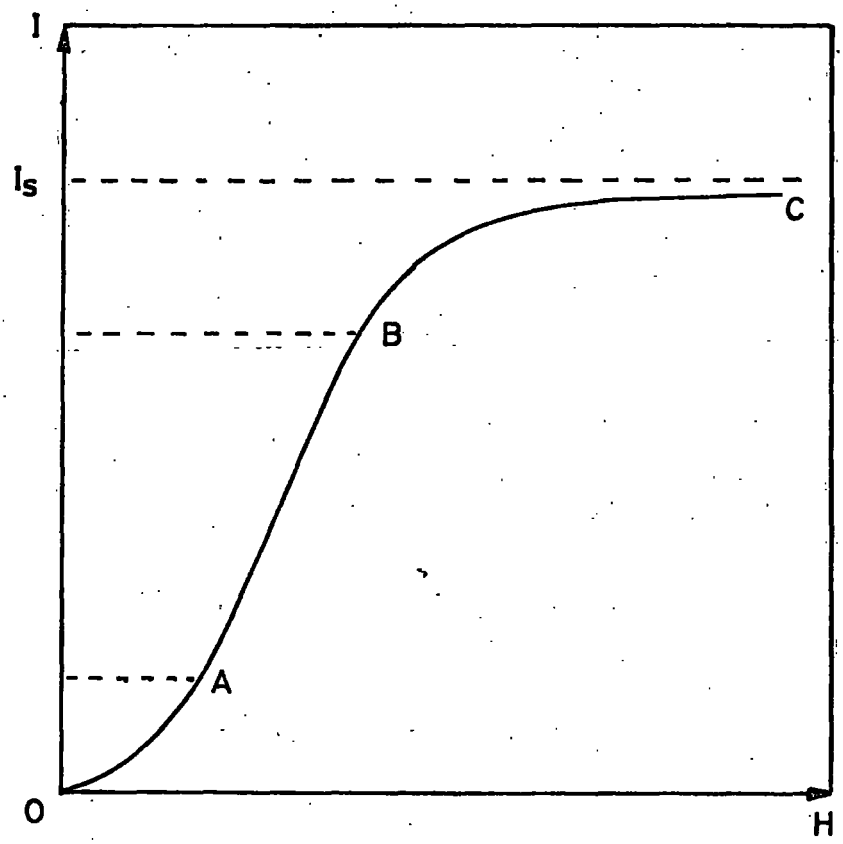

FIG. 1.5

TYPICAL MAGNETIZATION

CURVE

where I is the intensity of magnetization and D is the demagnetizing factor which is dependent upon the shape of the specimen. The effective field inside the sample H_{eff} is therefore less than the applied field by an amount H_D

$$\text{i.e. } \bar{H}_{eff} = \bar{H}_{ex} - D\bar{I} \qquad \ldots\ldots\ldots\ldots\ldots\ldots (1.5)$$

In the present work, it was found more convenient to work with the specific magnetization σ rather than I, and then convert back if necessary. The reason for this was that it was easier to weigh samples rather than measure the volume. The relation between I and σ is

$$I = \rho\sigma$$

where ρ is the density of the material.

$$\therefore \quad \bar{H}_{eff} = \bar{H}_{ex} - D\rho\sigma \qquad \ldots\ldots\ldots\ldots\ldots\ldots (1.6)$$

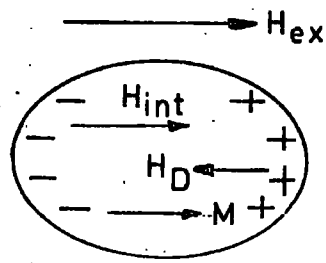

FIG. 1.6
DISTRIBUTION OF FREE POLES PRODUCED BY THE APPLICATION OF AN EXTERNAL FIELD

For a prolate ellipsoid, where the semimajor axis is 'a' and seminor axes b = c, then the demagnetizing factors parallel to these axes are D_a, D_b, D_c.

For a sphere, a = b = c

therefore $D_a = D_b = D_c$ $(= 4\pi/3)$

For a very long cylinder, which can be regarded as an ellipsoid with b = c and a = ∞, the demagnetizing factors are $D_b = D_c = 2\pi$ and $D_a = 0$.

In the case of samples whose shapes are not as simple as those above, the demagnetizing fields are non-uniform. It is then difficult or even impossible to find the corresponding demagnetizing factors.

However, if D is known it is possible to transform (σ vs H_{eff}) curves into (σ vs H_{ex}) curves and vice versa.

The magnetization process in large samples can be explained in terms of a series of domain wall displacements and magnetization rotations. If the sample is subdivided many times, the stage is reached where it contains but a single domain. There are no domain walls. Some of the questions which now arise are, what size must a sample be to consist of a single domain, and what are the magnetization processes when an external field is applied ? The next chapter therefore deals exclusively with fine particle theory.

CHAPTER 2

FINE PARTICLE THEORY

2.1. Introduction

In a large ferromagnetic sample the magnetization is in general not uniform. Instead the body is divided into domains. The magnetization of each domain is fairly uniform except for the effects of thermal agitation. As the size of the sample is decreased the formation of domain walls ultimately becomes energetically unfavourable. Eventually the body consists of a single domain. The magnetic properties of such particles would be expected to differ from those of larger samples.

For example in a spherical sample the surface atoms have a lower crystalline symmetry than those in the centre. As the particle size is reduced the ratio of the surface area to the volume is increased. Therefore the surface atoms represent a greater fraction of the total. In a cube of an f.c.c. crystal having an edge length of six lattice parameters, approximately 50% of the atoms are surface atoms. Six atomic spacings corresponds to an edge length of about 21Å in nickel. It may be therefore that the magnetocrystalline anisotropy effects in small crystals differ from those of larger samples. This surface anisotropy effect was first suggested by Néel (1). Actually it has been found that the magnetocrystalline energy density E_K in crystals with diameters as small as about 20Å does not differ greatly from that in larger crystals (2).

In ferromagnetic bodies, the magnetostatic energy favours a non-uniform magnetization configuration whilst the

exchange energy favours uniform magnetization. In large samples the long range magnetostatic forces predominate over the short range exchange forces. However upon decreasing the size of the sample, these roles are reversed. If the size of the particle is still further decreased, a stage is reached where the effects of thermal agitation override the exchange forces. The particles are then said to be superparamagnetic (3). It can therefore be seen that the size of single domain particles, whose magnetization is uniform, lies in some range between those sizes giving superparamagnetic and multidomain behaviour.

The critical size below which single domain behaviour occurs was the centre of discussion for a number of years. Originally, calculations were based upon comparing configurational energies of different models with that of a uniformly magnetized single domain ellipsoid (4). This method has been criticized (5), and its pitfalls will be discussed in a later section. In order to calculate this critical size it is necessary to consider the mechanisms of magnetization reversal and the various anisotropies that may be present.

2.2. Magnetization Processes

Consider a fairly large ferromagnetic sample magnetized to an intensity I in a positive field H. This value of I has been reached by a series of reversible and irreversible steps (see section 1.4) consisting chiefly of domain wall movements and magnetization rotations. When the field is reduced and finally reversed, the change in magnetization is again due to rotations, and domain wall movements.

If the size of the sample is reduced so that the multidomain configuration is inhibited, then the magnetization

changes within the particle must be due entirely to rotation of some form or other. The simplest mechanism for rotation of the magnetization vector is that in which all the electron spins are parallel at all times during reversal (6).

Before discussing this, it is perhaps necessary to introduce two types of field associated with the magnetization process. These are the coercive field H_c and the nucleation field H_n. H_c is that reverse field at which the magnetization becomes zero. H_n is the field at which the initially uniform magnetization first becomes unstable. This nucleation field can be best understood by considering a single domain ellipsoidal particle magnetized to saturation in the positive field direction. In order to dislodge the magnetization from this state, the applied field must in general overcome anisotropy, exchange and demagnetizing forces. The field at which this occurs is the nucleation field.

2.2.1. Coherent Rotation (6)

The process of magnetization change is governed by the energies of shape, stress and magnetocrystalline anisotropy together with those associated with exchange and demagnetizing effects. Initially though, only simple shapes and uniaxial magnetocrystalline anisotropy will be considered. The stress will be assumed to be zero.

Consider the prolate ellipsoid shown in figure 2.1, with polar semiaxis 'a' and equatorial semiaxis 'b'. At equilibrium the total free energy density is given by

$$E = K \sin^2 \phi - HI_s \cos \alpha \quad \ldots\ldots\ldots\ldots\ldots\ldots \quad (2.1)$$

where K is the total anisotropy constant. If K_1 is the magnetocrystalline anisotropy constant then

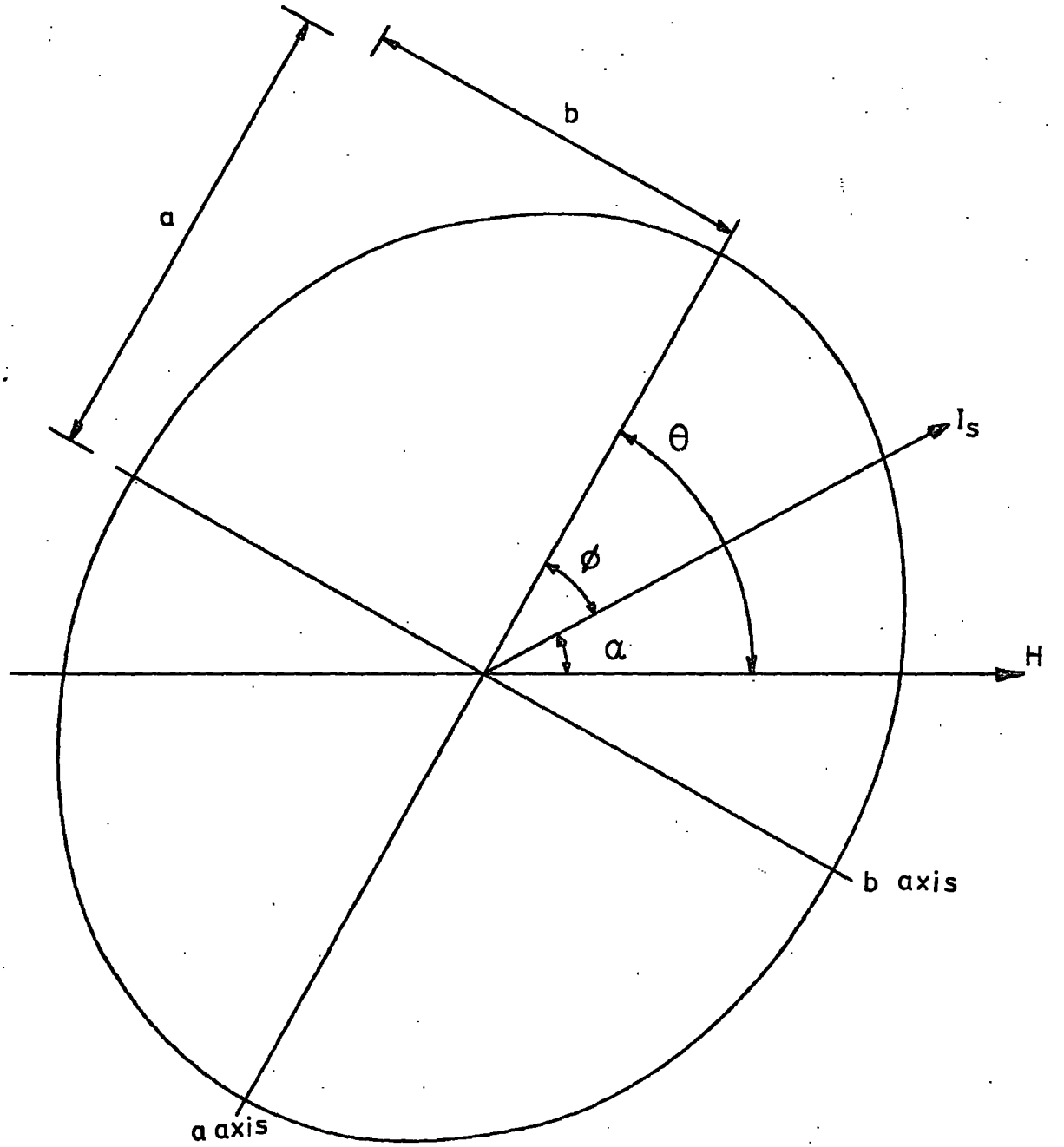

FIG. 2.1

DEFINITION OF ANGLES FOR

THE PROLATE ELLIPSOID

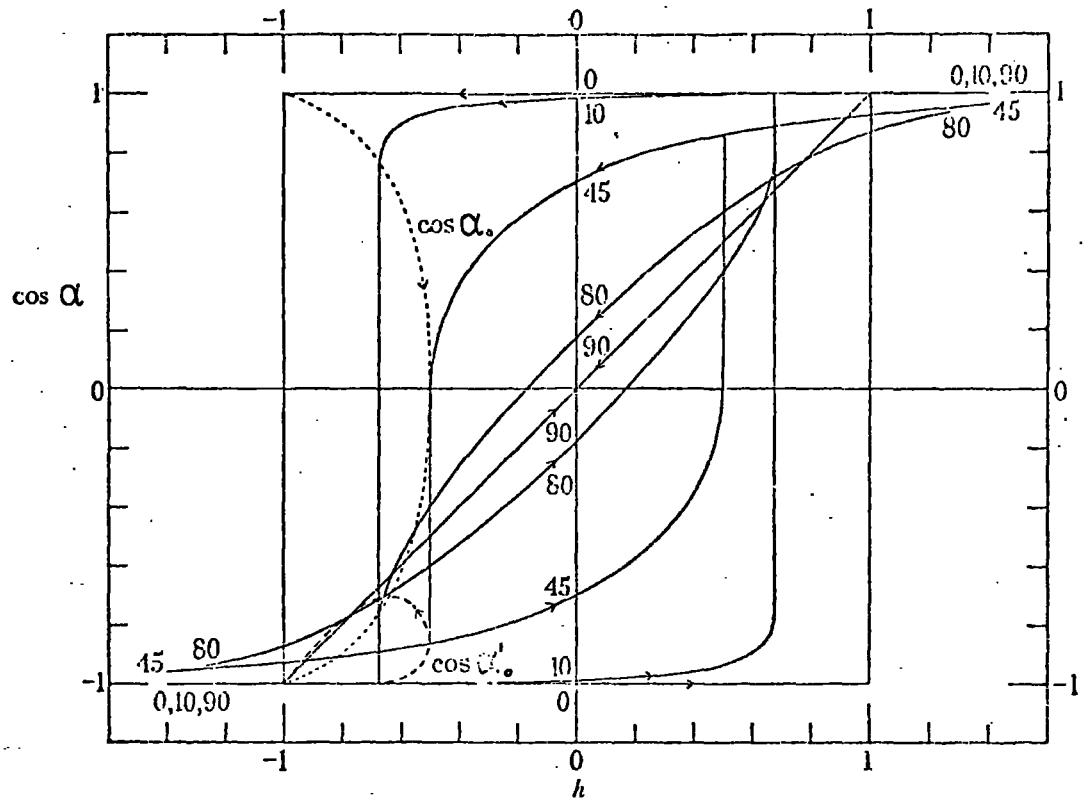

FIG. 2.2 Magnetization curves for prolate spheroids. The resolved magnetization in the positive field direction is given by $I_0 \cos\alpha$, where I_0 is the saturation magnetization. The field, H, is given by $H = (N_b - N_a) I_0 h$, where N_a and N_b are the demagnetization coefficients along the polar and equatorial axes. The angle, θ, between the polar axis and the direction of the field, is shown, in degrees, by the numbers on the curves. The dotted curves give $\cos\alpha_0$ and $\cos\alpha'_0$ where α_0 and α'_0 are the angles made with the positive field direction by the magnetization vector at the beginning and end of the discontinuous change at the critical value, h_0, of the field.

$$K = K_1 + \tfrac{1}{2} I_s^2 (D_b - D_a) \quad \ldots\ldots\ldots\ldots\ldots\ldots \quad (2.2)$$

D_b and D_a are the demagnetizing factors. There is no exchange energy.

For stable equilibrium in a given field H, the magnetization will point in a direction which makes the energy a minimum.

i.e. $\frac{dE}{d\phi} = 0$

$\therefore$ $2K \sin\phi \cos\phi - HI_s \sin(\theta - \phi) = 0$

This gives

$$K \sin 2\phi - HI_s \sin(\theta - \phi) = 0 \quad \ldots\ldots\ldots \quad (2.3)$$

If H is applied along the polar axis $\Theta = 0$, and if $\phi \ll 1$, it follows that

$$H_n = -\frac{2K}{I_s} = -H_K \quad \ldots\ldots\ldots\ldots\ldots\ldots\ldots \quad (2.4)$$

where H_K is the anisotropy field. The magnetization is stable in its original state as long as $H > -2K/I_s$. Let 'h' represent a reduced field equal to H/H_K.

Then $h = \frac{HI_s}{2K}$

Recalling that $\Theta = \phi + \alpha$, equation (2.3) can be rewritten as

$$\frac{1}{2} \sin 2(\Theta - \alpha) - h \sin \alpha = 0 \quad \ldots\ldots\ldots\ldots\ldots \quad (2.5)$$

Now 'h' is equivalent to a field in the H direction. Also, if I is the magnetization in the field direction, then $\cos\alpha$ is equivalent to a reduced magnetization ($\cos\alpha = I/I_s$). Stoner and Wohlfarth (6) solved equation (2.5) for 'α' in terms of 'h' and 'Θ'. They used the results to produce magnetization curves for different values of Θ (see figure 2.2).

Several points are worthy of note. Firstly, the K in expression (2.1) represents the total anisotropy. It is still valid even if the magnetocrystalline component is negligible. In this case, the polar axis of the ellipsoid still corresponds to an easy axis. This is the second point; that the prolate ellipsoid therefore possesses a uniaxial shape anisotropy.

Thirdly, the coercivity H_c (or h_c) is a maximum when the field is applied along the polar axis, and zero when applied along an equatorial axis. In this latter case, no hysteresis is observed. This is due to rotation which is completely reversible.

Normally in experimental work, an assembly of particles is studied. If these are non-interacting prolate ellipsoids oriented at random, then the shape of the resulting magnetization curve will be an "average" of all the individual curves. A reasonable guess at the reduced coercive force of the powder would be 0.5. By actual calculation Stoner and Wohlfarth (6) found $h_c = 0.479$, and the reduced remanence to be $\overline{\cos\alpha} = 0.5$.

The treatment of particles which have cubic magnetocrystalline anisotropy and zero shape anisotropy is more complicated (7)

The anisotropy energy density for a cubic crystal depends on the magnetization direction according to the relation (1.4).

i.e. $E_K = K_o + K_1(\alpha_1^2\alpha_2^2 + \alpha_2^2\alpha_3^2 + \alpha_3^2\alpha_1^2) + K_2(\alpha_1^2\alpha_2^2\alpha_3^2)$

Again the total energy density is given by the sum of the anisotropy energy E_K and the external field energy E_H

$$E = E_K + E_H$$

If rotation occurs in the (001) plane, equation (1.4) is simplified to

$$E_K = K_1 (1 - \cos 4\phi)/8 \quad \ldots\ldots\ldots\ldots\ldots\ldots \quad (2.6)$$

$$\sim K_1\phi^2 \text{ for } \cos 4\phi \rightarrow 1$$

The total energy is then given by

$$E = K_1\phi^2 - HI_s \cos(\theta - \phi) \quad \ldots\ldots\ldots\ldots\ldots\ldots \quad (2.7)$$

The equilibrium condition is given by

$$\frac{dE}{d\phi} = 2K_1\phi - HI_s \sin(\theta - \phi) = 0$$

If $\theta = 0$ and $\phi \ll 1$, it follows that

$$H_{K1} = \frac{2K_1}{I_s}$$

This is the maximum value of the coercive force. For an assembly of spherical particles with cubic crystalline anisotropy, oriented at random, Néel (8) calculated the coercive force to be

$$H_c = \frac{0.64}{I_s} K_1$$

There is however some question concerning this calculation (9). For cubic crystals, it is impossible to decide from energy calculations, which path the magnetization takes during reversal. Calculations of the remanence of a random assembly have yielded

$$I_r/I_s = 0.832 \quad \text{for} \quad K_1 > 0$$
$$I_r/I_s = 0.872 \quad \text{for} \quad K_1 < 0$$

Even though a powder may contain particles which have cubic crystallinity, it may be that the effect of shape produces a predominant uniaxial anisotropy.

Other particle shapes have been considered (6); for example the oblate ellipsoid where $b > a$ and also the general ellipsoid where $a > b > c$.

First consider an oblate ellipsoid. Because of the shape anisotropy, the equatorial plane is an easy plane; i.e. any direction in the plane is an easy direction. The polar axis is a hard direction. Because of the magnetization reversal processes, hysteresis is not observed although there is a discontinuity at $H = 0$.

In the case of the general ellipsoid, the magnetization no longer lies in the plane defined by the principal axis 'a' and the field direction. Fortunately however, to cover most cases, it is necessary to consider only prolate and oblate

ellipsoids.

A sphere for example is simply a special case of a prolate ellipsoid. Then, because $D_a = D_b = D_c$, the shape anisotropy is zero.

2.2.2. Incoherent Rotations (10, 11)

The discussion so far has assumed that a single domain particle in zero field remains so in an applied field. That is, the magnetization I, remains everywhere uniform, even during reversal. This is the essence of coherent rotation. The discussion has also assumed that rotation in unison is the lowest energy mode for the reversal of a single domain particle. By using that branch of magnetism known as micromagnetics (12, 13, 14) it has been found that other reversals mechanisms of lower energy can exist. These processes are known as incoherent rotations. Although the mathematics are involved and complicated, it is possible to discuss the results and their physical meanings in simple terms. To do this the shapes of particles have been restricted to simple geometries such as cylinders, ellipsoids, and spheres.

These incoherent modes of reversal are known by the names curling, buckling (5, 12, 15), and fanning (11).

(i) Curling may be best understood by imagining a parallel bunch of wires to be twisted together. The direction of the wires then gives the direction of magnetization. Because the magnetization remains parallel to the surface, no free poles are produced. Therefore no magnetostatic energy is produced. On the other hand both the exchange and anisotropy energies are increased. Since the exchange forces are short range, the field required to overcome them and initiate the curling mode

decreases with increasing particle size.

(ii) Buckling is represented by a sinusoidal variation of the magnetization vector. This fluctuation takes place along the direction of the original magnetization, and in a plane containing this direction. In a plane perpendicular to this, the spins are more or less parallel to each other. The wavelength of the fluctuation depends upon the particle radius. If the particle is cylindrical in shape, the wavelength tends to infinity as the radius tends to zero. In this case, the buckling mode can be approximated to that of coherent rotation. For any finite radii the buckling mechanism produces free poles of alternating sign on the surface. This results in a lower magnetostatic energy than in the case of rotation in unison. Buckling though increases the exchange energy. Even so the total energy remains smaller than for coherent reversal.

(iii) Fanning is the reversal mechanism proposed by Jacobs and Bean (11) to explain the magnetization processes in elongated single domain (ESD) particles. They suggested that ESD particles are actually composed of chains of spheres. The magnetization is assumed uniform for each sphere, and only dipole-dipole interactions are considered. During reversal, coherent rotation takes place in each sphere, but in the opposite sense for adjacent spheres.

These incoherent mechanisms are shown in figure 2.3. Reversal by one of these processes depends upon the particle shape and size. These in turn determine the nucleation field for a particular reversal. The mode of reversal is then the one which leads to the least negative nucleation field.

Coherent rotation

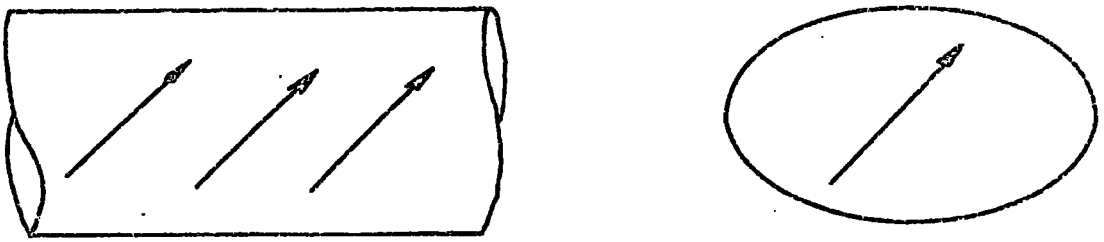

Curling

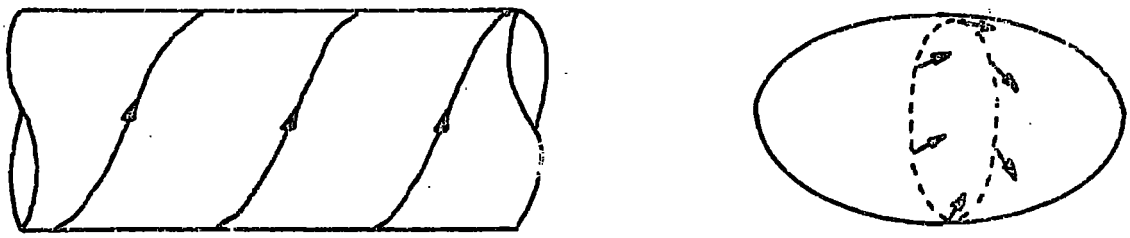

Buckling

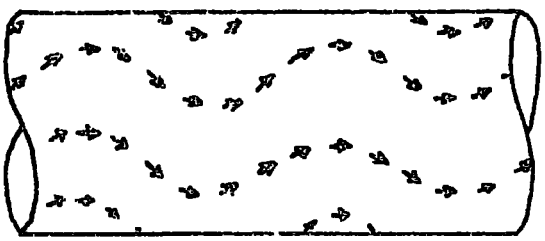

Fanning

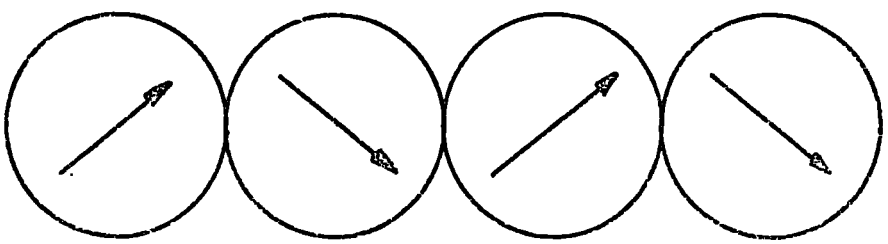

FIG. 2.3

MAGNETIZATION REVERSAL MECHANISMS

Consider the following three cases.

(a) The infinitely long cylinder whose axis is either parallel to or inclined to some field has been treated by Frei et al (5) and also Shtrikman and Treves (16).

At this stage it is convenient to introduce a reduced cylinder radius S which is given by,

$$S = b/b_o$$

where $b_o = A^{\frac{1}{2}}/I_s$

'b' is the cylinder radius and 'A' is the exchange constant. In the buckling mode, the nucleation field is given by,

for $S \ll 1$

$$H_n \sim \frac{-2K}{I_s} = \frac{-2K_1}{I_s} - 2\pi I_s \quad \ldots\ldots\ldots\ldots\ldots\ldots (2.8)$$

and for $S \gg 1$

$$H_n \sim \frac{-2K_1}{I_s} - 2.58\,\pi\, I_s\, S^{-\frac{2}{3}} \quad \ldots\ldots\ldots\ldots\ldots\ldots (2.9)$$

For $S \ll 1$, the nucleation field approximates to that for coherent rotation. For the curling mode in an infinite cylinder, the nucleation field is given by

$$H_n = \frac{-2K_1}{I_s} - 2.16\,\pi\, I_s S^{-2} \quad \ldots\ldots\ldots\ldots\ldots\ldots (2.10)$$

The reduced nucleation field h_n is plotted as a function of S for the different reversal mechanisms in figure 2.4. It can be seen that at small radii the reversal approximates to rotation in unison, and at large radii the reversal is due to curling rather than buckling.

Rotation in unison, and curling mechanisms have been studied in spheres and prolate ellipsoids by Shtrikman and

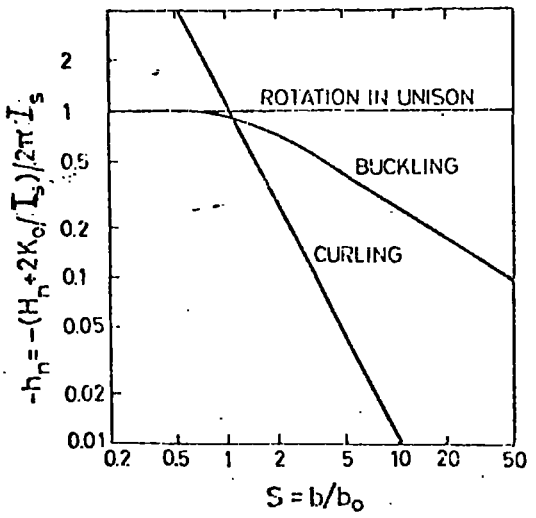

Reduced nucleation field $h_n = (H_n + 2K_0/I_s)/2\pi I_s$ of infinite cylinders as a function of the reduced cylinder radius $S = b/b_0 = b I_s A^{-1/2}$, calculated for various modes of nucleation in fields parallel to the cylinder axes.

FIG. 2.4

Treves (12) and others (5, 17). They have shown that these two processes are the reversal modes for particles with small and large radii 'b' respectively.

(b) For a sphere possessing only uniaxial magnetocrystalline anisotropy, the nucleation field is given by

for $S \leqslant 1.44$

$$H_n = -\frac{2K_1}{I_s} \qquad \ldots\ldots\ldots\ldots\ldots\ldots\ldots\ldots \quad (2.11)$$

and for $S > 1.44$

$$H_n = \frac{4}{3}\pi I_s - 2.78\,\pi I_s S^{-2} - \frac{2K_1}{I_s} \qquad \ldots\ldots\ldots \quad (2.12)$$

i.e. for radii 'b' less than $1.44\,A^{\frac{1}{2}}/I_s$ the reversal mechanism is by rotation in unison.

(c) For a prolate ellipsoid whose semimajor axis is 'a' and semiminor axis is 'b', the demagnetizing factors are D_a and D_b.

If a field is applied parallel to the 'a' axis, the nucleation field is given by,

for rotation in unison

$$H_n = \frac{-2K_1}{I_s} - I_s (D_b - D_a) \quad \ldots\ldots\ldots\ldots\ldots\ldots (2.13)$$

and for curling,

$$H_n = \frac{-2K_1}{I_s} + I_s D_a - 2\pi k I_s S^{-2} \quad \ldots\ldots\ldots\ldots (2.14)$$

where k is a constant which varies from 1.08 for an infinite cylinder to 1.39 for a sphere. Equation (2.14) therefore represents a general expression for the nucleation field for curling. The reversal mechanism is again the one with the least negative nucleation field. For rotation in unison this is independent of the radius. However, the nucleation field for curling is strongly dependent upon the dimensions of the particle.

In the fanning mode, it is assumed that all the spheres are isotropic, and that only dipole-dipole interactions take place. It is also assumed that the spheres either touch at a point or are slightly displaced from each other. The exchange forces are neglected. The fanning mechanism then depends upon three things. These are the number of particles in a chain, the inclination of the chain to the field and also on whether the ends of the chain meet.

Jacobs and Bean postulated two fanning mechanisms, symmetric and nonsymmetric fanning. For symmetric fanning it is assumed that the angle of fanning is constant along the length of the chain. This applies for chains of two spheres and for infinitely long chains whose ends meet. In aligned chains of finite and semi-finite length an end effect occurs.

Consider a chain of n spheres, each with a moment m, and whose centres are separated by a distance r. Let a field be applied along the chain, and let ϕ_i be the angle between the magnetization of the ith sphere and the chain axis.

For parallel rotation $\phi_1 = \phi_2 = \phi_i = \phi$. The total energy is given by (11)

$$E = \frac{m^2}{r^3} n K_n (1 - 3\cos^2\phi) - nmH\cos\phi$$

where $K_n = \sum_{i=1}^{n} (n - 1)/ni^3$

the coercivity is then given by

$$H_{cn} = - \frac{m}{r^3} 6K_n \qquad \ldots\ldots\ldots\ldots\ldots\ldots (2.15)$$

For symmetrical fanning, $\phi_1 = -\phi_2 = \phi_3 = \phi$. This time the total energy is given by

$$E = \frac{m^2}{r^3} nL_n (\cos 2\phi - 3\cos^2\phi)$$

$$+ \frac{m^2}{r^3} nM_n (1 - 3\cos^2\phi) - nmH\cos\phi$$

K_n, L_n, & M_n are scale factors dependent on n.

where

$$L_n = \sum_{i=1}^{\frac{1}{2}(n-1) < i \leq \frac{1}{2}(n+1)} (n - (2i - 1))/n (2i - 1)^3$$

$$M_n = \sum_{i=1}^{\frac{1}{2}(n-2) < i \leq \frac{1}{2}n} (n - 2i)/n(2i)^3$$

$$K_n = L_n + M_n$$

this gives the coercivity for n spheres

$$H_{cn} = - \frac{m}{r^3} (6K_n - 4L_n) \qquad \ldots\ldots\ldots\ldots\ldots (2.16)$$

Thus fanning leads to a lower coercivity than rotation

in unison. If the spheres are touching $m/r^3 = \pi I_s/6$.

Experimentally measured values of coercivity are normally less than those predicted for coherent rotation. Incoherent rotations however lead to lower predicted values. This then is to some extent indirect evidence of the existence of incoherent reversal mechanisms.

2.3. Particle Anisotropies (18)

So far only shape and magnetocrystalline anisotropies have been considered. Other anisotropies do exist. These have been neglected in the preceding sections in an attempt to simplify the mathematics. In an assembly of real particles, the effect and type of anisotropy may vary from one particle to the next. Taken over the assembly as a whole, the effects may be small, but in localized areas they may become significant. Other forms of anisotropy which occur are stress, interaction, surface and exchange anisotropy.

The internal energy density E_i for a simple magnetically uniaxial particle is given by (c.f. equation 2.1)

$$E_i = K \sin^2\phi \qquad \ldots\ldots\ldots\ldots\ldots\ldots \quad (2.17)$$

where the symbols have been defined earlier. If a particle with no shape or crystal anisotropy is acted upon by a uniaxial stress T', the magnetoelastic energy density E_m is given by

$$E_m = \frac{3}{2} \lambda_s T' \sin^2\phi \qquad \ldots\ldots\ldots\ldots\ldots\ldots \quad (2.18)$$

where λ_s is the saturation magnetostriction constant. By comparing equations (2.17) and (2.18) it can be seen that the stress produces an equivalent uniaxial anisotropy whose constant is given by

$$K = \frac{3}{2} \lambda_s T' \qquad \ldots\ldots\ldots\ldots\ldots\ldots \quad (2.19)$$

Interaction anisotropy arises in configurations of otherwise isotropic spherical particles. For example in a chain of spheres the dipole-dipole interaction between the particles causes the axis of the chain to be one of easy magnetization.

The effects of surface anisotropy were discussed in the introduction to this chapter.

Exchange anisotropy is an interfacial effect between two different magnetic substances (3). For example between an antiferromagnetic and a ferromagnetic (or ferrimagnetic) material. The effect has been observed in cobalt particles which have been partly oxidised. Cobaltous oxide is an antiferromagnetic material with a Néel temperature of about 300°K. Pure cobalt has a high Curie temperature and so is still ferromagnetic above 300°K. If a field is applied to the particles, at a temperature not too far above 300°K, the cobalt moments will tend to align whereas those in the oxide will hardly be affected. On cooling through the Néel temperature, the oxide moments may be affected by spin-spin exchange interactions at the interface. Upon reversal of the applied field, the moments in the cobalt are reversed, but those deep in the oxide are unaffected. The net result of the exchange anisotropy is to shift the hysteresis loop along the field axis.

2.4. Critical Particle Size (19, 20)

Early estimates of the critical size below which a particle consists of a single domain were based upon comparing configurational energies of different models. In other words the energy of a single domain particle was compared with that of a particle which had a different magnetization distribution.

Calculations were made for various configurations in zero applied field. The size at which the single domain energy was less than or equal to any other energy was taken to be the critical size.

From the preceding sections it should be apparent why there are serious objections to this method.

First of all the calculations were made for zero applied field; that is, at remanence. Secondly it was assumed that a single domain particle in zero field, remains so in an applied field. It was shown earlier that this is not necessarily so. Instead the particle can reverse its magnetization incoherently, in which case the configuration is not single domain in nature. The mode of reversal is not determined by the remanence, but by the nucleation field.

There is another serious objection to the method of comparing configurational energies. That is the implication that at the critical size and in the absence of a field, the single domain configuration can change spontaneously into some other configuration and vice versa. This would result in the disappearance of hysteresis at this point. It is therefore insufficient to compare configurational energies to try to obtain a value for the critical particle size. Indeed for larger particles, the incoherent processes sometimes represent lower energy modes.

Instead, the problem is to find that size below which a single domain particle reverses its magnetization coherently.

Three simplified cases can be considered. The first is when shape anisotropy predominates, the second when magnetocrystalline anisotropy predominates, and the third case

is when the two are approximately equal.

(i) Dominant shape anisotropy. In this case the nucleation field for coherent reversal is given approximately by

$$H_n \sim -I_s(D_b - D_a) \quad \ldots\ldots\ldots\ldots\ldots\ldots \quad (2.20)$$

This is to be compared with the nucleation fields for other reversal processes. The three shapes considered so far are ellipsoids, spheres and cylinders. In the first two the incoherent mechanism is curling. But in cylinders, buckling is an intermediate process between curling and coherent rotation. It can be shown though that both the incoherent processes lead to the same critical size. Therefore curling alone will be taken as the incoherent reversal mechanism.

Suppose the particles are ellipsoidal in shape. There is little or no magnetocrystalline anisotropy, hence $K_1 = 0$. Using the same symbols as before, the nucleation field for curling is then given by equation (2.14).

$$H_n \sim D_a I_s - 2\pi k I_s S^{-2} \quad \ldots\ldots\ldots\ldots\ldots \quad (2.21)$$

The nucleation field for spheres and cylinders can be found by the choice of a suitable value of k. Comparing (2.20) and (2.21) gives the critical particle radius as

$$b_c = \left\{ \frac{2\pi k A}{D_b I_s^2} \right\}^{\frac{1}{2}} \quad \ldots\ldots\ldots\ldots\ldots\ldots \quad (2.22)$$

for a sphere, $D_b = 4\pi/3$, $k = 1.39$

$$\therefore \quad b_c = \left\{ \frac{2.08A}{I_s^2} \right\}^{\frac{1}{2}} \quad \ldots\ldots\ldots\ldots\ldots\ldots \quad (2.23)$$

for an infinite cylinder, $D_b = 2\pi$, $k = 1.08$

$$\therefore \quad b_c = \left\{ \frac{1.08A}{I_s^2} \right\}^{\frac{1}{2}} \quad \ldots\ldots\ldots\ldots\ldots\ldots \quad (2.24)$$

One interesting point is that for the sphere. Since $D_b = D_a$ and $K_1 = 0$, it is purely isotropic. The nucleation field and the coercivity are both zero. Therefore the critical particle size is calculated at remanence.

(ii) Dominant magnetocrystalline anisotropy. In this case, the nucleation field for rotation in unison is

$$H_n = \frac{-2K_1}{I_s} = H_c$$

But this also happens to be the nucleation field for curling. The expression is independent of particle size. Experimentally however, the coercivity of samples with large magnetocrystalline anisotropy is found to be strongly size dependent. This is known as Brown's Paradox. Wohlfarth (18) made a "very tentative estimate" of the critical size based upon dimensional grounds. If only A and K_1 enter the expression,

$$b_c \sim (A/K_1)^{\frac{1}{2}}$$

(iii) Equal shape and crystalline anisotropy. In this case, $-2K_1/I_s$ enters both expressions for the nucleation field. Upon comparing the two, it vanishes. Therefore the critical particle size is again given by expression (2.22).

At the other end of the scale is the critical size between single domain and superparamagnetic behaviour. This point would be expected when the energy of thermal agitation kT is very much bigger than the energy barrier Kv, where k is Boltzmanns constant and v is the particle volume. It has been shown that the size, above which single domain behaviour may be observed must satisfy (21)

$$b_s > \left\{\frac{75}{4}\ \frac{kT}{\pi K}\right\}^{\frac{1}{3}} \qquad \text{.....} \qquad (2.26)$$

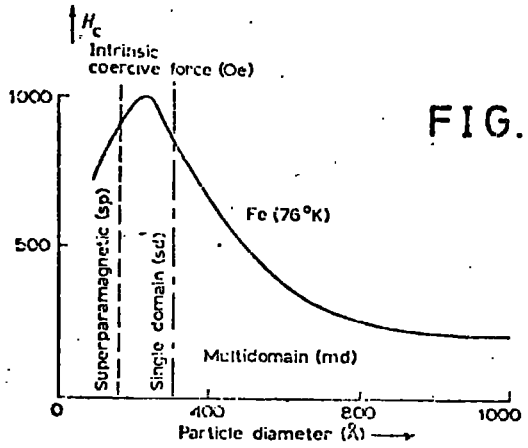

FIG. 2.5

Coercive force for iron powder as a function of particle diameter (MEIKLEJOHN [1953]).

Experiment has shown (22, 23) that the coercivity of fine particles is size dependent, reaching a maximum value in the range of single domainedness (see figure 2.5). This then provides an alternative definition for the critical particle size (18). At sizes above this, inhomogeneous reversals occur, leading to lower coercivities. As the size is increased, it becomes more and more favourable for the formation of domain walls; again resulting in a lowering of the coercivity. Eventually, the coercivity reaches the small but finite value of bulk samples.

At sizes below that for single domainedness a decrease in coercivity is also observed. This behaviour is due to there being an increasing probability of spontaneous reversal by thermal activation.

As far as hard magnetic materials are concerned, it is desirable to have a high coercivity whilst still retaining a

high remanence to saturation ratio. These two requirements would seem to be fulfilled by the use of aligned single domain particles.

Real powders are not normally single sized, but have a distribution of sizes. This means that they are not necessarily composed purely of single domain particles. In an attempt to learn more about real particles, a number of investigations have been carried out over the years.

2.5. Experiments on Fine Particles

Measurements that have been made on fine particles have included those of magnetization, coercivity, torque and remanence.

The saturation magnetization has been measured so that it can be compared with that of bulk material. Investigations have also been made into the size and temperature dependence of the saturation magnetization (24).

In an effort to produce new permanent magnet materials, interest in the increased coercivity of fine particles runs high. The coercivity has been measured as a function of size and temperature (25). In fact these two results can give information concerning the behaviour of the critical size at different temperatures. The angular variation of the coercivity has also been studied (26). The significance of this is that it can show whether or not incoherent reversals are operative.

Torque curves have also been obtained for fine particles. To do this, the particles are aligned and then fixed in some sort of binder or wax. This is subsequently cut into discs for

use in a torque magnetometer. It has been possible by this method to obtain information about the anisotropy of fine particles (27, 28). Because the sample is in the form of a disc, the shape anisotropy of the whole assembly has no effect. However the shape anisotropy due to the particles alone can be assessed.

Other types of measurement have been made, but one of the most important is that of remanence curves. Remanence curves are concerned only with irreversible changes whereas hysteresis curves are determined by both reversible and irreversible processes. Remanence can be acquired in a number of ways.

The static remanence $I_r(H)$ is that remanence which is acquired after demagnetization, and the subsequent application and removal of a d.c. field H. $I_D(H)$ is the d.c. demagnetization remanence which is acquired by saturating in one direction and then applying and removing a d.c. field H in the opposite direction. Two other forms of remanence occur, the a.c. demagnetization remanence $I_D'(H)$ and the anhysteretic remanence $I_{ar}(H)$.

$I_D'(H)$ is acquired after d.c. saturation and the subsequent application of a slowly diminishing a.c. field of initial amplitude H. $I_{ar}(H)$ is acquired after the application of a d.c. field H, superposed with a decreasing a.c. field of initially large amplitude.

For an assembly of uniaxial non-interacting particles there exist a set of relations between the remanence curves (29).

These are independent of the reversal mechanism (20) and are given by

$$I_D(H) = I_r(\infty) - 2I_r(H) \quad \ldots\ldots\ldots\ldots\ldots \quad (2.27)$$

$$I'_D(H) = I_r(\infty) - I_r(H) \quad \ldots\ldots\ldots\ldots\ldots \quad (2.28)$$

$$\therefore \quad I'_D(H) = \frac{1}{2} I_r(\infty) + \frac{1}{2} I_D(H) \quad \ldots\ldots\ldots\ldots\ldots \quad (2.29)$$

$$I_{ar}(H) = I_r(\infty) \quad \ldots\ldots\ldots\ldots\ldots \quad (2.30)$$

where experimental curves depart from these, the cause is generally ascribed to interaction effects (31).

In connection with the above relations, a field known as the remanence coercivity H_r is introduced. H_r is defined as the field for which the d.c. demagnetization remanence is zero.

i.e. $$I_D(H_r) = 0 \quad \ldots\ldots\ldots\ldots\ldots \quad (2.31)$$

It then follows that,

$$I_r(H_r) = I'_D(H_r) = \frac{1}{2} I_r(\infty) \quad \ldots\ldots\ldots\ldots \quad (2.32)$$

For a random assembly of non-interacting particles, it has been shown that (30)

$$H_r/H_c = 1.094$$

Actual experimental values of this ratio are usually higher than this. This is thought to be due to a distribution of anisotropies or shapes in real powders (29).

The idea of a distribution of anisotropies can be extended to include distribution of particle sizes, shapes etc. This has given rise to two mathematical possibilities. First, given a particular distribution to calculate the magnetic

properties of the assembly, and conversely, given the magnetic properties, to calculate the distribution.

These seem to be formidable tasks, but in several cases they have been attempted. Gaunt (31) for example, found a distribution of anisotropies which produced a value of H_r/H_c in agreement with his experimental value. On the other hand, Johnson and Brown have used remanence curves in order to find the distribution of axial ratios for ellipsoidal particles (32). The distribution they predicted differed from that obtained by direct observation (i.e. electron microscopy). Two reasons have been given. First, incoherent reversals were neglected; it was assumed that reversal took place by rotation in unison. Secondly, particle interactions were neglected.

The effect of particle interactions cannot be neglected. In most of the preceding chapter it has been assumed that the particles in an assembly are magnetically isolated from each other. This is unlikely to be the case for real powders, unless the particles are greatly dispersed. Instead, the particles are expected to interact with each other.

An attempt has been made to assess both theoretically and experimentally the degree of interaction. It is difficult to measure a quantity which can be accurately described as the 'interaction factor'. In remanence curves for example, the deviation of the experimental curves from the theoretical ones is assumed to be due to interactions. The difference in the areas is then taken as a quantity which depends upon the amount of interaction (18). However, it cannot be taken as a reliable measure for some mean absolute magnitude of the interaction.

It would appear that "hardly any general conclusion can be derived from experiment alone" (20).

Interaction effects should be small, provided the particles are well separated or dispersed. The degree of separation of the particles is given by the packing factor 'p'. This is defined as the ratio of the sum of the volumes of the magnetic particles, to the volume of the whole assembly. The coercivity is given by

$$H_c(p) = H_c(p=0)(1-p) \quad \ldots\ldots\ldots\ldots\ldots \quad (2.33)$$

Hence at very low values of p, the coercivity is hardly affected.

It is therefore generally expected that experimentally measured properties will be different from theoretical values.

CHAPTER 3

FERROMAGNETIC MATERIALS

The choice of materials which can be produced in micropowder form depends to some extent upon what is known of bulk materials. Experience of the properties of bulk ferromagnetic substances would suggest that these may produce good ferromagnetic particles. This at least provides some sort of starting point.

However, due to the technological importance of magnetism, there exist today a large number of ferromagnetic materials. Even so, there are only three pure metals which exhibit ferromagnetism at room temperature. These are iron, cobalt and nickel. These elements all have unfilled 3d shells which can act co-operatively. As explained in Chapter 1, this is the origin of ferromagnetism. Most other ferromagnetic materials are produced by alloying one or more of these pure metals with each other or with other 'non-magnetic' metals. There are exceptions however. Some ferromagnetic materials do not contain either iron, cobalt or nickel. For example the so-called Heusler alloys are based on the Cu-Al-Mn system. The magnetic properties of these alloys depend upon the Mn-Mn interatomic distances and upon the degree of ordering.

Some alloys have been produced specifically for use as hard magnetic materials and some for use as soft magnetic materials. Figure 3.1 shows the distribution of relative permeability and coercivity for different magnetic materials (1).

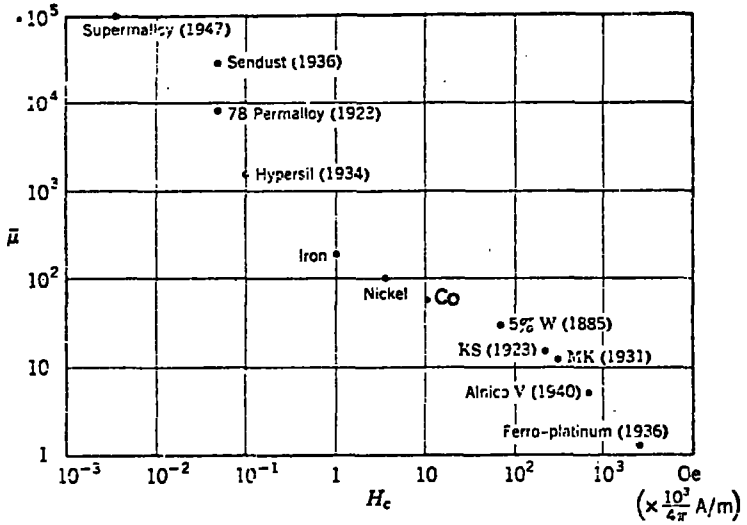

Fig. 3.1 Relative permeability and coercive force of various magnetic materials

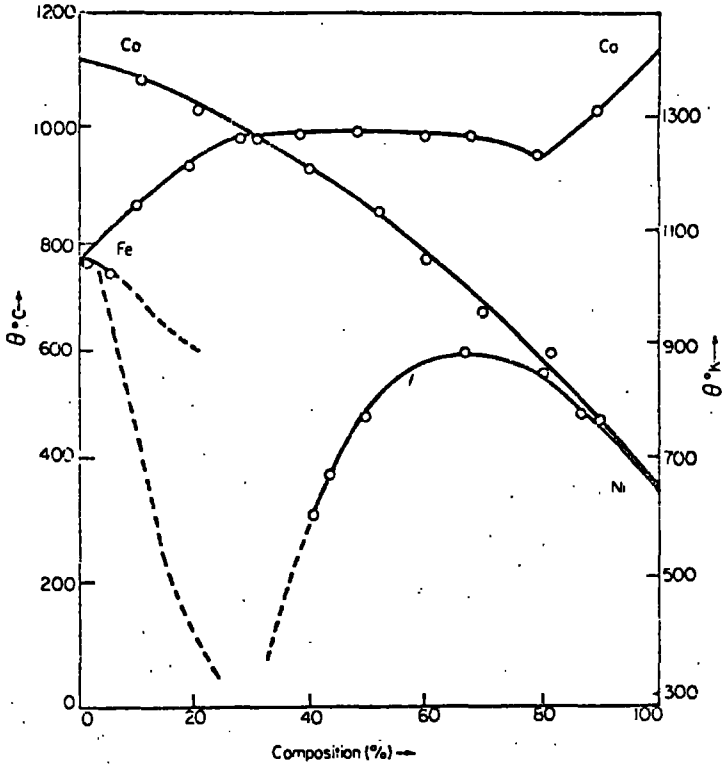

Figure 3.2 Magnetic transformation temperatures of Fe–Co, Fe–Ni and Co–Ni alloys

The object of the present investigation was to try to produce micropowders which possessed hard magnetic characteristics. At first sight the properties of bulk iron, cobalt and nickel would tend to exclude them from this category. However interest has grown because of the possible increase in remanence and coercivity that might accrue from their particulate form. These may then be suitable materials for permanent magnet use.

The magnetic properties of bulk iron, cobalt, iron-cobalt alloys and nickel have already been extensively researched. In addition some fine particles have been studied. In an attempt to produce further information regarding micropowders, these materials were used in the present investigation.

Another reason why these materials were chosen is that they have relatively high Curie temperatures. The variation of these temperatures with composition for iron-cobalt alloys is shown in figure 3.2 (2). For pure nickel the Curie temperature is 358°C (3). Therefore the magnetization of these metals is fairly insensitive to small temperature fluctuations around room temperature.

In bulk specimens of iron-cobalt alloys the saturation magnetization reaches a maximum near the composition $Fe_{65}Co_{35}$. The dependence of the magnetization upon the composition is shown in figure 3.3 (4). At room temperature (291.5°K) the saturation magnetization for bulk nickel is 54.49 e.m.u/gm (5).

Another important factor in the magnetic properties of materials is the magnetocrystalline anisotropy. The

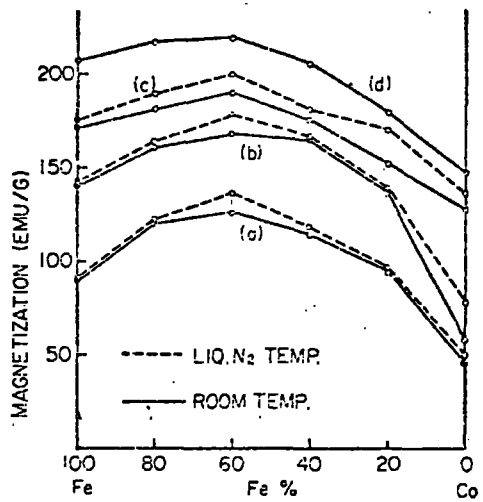

Fig.3.3 Saturation magnetization of Fe-Co alloy fine particles whose average radii are 50 Å (a), 120 Å (b) and 350 Å (c). Those of bulk specimens are also shown (d).

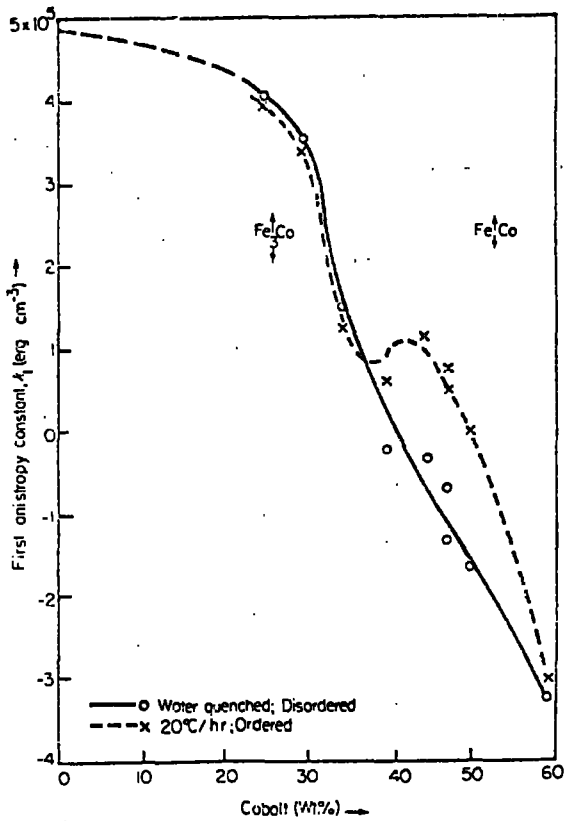

Figure 3.4 The first anisotropy constant for the Co–Fe alloys

variation of the first anisotropy constant K_1 with composition is shown for the b.c.c. Fe-Co alloy series in figure 3.4. The two sets of results come from Kittel (6) and Hall (7). Cobalt can be hexagonal or face centred cubic at room temperature. The magnetocrystalline energies are different (see Chapter 1).

However in the hexagonal form (8),

$K_1 \sim 5.1 \times 10^6$ erg/c.c.

$K_2 \sim 1.0 \times 10^6$ erg/c.c.

and in the cubic form (9)

$K_1 \sim -8.3 \times 10^4$ erg/c.c.

$K_2 \sim -1.6 \times 10^4$ erg/c.c.

where K_2 is the second anisotropy constant.

For f.c.c. nickel at room temperature, the anisotropy constants are (10)

$K_1 \sim -4.5 \times 10^4$ erg/c.c.

$K_2 \sim 2.3 \times 10^4$ erg/c.c.

CHAPTER FOUR

EXPERIMENTAL TECHNIQUES

4.1 SPECIMEN PREPARATION

The materials used in this investigation were either elemental metals or alloys. The elemental metals were usually in the form of thin wire.

The alloys were made by melting together the stoichiometric quantities of the individual components in an arc furnace. The melting took place on a water cooled copper hearth, in the presence of argon gas. The argon used was Purargon. That is high purity argon with less than 3 p.p.m. of oxygen. The components were melted together at as low a temperature as possible so as to minimise the loss of material due to evaporation. The resulting flat bottomed buttons were reversed and re-melted several times to ensure complete alloy homogeneity. The buttons were sliced into thin rods, using clean hacksaw blades, as this form was most convenient for later work.

The elemental metals used in this investigation had purities of 99.99%.

4.2 PARTICLE PRODUCTION

Ultrafine particles of the metals and alloys were produced by an evaporation-condensation technique. This technique was first used by Beek (1) et al in their study of the catalytic action of evaporated metal films. The method essentially involves evaporating metal from a hot filament. This is performed in a gas, usually inert, which is at a low pressure (somewhere between 10^{-1} and 30 torr). The apparatus used in the present investigation is shown in figure 4.1.

An evaporation chamber is connected to a diffusion pump and rotary pump. Coming through the base plate are a pair of electrical lead throughs. This enables a tungsten filament to be heated inside the bell jar.

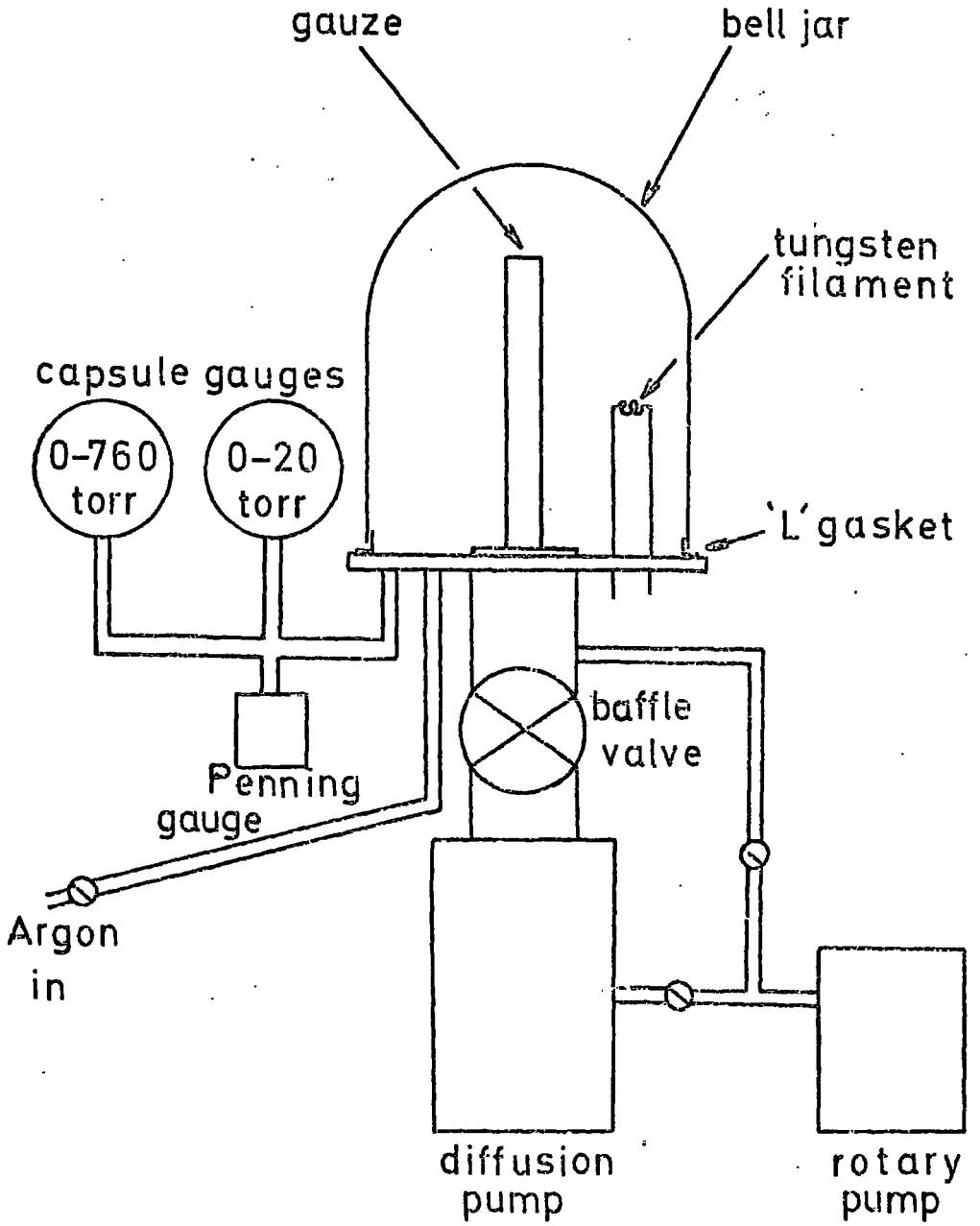

FIG. 4.1

EVAPORATION - CONDENSATION UNIT

The material to be evaporated was placed on the filament inside the chamber. This was evacuated to about 10^{-4} torr and then flushed with Purargon gas to reduce the amount of residual air. The bell jar was re-evacuated, and argon allowed to re-enter. The gas flow was adjusted so that at the required pressure it just counterbalanced the pumping speed of the rotary pump. This ensured a continuous gas flow at constant pressure. The dynamic method was adopted in order to speed the deposition and collection of the particles. In a static situation where the pumps and the gas bottle are isolated, the particles acquire a low terminal velocity (2) and seem to hang in the gas.

The filament was heated by means of increasing and decreasing, alternately, the power through it. This was done by hand. About 10-15 cycles were necessary, and it ensured that when the material 'boiled' and the particles were driven off, they were fairly free from contamination by the filament (3). The evaporation takes about 30-45 seconds by this method. Particles produced were collected from paper placed in the bell jar and on the base plate. Transition metals and their alloys were used to produce ultrafine particles by this process.

After each evaporation the bell jar and base plate had to be cleaned thoroughly using acetone. Every so often the bell jar was cleaned using benzene and Decon 90. Instead of using argon, the evaporation was sometimes carried out in the presence of air at low pressure. This was done to see if there was any appreciable increase in the oxide content of the particles, and how this affected the magnetic properties.

4.3 CRYSTAL STRUCTURE DETERMINATION

The crystal structures of the particles were compared with those of the bulk materials. This was done by X-ray powder photography, using a Phillips 360 mm circumference, Debye-Scherrer camera and cobalt $K\alpha_1$ radiation. The film was analysed in the normal way and 'd' values were computed using a simple FL/1 computer programme (see Appendix B). Comparison between the results for particles and the bulk material is given in Chapter 5.

4.4 ELECTRON MICROSCOPY

In addition to X-ray methods, electron microscope studies were carried out to determine the size distribution of the particles. The particles were allowed to settle on copper grids during evaporation. Prior to this, the grids had been covered in a thin film of graphite so as to act as a substrate for the particles.

Initially, clean glass microscope slides were soaked in a weak soap solution and then allowed to dry. These were placed in an ordinary evaporator and covered in a thin film of graphite. It was then necessary to transfer the graphite from the glass slides to the copper grids. In order to do this, the graphite film was cut into small squares using a sharp razor blade. The slides were then slowly submerged in a clean beaker containing distilled water. The water on the dry soapy surface of the slides enabled the graphite squares to be floated from the glass. Copper grids held by tweezers were brought up under the graphite so that the square film covered the grid. These had to be dried carefully using blotting paper since they could easily be damaged. The grids were stored in small tablet capsules until they were needed.

4.5 MAGNETIC MEASUREMENTS

There are various methods of measuring magnetization. These usually depend upon any one of three basic effects produced by a magnetic sample. They can be summarized as:

(a) the measurement of an induced voltage or current due to the sample

(b) the measurement of the force acting on the sample

(c) the measurement of the magnetic field produced by the sample.

The magnetic properties of the fine particles in this study were investigated using two pieces of apparatus which relied upon (a) and (b).

The first was the Pulsed Field Magnetometer (4) (5). This was used to obtain traces of magnetization versus field on an oscilloscope.

The magnet coil of a pulsed field system can be considered to consist of an inductance L and a resistance R, the latter being due to the resistance of the coil winding and the leads. A magnetic field can be produced by discharging a high voltage from a capacitor bank C, through the magnet coils. The circuit then behaves as an LCR circuit. The field thus produced is oscillatory, with an amplitude which decays exponentially. This damped S.H.M. is typical of such circuits.

Pick-up coils are placed about the sample inside the magnet. Signals from these coils are integrated in order to produce outputs proportional to the field and the sample magnetization. Stray signals due to noise or phase differences can be removed or partly removed by the addition of compensating signals.

From the corrected signals, a hysteresis loop of magnetization against field, can be displayed directly on an oscilloscope.

The second piece of apparatus used in the magnetic studies was a Faraday Balance Magnetometer (6) (7). Essentially, this measures the apparent change in weight, or more correctly, the force acting on a sample in the presence of a non-uniform magnetic field. A signal proportional to this force can be displayed on a pen recorder either as a function of field or temperature.

More detailed accounts of these pieces of equipment are given in the following sections. It should be noted however that neither gives an absolute measurement, but each needs to be calibrated against some known standard.

4.6 THE PULSED FIELD MAGNETOMETER

The pulsed field magnetometer has been extensively covered by Poldy (5) and Hunter (8), and only the salient points of the technique will be outlined here. A magnetic specimen is placed in the centre of a coil through which a stored charge may be passed giving an intense magnetic field pulse. Pick-up coils are used to measure the magnetization of the sample (figure 4.2).

CONSTRUCTIONAL DETAILS

4.6.1 THE MAGNET

Pulsed magnetic fields were produced by discharging a 2000 μF capacitor through a coil which had been machined from a solid block of beryllium-copper alloy (2% Be). The addition of beryllium increases the tensile strength of the coil so that it does not distort easily under high fields. As an additional measure the coil was potted in araldite. The method of charging and discharging the 2000 μF capacitor bank is shown in figure 4.3. The maximum voltage obtainable from the power supply is 2 kV. This means that 4 kJ of energy is discharged through the magnet coil. The time variation of the magnetic field can be found by solving the differential equation for the sum of the voltages in an LCR circuit.

$$\text{i.e.} \qquad L\frac{di}{dt} + iR + \frac{q}{C} = 0$$

$$\text{or} \qquad L\frac{d^2i}{dt^2} + R\frac{di}{dt} + \frac{i}{C} = 0 \qquad \ldots\ldots\ldots \quad (4.6.1)$$

At time t = 0, the capacitor is charged to a voltage V, and the current is zero.

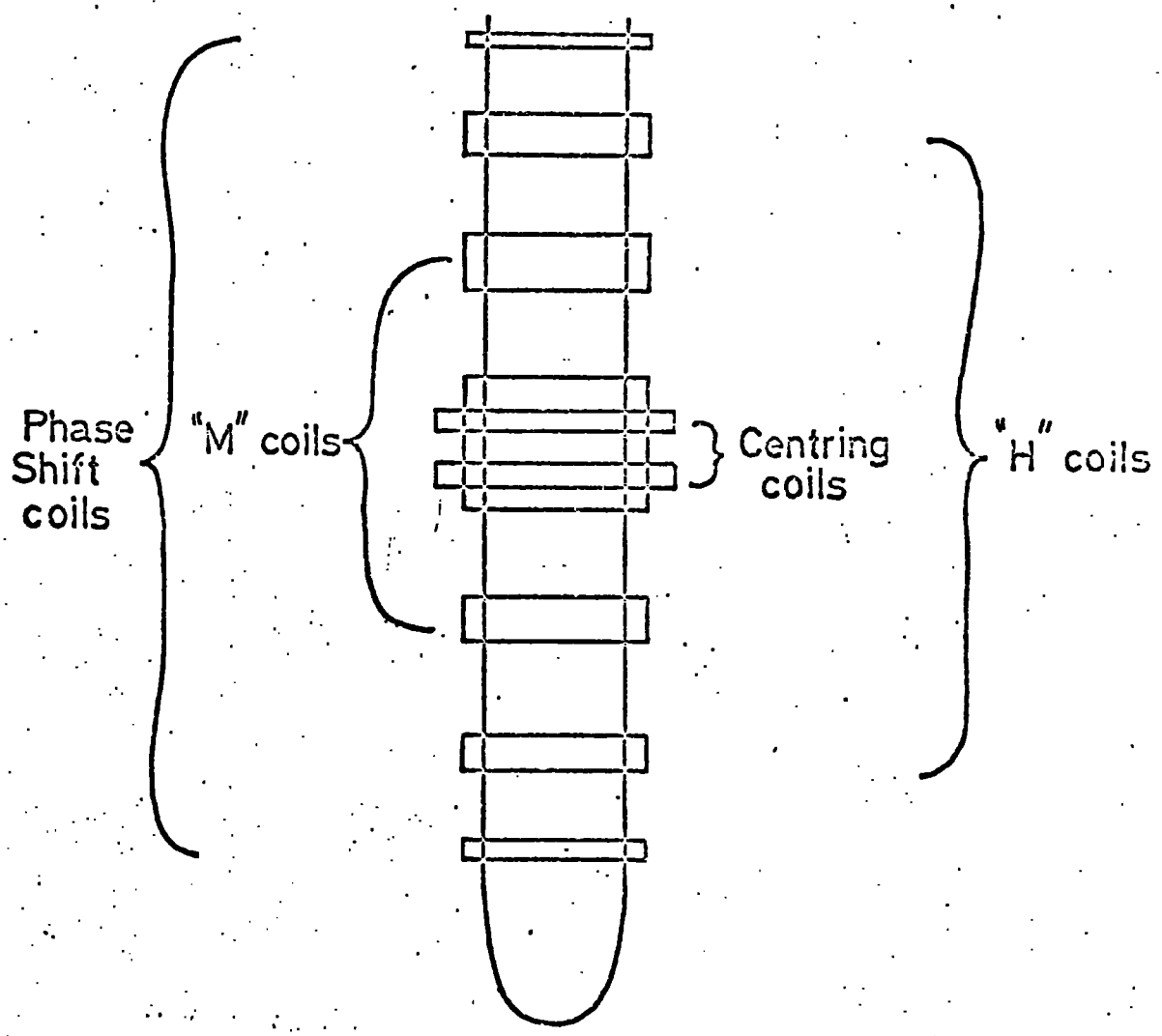

FIG. 4.2

Pick-up coil assembly used for measuring the magnetisation of a specimen in a measured applied field.

FIG. 4.3 Power Supply For Capacitor Bank

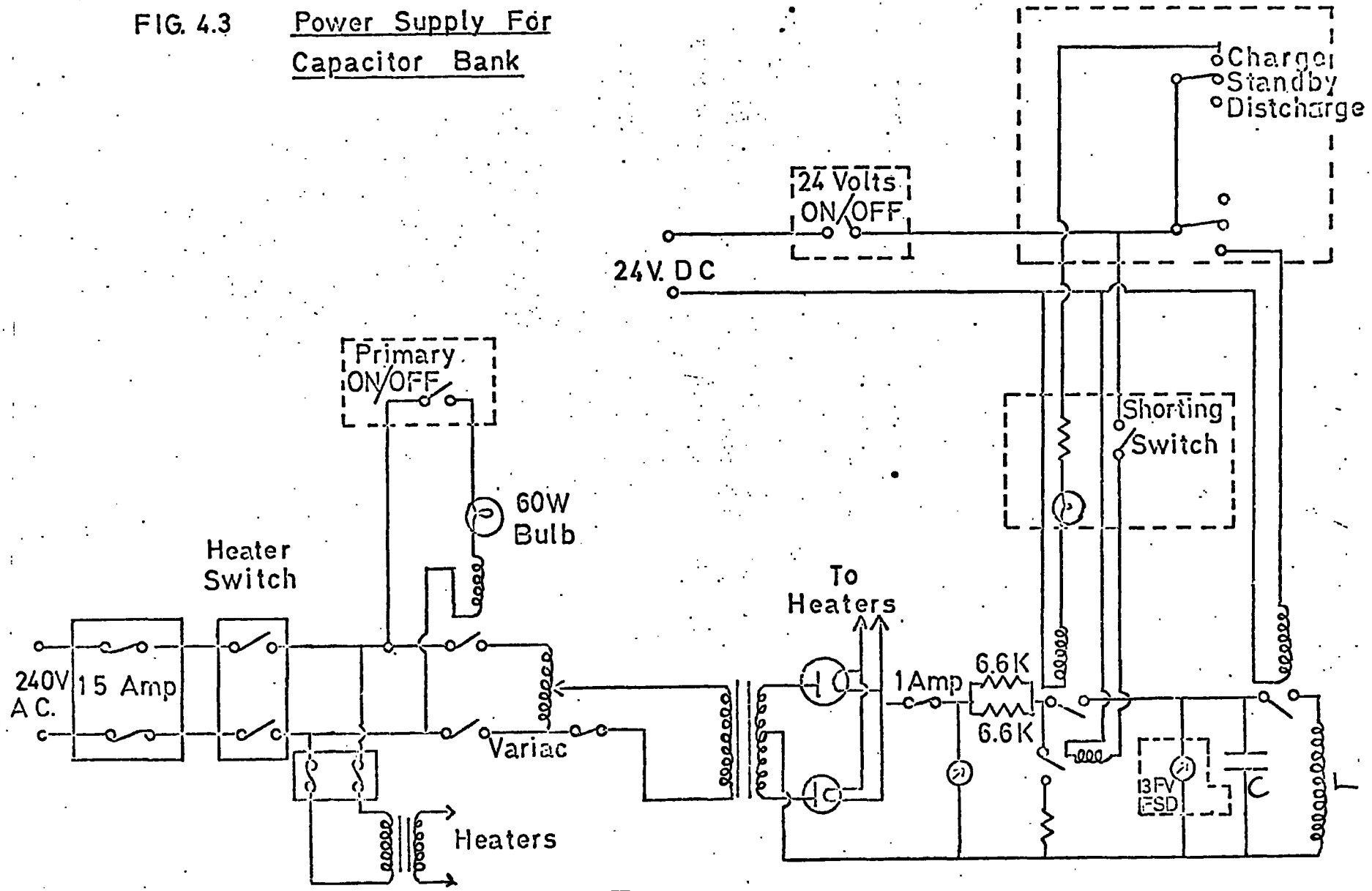

The solution then is

$$i = \frac{V}{L} \exp\left[-\frac{Rt}{2L}\right] \quad \frac{\mathrm{Sin}\omega t}{\omega} \quad \ldots\ldots\ldots\ldots\ldots\ldots \quad (4.6.2)$$

where $\omega = \left\{\frac{1}{LC} - \frac{R^2}{4L^2}\right\}^{\frac{1}{2}}$

The form of the current is that of a sine wave whose amplitude is decaying exponentially with time. Now $V/L\omega$ has the dimensions of current.

Let $i' = \frac{V}{L\omega}$

$$\therefore \quad i = i' \exp\left[-\frac{Rt}{2L}\right] \mathrm{Sin}\omega t \quad \ldots\ldots\ldots\ldots\ldots \quad (4.6.3)$$

The resulting magnetic field will have a similar form (c.f. 4.6.6)

i.e. $H(t) = H' \exp(-\lambda t) \mathrm{Sin}\omega t \quad \ldots\ldots\ldots\ldots\ldots \quad (4.6.4)$

where $\lambda = \frac{R}{2L}$

To make the exponential term as close to unity as possible, the resistance of the coil and associated leads is kept as small as possible. This is accomplished by making the magnet windings of large cross sectional area, and using large diameter connecting leads. The resistance can also be reduced by immersing the coil in liquid nitrogen. The period of the magnetic field of such a system was found to be about 2.5 milliseconds, and the maximum field about 150 kOe. Such a large field however was not needed for the present investigations. The form of this magnetic field is shown in figure 4.4.

4.6.2 Field Measurement

The magnetic field produced by the pulsed magnet is measured by means of a pick-up coil wound with a total of thirty turns. This coil is placed close to the sample but not so close that it is affected by the magnetization of the sample. Therefore the coil does not give

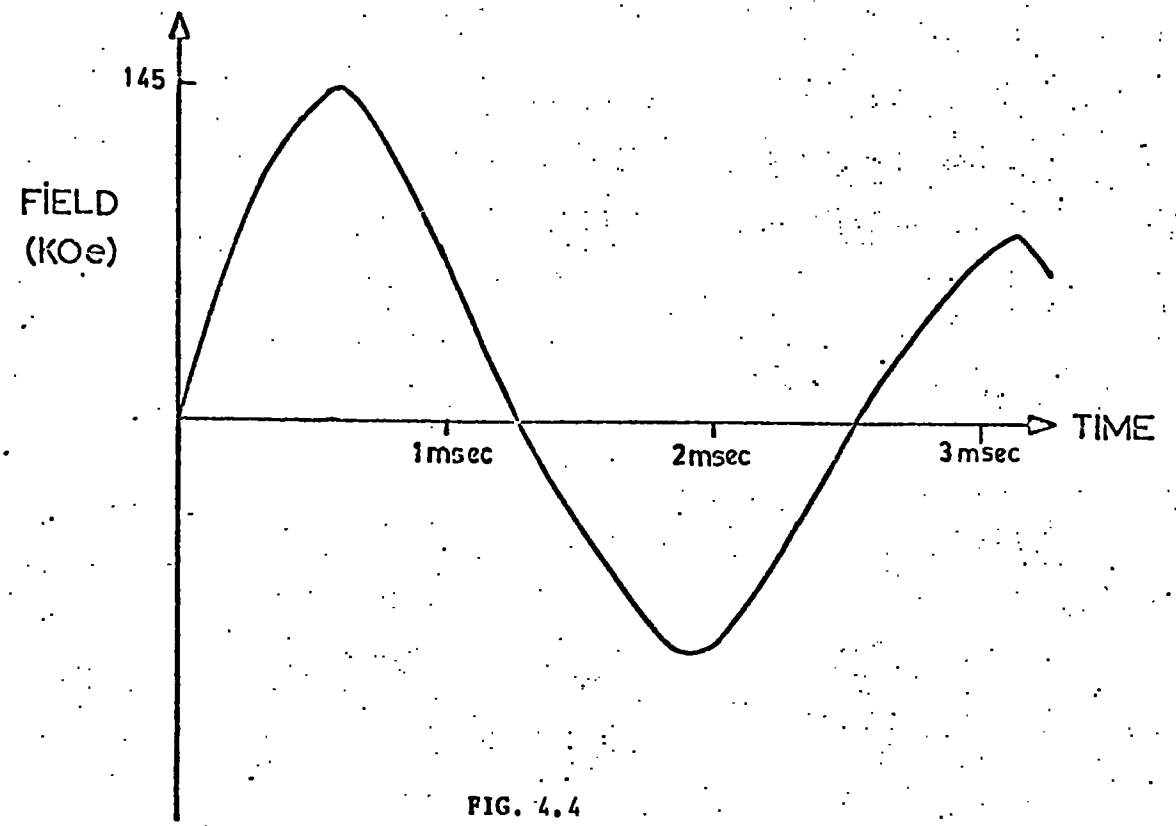

FIG. 4.4
Variation of field with time using the pulsed field magnet

the true field at the sample which is in the maximum field position. Although the field is a function of position as well as time, Poldy points out that the time dependence is not a function of position at a given time t. Therefore the field in the H coil is proportional to the field at the sample. However the output from a single coil will vary with position making its location critical for accurate measurements. This difficulty is overcome by winding the coil in two halves, one above and one below the centre of the magnet. A slight change in the vertical position of the pick-up coil results in an increase in signal from one coil which is counterbalanced by a decrease in signal in the other. The signal is therefore insensitive to slight vertical movements.

The output from the pick-up coils is proportional to dH/dt. To obtain a measure of H, this signal must be integrated. This was done electronically using the circuit shown in figure 4.5.

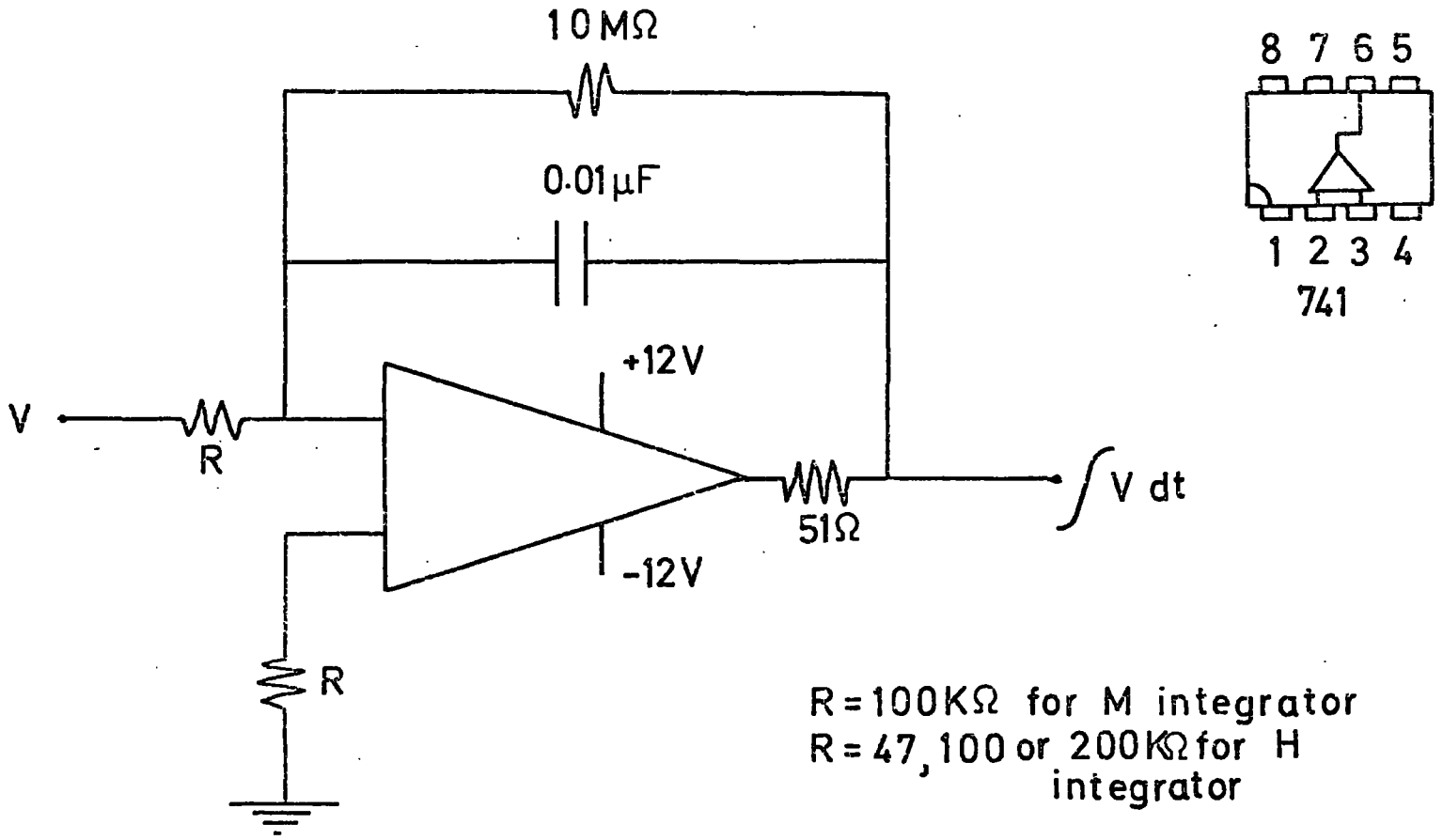

FIG. 45

ELECTRONIC INTEGRATOR

4.6.3 Calibration of the H-signal

Poldy describes two methods of H calibration. The first relies upon observing the M versus H curve for a substance which has a known critical field; and the second method which is less direct is concerned with calculating the sensitivity of the H signal from first principles.

In the first case, $Zn\ Cr_2Se_4$ was used. The critical field value of 64kOe was used for calibration purposes. This was the method that Poldy and Hunter both preferred to rely upon for accuracy. However, Hunter in later work (8) points out that the size of the critical field is dependent upon the rate at which the external field is applied. This implies that the experimental determination of the H calibration may not be so reliable. Poldy's theoretical estimate still relies upon several electrical measurements, each of which may introduce errors. It is possible however to calculate the H sensitivity by taking only one 'electrical' reading. That is the deflection produced on the oscilloscope for the maximum field. The latter can be found as follows. For maximum or minimum field,

$$\frac{di}{dt} = \frac{dH}{dt} = 0$$

This gives $\tan\omega t_m = \frac{2L\omega}{R}$ ..... (4.6.5)

where t_m is the time for maximum field

$$\therefore \quad i_m = i' \exp\left[\frac{-Rt_m}{2L}\right] \operatorname{Sin} \omega t_m$$

and for a solenoid

$$H_m = \frac{ni_m}{\ell} \qquad (A/m)$$

Hence $H_m = \frac{n}{\ell} i' \exp\left[\frac{-Rt_m}{2L}\right] \operatorname{Sin} \omega t_m$ ..... (4.6.6)

If τ is the period of the oscillation then,

$$\omega \tau = 2\pi$$

from the display of the field, (figure 4.4)

$$\tau = 2.5\ 10^{-3}\ s$$

$$\therefore \quad \omega = 2.51\ 10^{3}\ s^{-1}$$

also from the oscilloscope trace,

$$t_m = 0.60\ 10^{-3}\ s$$

$$\therefore \quad \omega t_m = 1.506$$

(4.6.5) $\rightarrow$ $$\frac{2L\omega}{R} = \tan(1.506) = 15.4$$

$$\therefore \quad \frac{R}{2L} = \frac{\omega}{15.4} = 163$$

Let $$A = \exp\left[-\frac{Rt_m}{2L}\right] \operatorname{Sin} \omega t_m$$

Then $$A = \exp\left(-163 \times 0.6 \times 10^{-3}\right) \operatorname{Sin}(1.506)$$

$$= 0.905$$

Hence the maximum field

$$H_m = \frac{ni'}{\ell} \times (0.905)$$

$$= \frac{n}{\ell}\frac{V}{L\omega} \times (0.905)$$

The inductance L can be found from the dimensions of the coil

$$L = \pi \mu_o n^2 r^2 / \ell \approx 25 \mu H$$

$$n = 36, \quad V = 2kV, \quad \ell = 0.09 \text{ metres}$$

$$\therefore \quad H_m = 1.15 \times 10^{7}\ A/m$$

$$= \underline{\underline{144.5\ kOe}}$$

This figure agrees quite favourably with that obtained by Poldy, lying half way between his estimated values.

This field produced a deflection of 5.2 cm on the (x1, 200K) setting. Thus the sensitivity of the H axis of the oscillogram on this range is 27.8 kOe/cm.

It is also interesting to calculate the theoretical value of resistance R.

$$\frac{R}{2L} = 163$$

$$L = 25\ 10^{-6}\text{H}$$

$$\therefore\ R = 8.2\ 10^{-3}\text{ohms}$$

It is now possible to find the H sensitivities of the other ranges thus enabling estimates of the coercivities of different samples to be made.

4.6.4. Magnetization Measurement

The magnetization of a specimen is measured by means of a pick-up coil placed close to the sample. The output from this coil is dependent upon the rate of change of magnetization, dM/dt, of the sample, and also upon the rate of change of field dH/dt. By removing the dH/dt component, it is possible to integrate the remaining signal to find the magnetization of the specimen.

To remove the effect of the applied field, a second identical pick-up coil is wound in series opposition to the first. Therefore in the absence of a sample the total output should be zero. However the two coils are in different fields, the first one being in the maximum field position. This results in a non-zero signal which can be balanced out electronically by adding part of the signal from the H pick-up coils.

As in the case of the H coils, the above system would be sensitive to the position of the coils. To overcome this the second pick-up coil is split, and each half placed symmetrically above and below the first coil. A complete circuit for the M and H detection system is shown in figure 4.6. With the H dependence removed from the M pick-up coils, the signal can be integrated using the circuit shown in figure 4.5.

Ideally, with no sample, the M against H display should be a horizontal straight line. However, because of eddy currents, the trace is

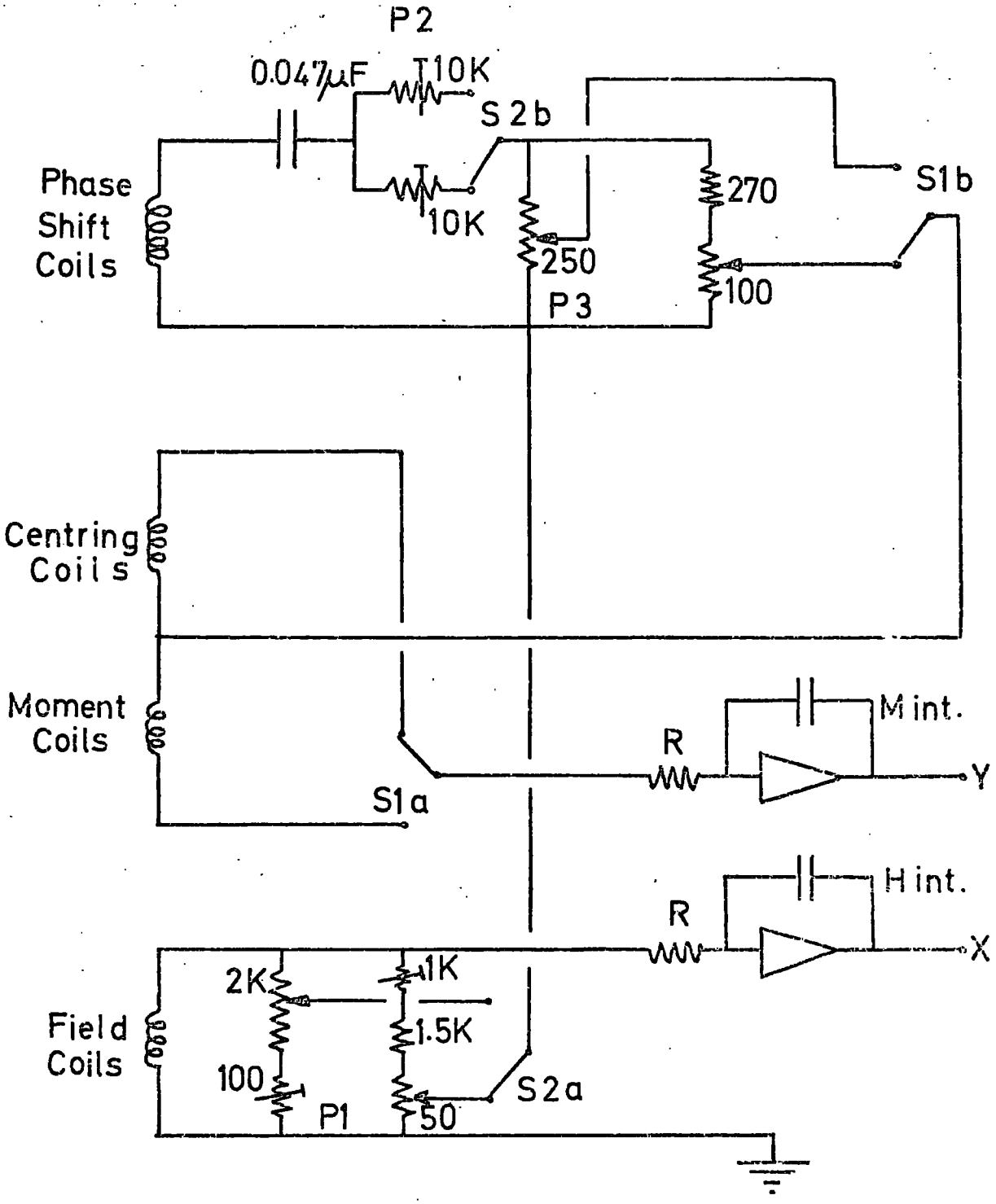

FIG. 4.6

CIRCUIT USED IN PULSED

FIELD MEASUREMENTS

found to have an elliptical shape. The amplitude and phase angle of the ellipse can be minimised by adding a correction signal of equal and opposite amplitude and phase. This signal is obtained from a pair of coils called the Phase Shift Coils (figure 4.6), and is added to the M signal. The required phase shift is obtained by varying the potentiometer P2, and the correct amplitude by varying potentiometer P3. When taking measurements these potentiometers were adjusted to give a no sample trace which was as close to the horizontal as possible.

To allow for residual eddy current noise, oscillograms with and without samples were obtained at identical applied fields. The noise components could therefore be subtracted off.

4.6.5. The Centring Coils

To be sure that any calibration holds for all samples, it is imperative to ensure that all the samples are measured in the same field position. This in fact should be the maximum field position.

To locate the sample accurately at this point, a pair of coils called the centring coils are employed. These are wound in opposition and placed symmetrically above and below the maximum field position. When centring the sample, the M integrator is switched from the moment coils to these coils. When the sample is half way between the coils, in the maximum field position, the output is zero. If the sample is anywhere else, a hysteresis loop is produced. This then is a simple method of centring the specimen.

4.6.6 Calibration of the M signal

The saturation magnetization of iron is known accurately and this was used for calibration purposes. Several powdered iron samples were used in the magnetometer, and the resulting hysteresis loops obtained. The size of the saturation signals M_s, in millivolts was plotted against the mass of the samples (see figure 4.7).

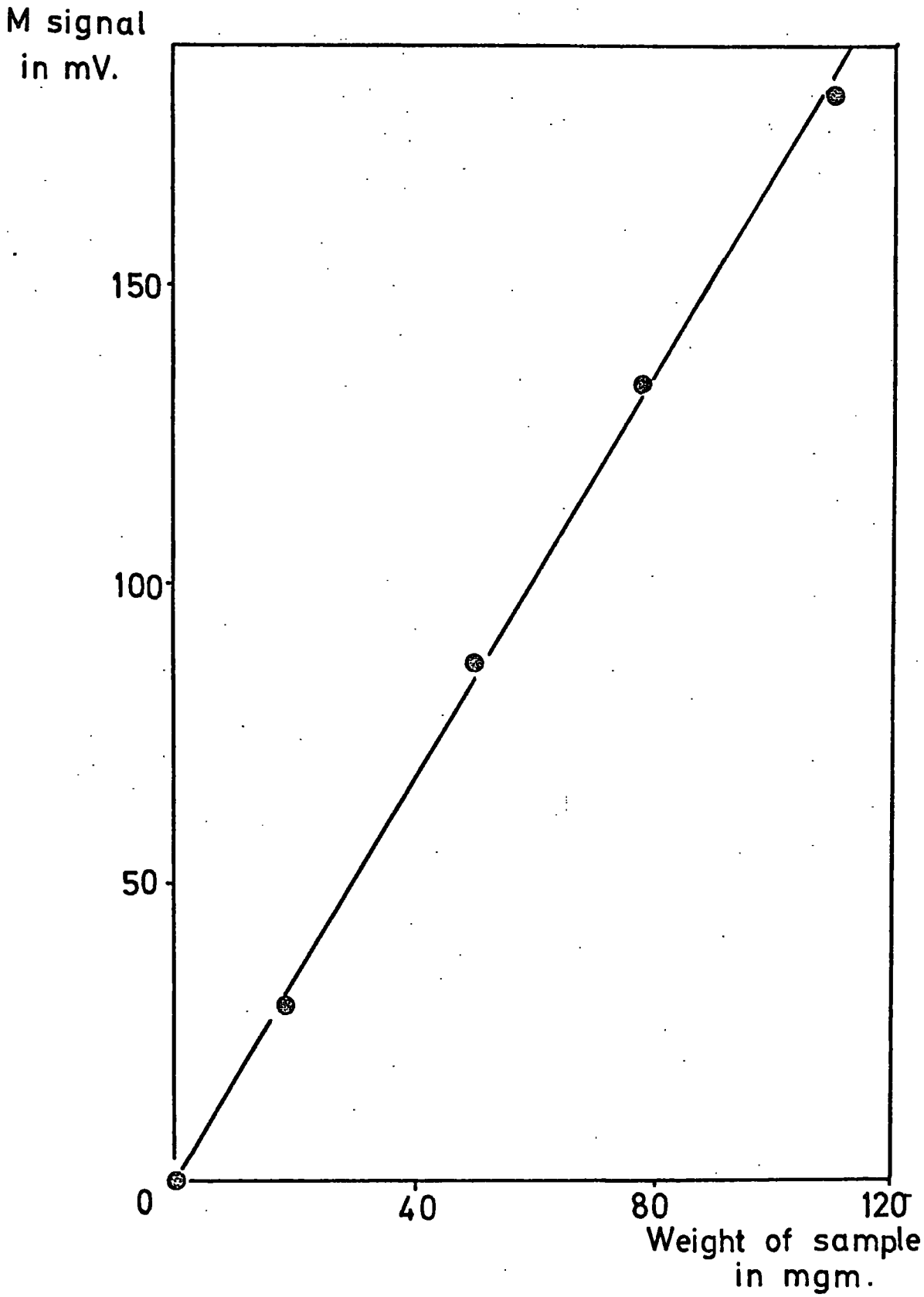

FIG. 4.7

Calibration of M signal

The gradient of this graph is given by

$$g = \frac{\Delta \text{Ms signal in mv}}{\Delta \text{mass of sample}} = \frac{167}{100} = 1.67$$

The specific magnetization of a sample is given by

$$\sigma = \frac{k \times \text{Msignal in mv}}{\text{mass of sample in mgm}}$$

For the iron standard

$$\sigma_s(Fe) = k.g$$

$$\therefore \quad k = \frac{\sigma_s(Fe)}{g} = \frac{218}{1.67} \text{ e.m.u/V}$$

Thus for any sample

$$\sigma(\text{sample}) = \frac{130.5 \times \text{Msignal in mV}}{\text{mass of sample in mgm}}$$

The units of σ are then e.m.u/gm

Using the pulsed field magnetometer it is thus possible to measure magnetization and coercivity for different samples. However for the particles under investigation there is some doubt on the accuracy of the magnetization results obtained by this method. The reasons for this are two fold although they may appear to be synonymous.

Firstly, the amount of material was small and the errors in weighing were greater than if a larger sample had been available. In addition there was a limit to the amount of material which could be put in the sample holder. This was because the packing efficiency of the particles was low, and the volume was filled with a comparatively small mass of powder.

The second reason was that with such small amounts of material, the signal was small, and in some cases was comparable to the size of the noise component.

The samples under investigation generally had high Curie temperatures. This meant that even the room temperature magnetization

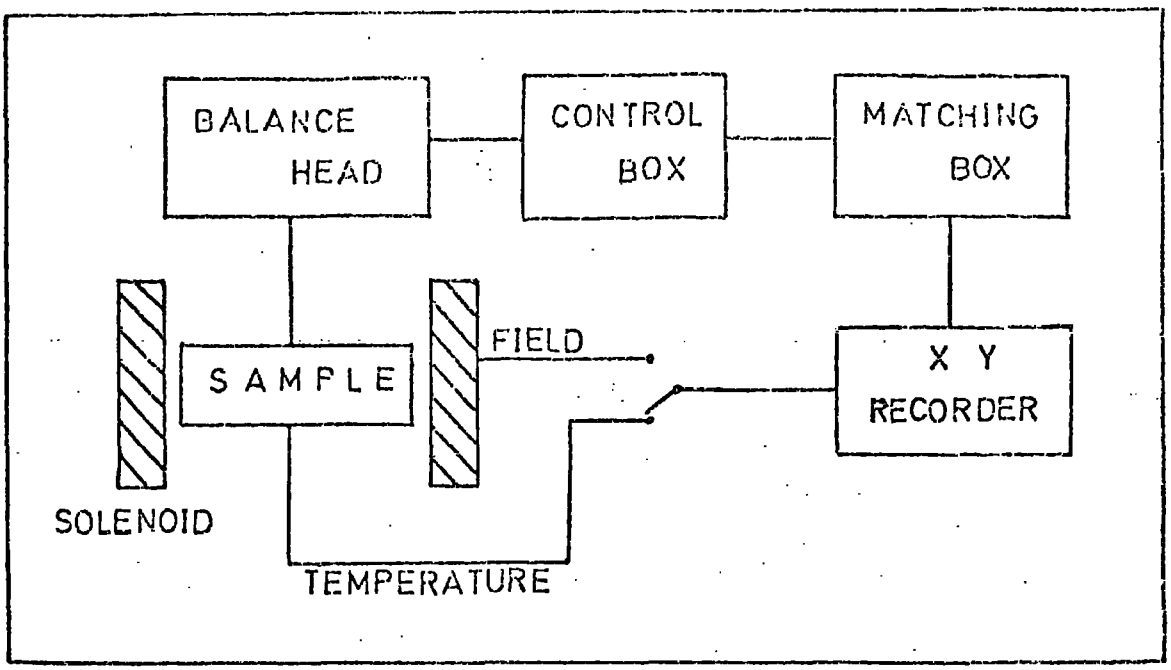

FIGURE 4.8

BLOCK DIAGRAM OF THE FARADAY BALANCE

was on the upper, more constant part of the Brillouin curve. Therefore although the measurements were made at 77°K the magnetization results should not differ too much from those expected at room temperature.

4.7. THE FARADAY BALANCE MAGNETOMETER

Principle of Operation

A Faraday Balance Magnetometer for susceptibility and magnetization measurements was designed and constructed in the laboratory. The principle of operation relies upon the fact that for a specimen magnetized in a field H_z and field gradient dH_z/dz, there exists a force F_z on the specimen.

This force is proportional to the susceptibility per unit mass of the specimen. In the experiment, an electronic balance was used to measure this force. The balance had a direct pen recorder output. This made it possible to display on an X-Y recorder, traces of force versus field and force versus temperature. A block diagram of the system is shown in figure 4.8.

4.7.1 Construction of the Magnetometer

In order that the magnetometer be versatile, that is, that it could be used for a variety of experiments, it was designed to take different demountable fittings. So that low temperature work could be carried out the system was designed to accept a cryostat. This enabled materials under investigation to be cooled to liquid helium temperature. At room temperature the cryostat could be left in place, or removed so that a simpler arrangement could be employed. These two modifications of the magnetometer are shown in figures 4.9a and 4.9b.

1. Solenoid, gradient coil, and power supplies

The magnet used to produce the field H_z was an oil cooled solenoid. Originally, the solenoid had been cooled by water but this led to electrolytic decomposition of the copper windings. This had the effect of producing localized hot spots due to thinning. Paraffin was tried as a coolant but this tended to perish the rubber seals, which had to be replaced periodically. Finally, transformer oil was adopted as the coolant. A table comparing the different cooling agents relative to water, is shown below (9). (The values given are average values)

	Water	Paraffin	Transformer Oil
Specific Heat	1	0.51	0.45
Viscosity	1	0.50	32
Conductivity	1	0.20	0.22
Density	1	0.80	0.88
Latent Heat of Vapourization	1	0.065	0.067

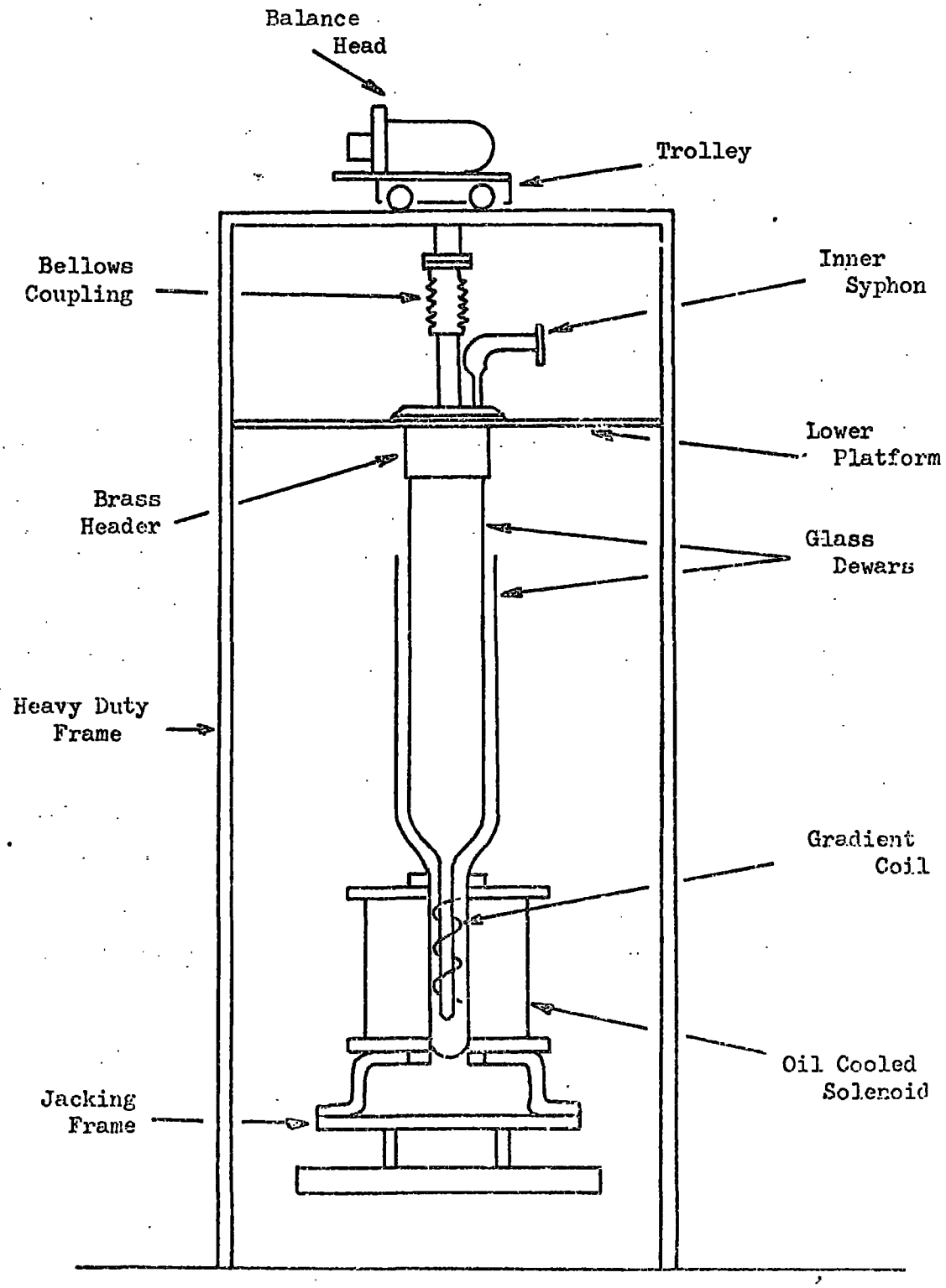

FIG. 49a

FARADAY BALANCE MAGNETOMETER
FOR LOW TEMPERATURE WORK

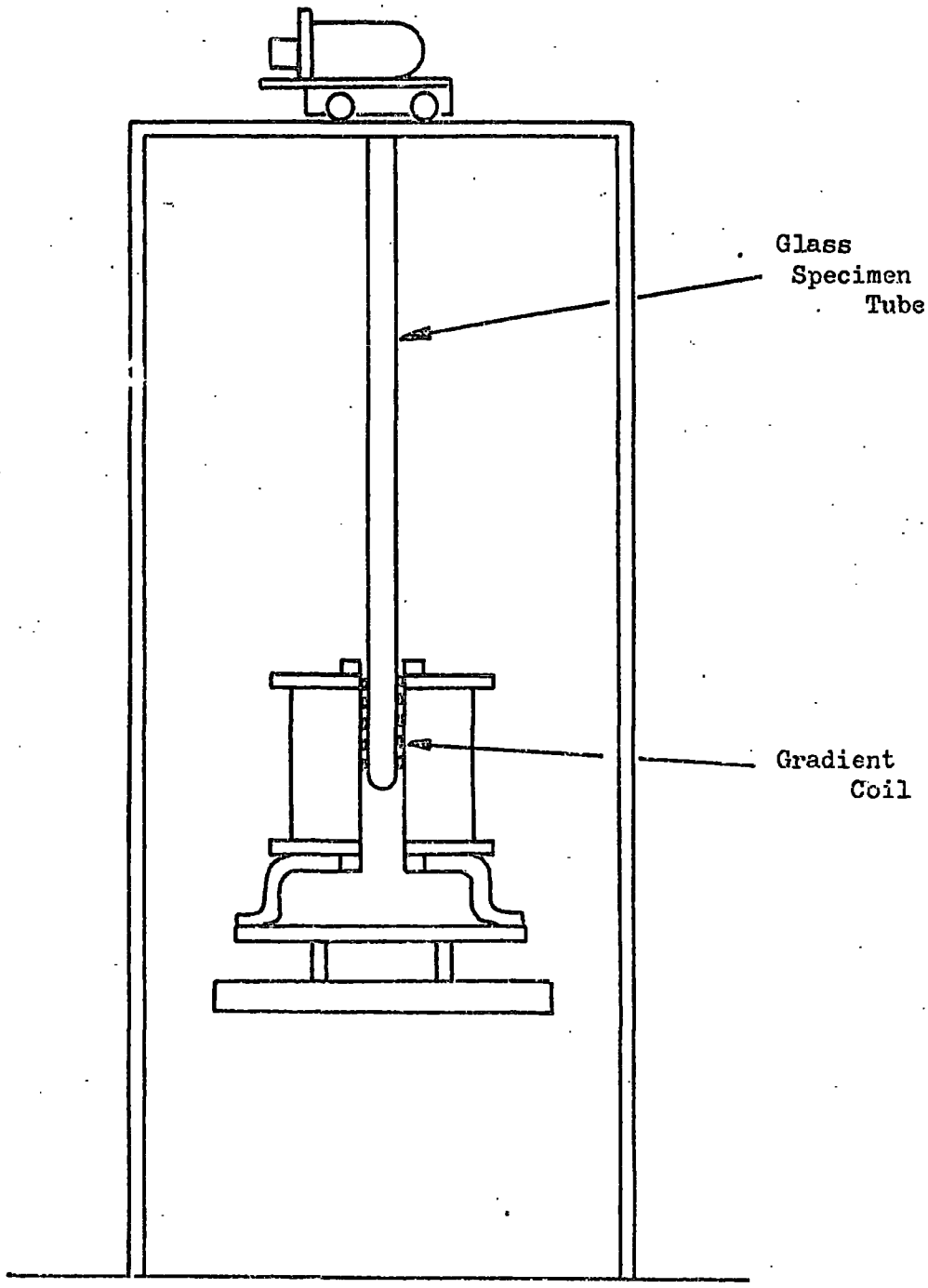

FIG. 4.9b

FARADAY BALANCE MAGNETOMETER
FOR ROOM TEMPERATURE WORK

The transformer oil was pumped through the solenoid within a recirculating system. Since the cooling efficiency of the oil was inferior to that of water, the closed circulating system was jacketed by three additional heat exchangers. These were cooled directly with water from the main.

It was also found that the rubber seals perished to a lesser degree when transformer oil was used. The solenoid itself was wound with copper strip in the form of 'pancakes'. Within each pancake, one turn of copper was insulated from the next by nylon fishing line which had been twisted round the copper strip. Alternate pancakes were oppositely wound and interconnected alternately at the centre and outside. This ensured that when they were all connected, the field due to each one was in the same direction. Each pancake was insulated from the next by the insertion of thin tufnol spacers. The solenoid was enclosed in a brass cylinder which had tufnol end pieces. The terminals for the solenoid were brought out through these end plates.

The power for the solenoid was derived from a Brentford Stabilized D.C. supply. The solenoid had a nominal resistance of 1 ohm. The voltage across the solenoid could be swept up to 120 volts for a current of 120 amps. However, the magnet could only be run continuously at 50 volts. Continuous running above this voltage led to excessive heating. The supply had two modes of operation. These were the current stabilized and the voltage stabilized modes. For the purpose of this experiment, the supply was operated in the former. The current stabilization overcomes any variation of field due to

resistance changes which may have resulted from heating effects. The magnetic field due to the solenoid was calibrated using a fluxmeter and Hall probe. Details of the calibration together with the graphs are given in APPENDIX A.

At a constant current, and hence a constant field, the field gradient at any given point inside the solenoid was constant. However when the field was varied, the field gradient changed. This variation of the field gradient for different values of magnet current is shown in figure 4.10. For force measurements, it was desirable to have as few variable parameters as possible, i.e. to have only the field varying at constant temperature, or the temperature changing at constant field. To overcome the changing field gradient, it was necessary to insert a supplementary gradient coil into the centre of the solenoid. This produced a constant field gradient. It will be shown later, in the section dealing with the interpretation of measurement, that the gradient due to the main solenoid can then be subtracted out. The power for the supplementary coil was derived from the 24 volt D.C. wall supply which had an A.C. ripple of about 2 volts amplitude. This was smoothed to about 0.2 volts using the circuit shown in figure 4.11. In order that the current through the gradient coil could be controlled, a large rheostat was placed in series with the coil. This also acted as a current limiter, ensuring that the current through the coil was well below the safety level. A meter was included in the circuit to monitor the coil current, which was kept below five amps.

The field signal for the X-Y recorder was obtained by tapping off the voltage across the current reading meter of the

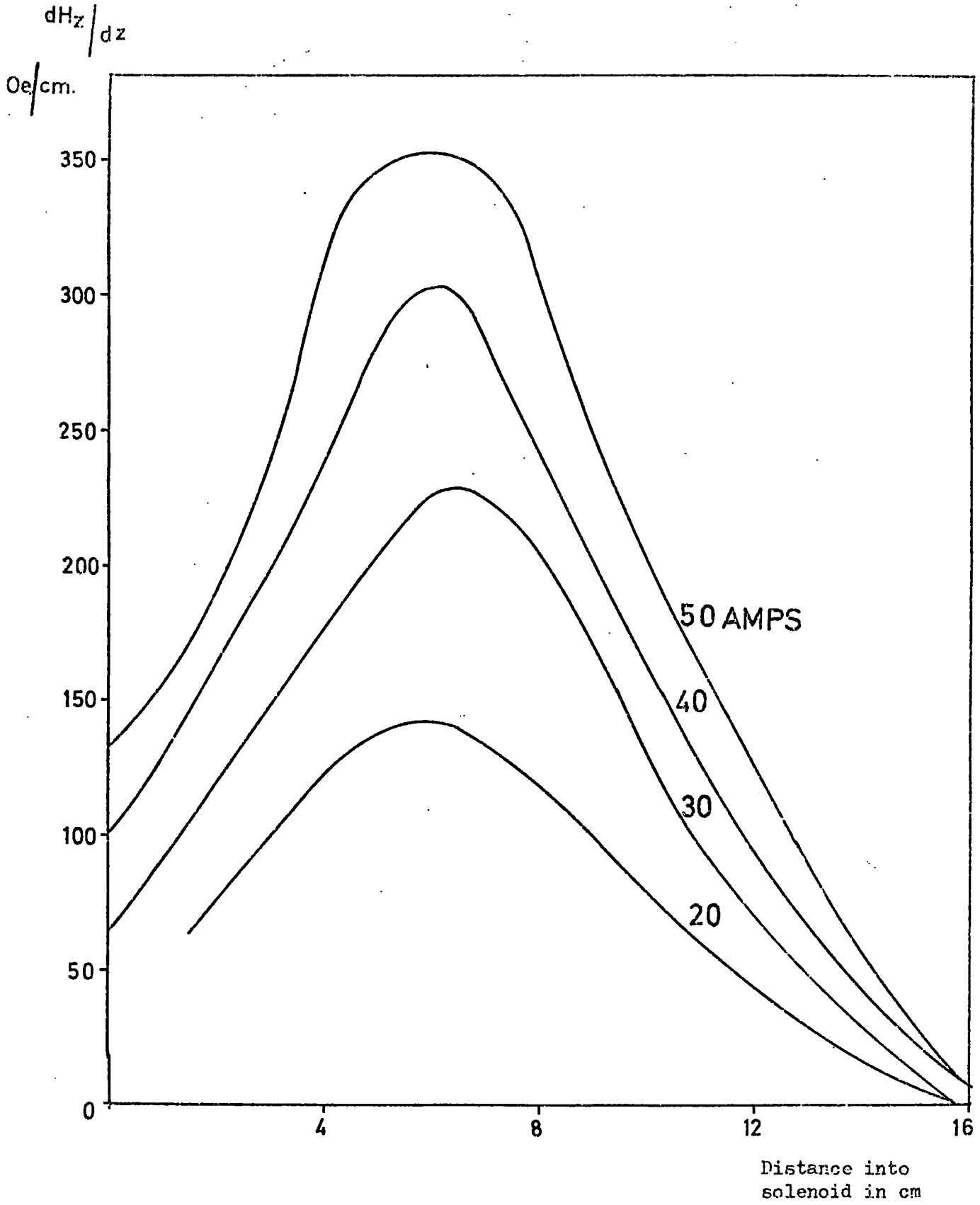

FIG. 4.10

VARIATION OF FIELD GRADIENT
INSIDE SOLENOID

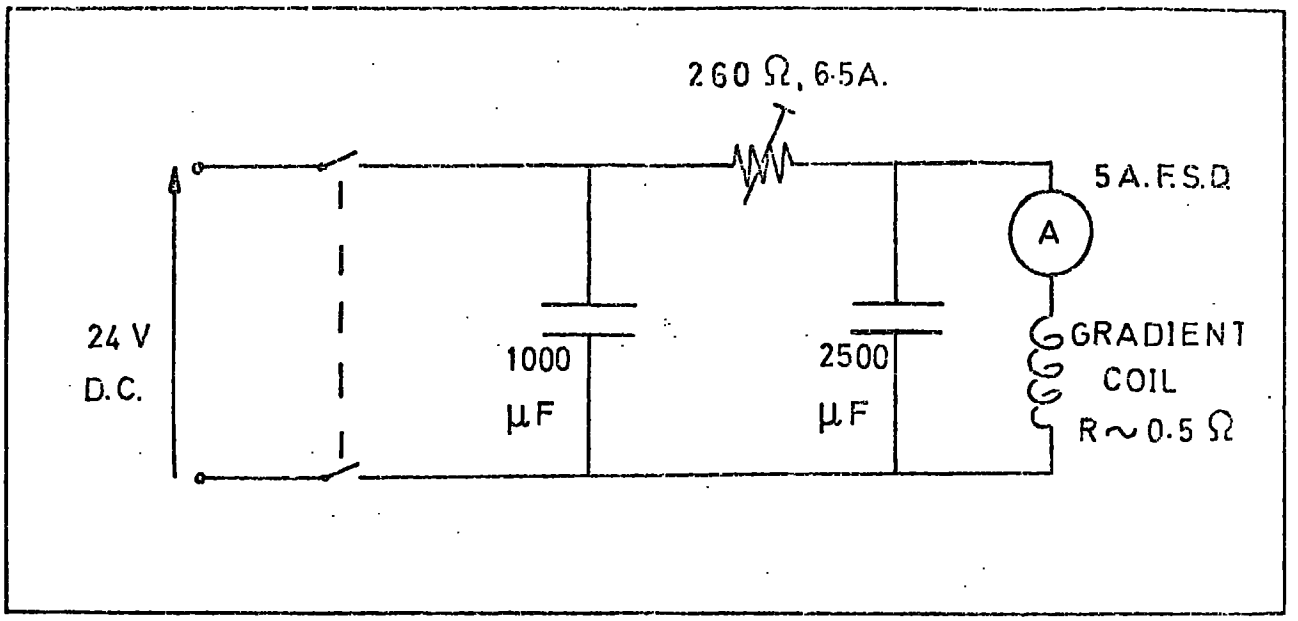

FIG. 4.11

SMOOTHING CIRCUIT FOR
GRADIENT COIL SUPPLY

Brentford power supply. The impedance of the recorder was 1 MΩ and that of the meter 20Ω, so no appreciable current was drained from the meter.

The solenoid, together with the gradient coil, was mounted upon a metal framework which formed part of a hydraulic jacking system. This enabled the solenoid to be raised or lowered to any height, and also made it easier to remove the glass dewars. The total movement of the magnet was 48 cm.

2. The Balance and Electronics

The force on a specimen was measured using an electronic microforce balance. The model used was the 2CT5, made by C.I. Electronics Ltd. The balance head was mounted in a detachable glass envelope. This was fitted with two male B34 joints, which enabled the envelope to be sealed up and evacuated. It could then be left under vacuum, or repressurized with helium gas.

The basic balance head construction is shown in figure 4.12. The balance arm or beam was made of an aluminium-beryllium-copper alloy. It was thus strong as well as being light. The beam

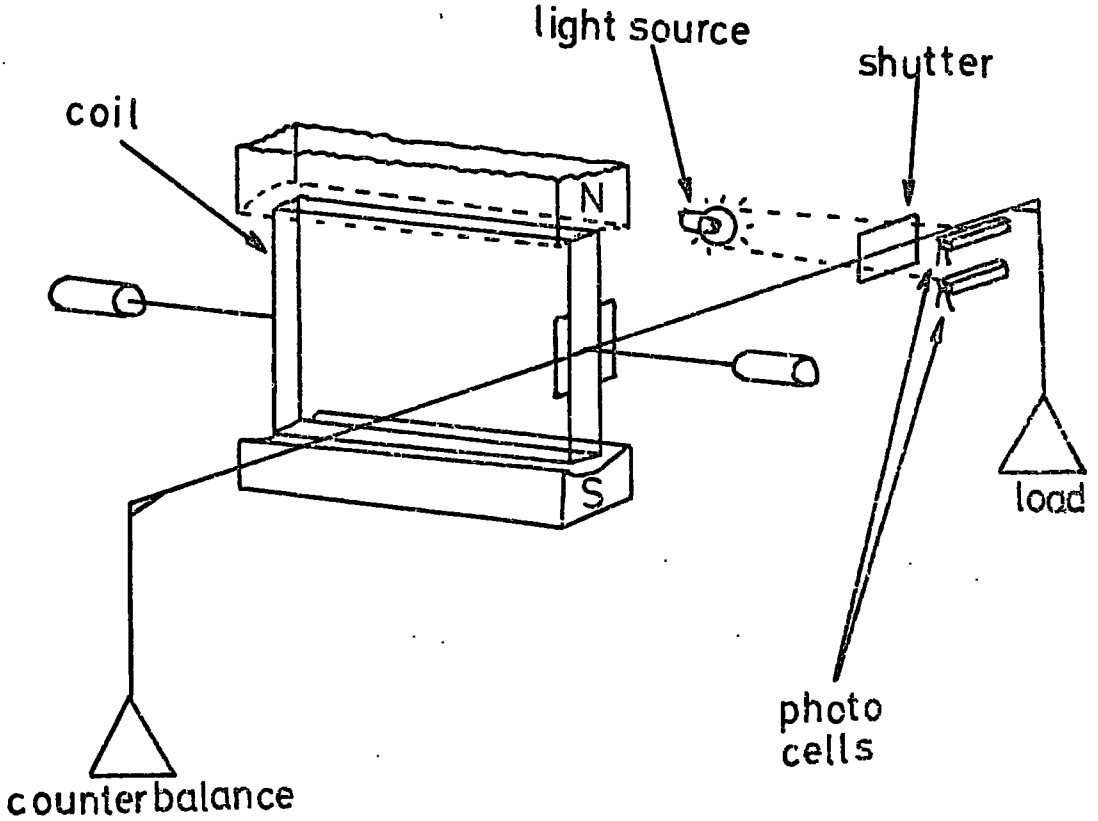

FIG. 4.12

BASIC BALANCE HEAD CONSTRUCTION

carried a shutter which was positioned between a lamp and a pair of silicon photocells. These cells electronically detected the balance condition. The centre of the beam was attached to a movement coil. This was free to rotate in a magnetic field when a current flowed through its windings.

The balance condition was maintained by an electronic servosystem which acted in such a way as to maintain equal illumination on the photocells. These photocells form part of a sensitive bridge circuit. The actual electronics are not shown but the principle is illustrated in the simplified circuit in figure 4.13. In equilibrium, the photocells have equal resistance, and so no bridge current flows. A slight displacement of the beam upsets the balance condition. This results in unequal illumination of the photocells, causing their resistance to change. This in turn produces a bridge current which flows through the movement coil, giving rise to a restoring torque. The torque is sufficient to return the beam to its original position minus the slight deflections inherent in any servosystem.

Associated with the balance head is a control box and a matching box. These contain most of the electronics, and enable an electrical output to be applied to the pen recorder. The control box could be switched to operate off a battery or off the mains. In the present experiment it was mains operated. The primary functions of the control box are to zero and calibrate the balance output. The zero facility enables electrical taring of up to 21.79 mgms by the use of the coarse, medium and fine controls. The balance is calibrated by weighing known standards and adjusting the output. There is a calibration control for each of the five ranges.

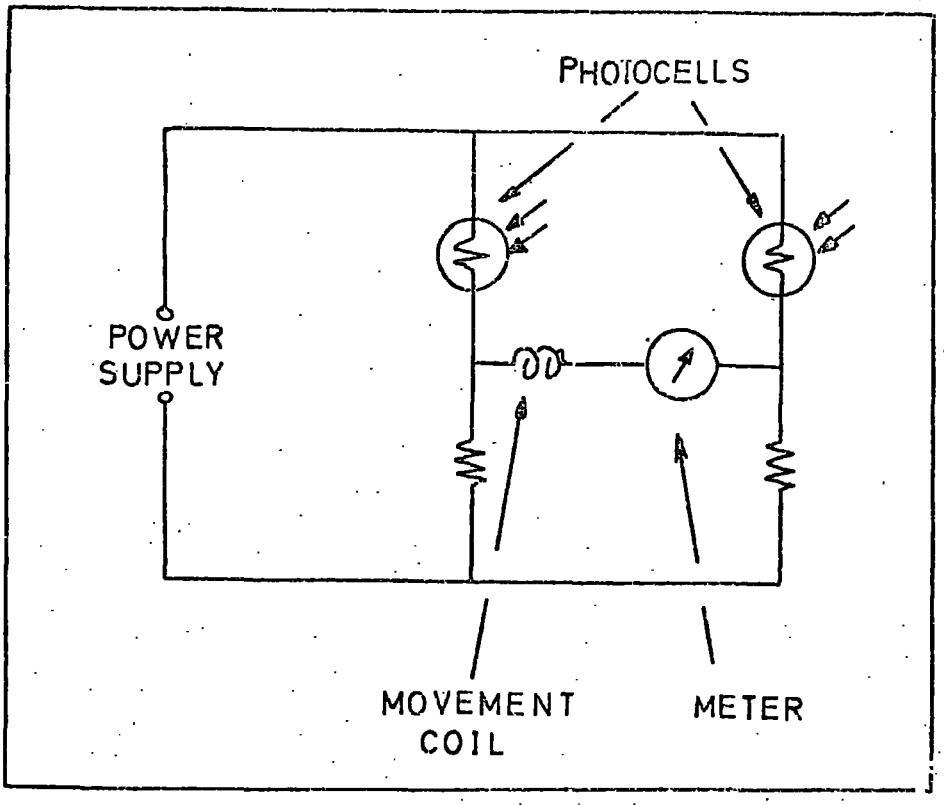

FIG. 4.13
SIMPLIFIED BRIDGE CIRCUIT

The matching box is placed between the control box and the pen recorder. The main role of this is to match the output of the balance to the input of the recorder.

The matching box has three controls. The ratio control is really a potential divider and effectively increases the measuring capabilities of the pen recorder. It allows extra full scale deflections intermediate between those normally obtained from the recorder. This increases the accuracy of the device. The ratio control also ensures that an impedance of 5000 ohms is presented to the balance. The second control is the set gain control, which provides a variable calibration facility for the pen recorder. The third control is for damping. By means of a switch, different amounts of damping could be introduced to reduce the 'noise' level. The switch simply introduces more capacitance into the network; the larger the capacitance, the greater the damping. The higher levels of damping were found to be

unacceptable in the present experiment since these led to an increase in the response time of the balance. Therefore the electrical damping was kept to a minimum.

3. Mechanical Consideration

The glass envelope which contains the balance head was mounted on a trolley. The platform of the trolley was constructed from 'dural', and was mounted on stainless steel bearings which were used as wheels. The trolley was free to run in tracks at the top of a heavy duty metal frame. The purpose of the trolley was to simplify the loading of the balance.

As can be seen from figures 4.9a and 4.9b, for room temperature work, the specimen tube was simply a glass one which mated up with the B34 fitting on the balance envelope. It was then held in place by means of an adjustable slider. For low temperature work, a more elaborate system was required. This is shown in figure 4.14. The brass header shown is in two main pieces. These bolt in place on the lower platform to provide vacuum sealing for the specimen tube and the inner dewar. The specimen tube is fixed in place by means of the gland nut and 'O' ring. The inner dewar seats on the rubber gasket shown, and is sealed on the outside with a rubber sleeve. Between the brass header and the balance is a jointed semi-flexible coupling. This incorporates a bellows system which serves two important purposes. Firstly, when depressed it provides more room for loading and unloading specimens. Secondly, it ensures that no undue strain is exerted on the glassware should there be any misalignment. Another gland nut is incorporated in the top header plate. This allows the insertion and sealing of a stainless steel half transfer syphon. The lower platform to which the brass header

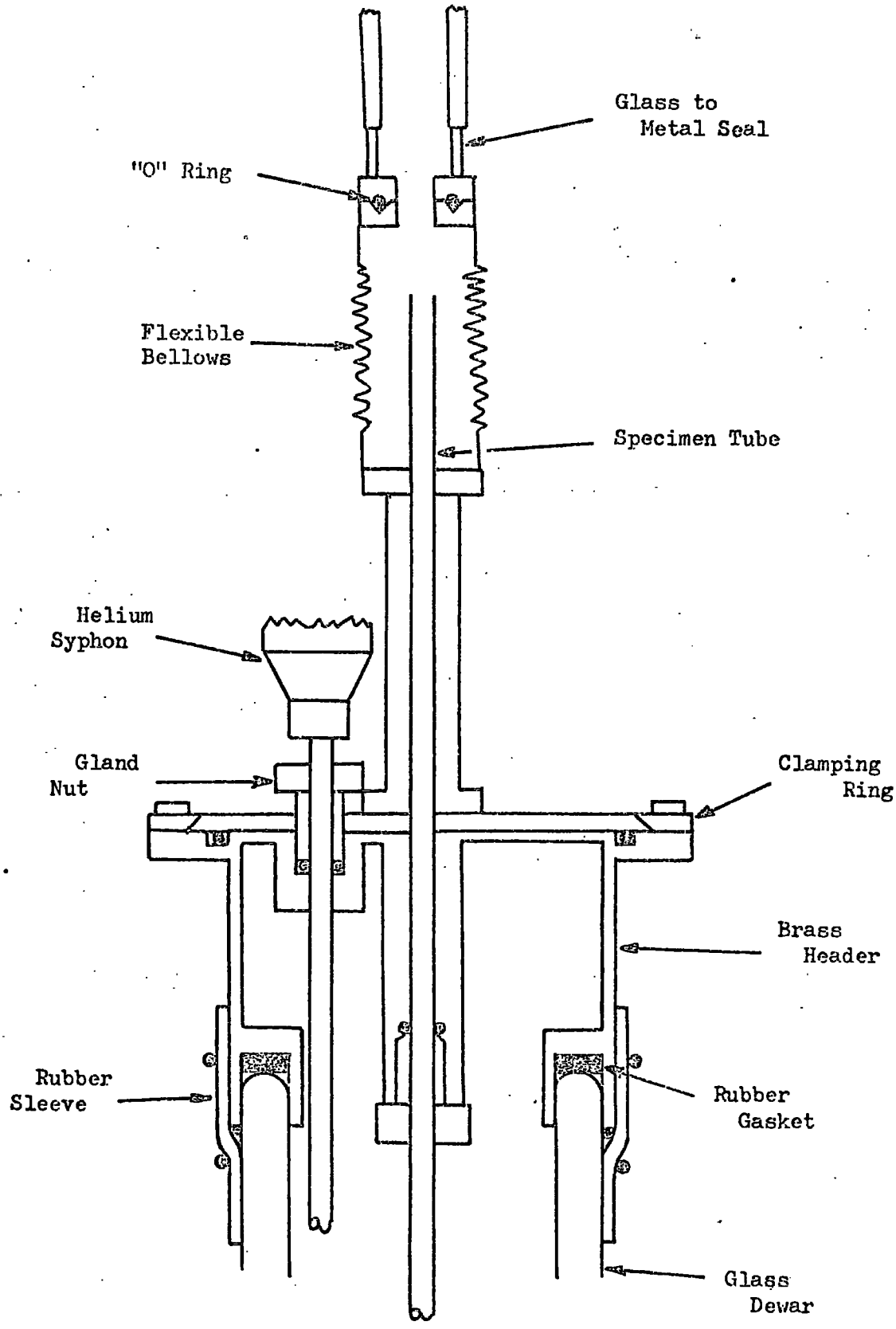

FIG. 4.14

BRASS HEADER ASSEMBLY

bolts, is also made of brass. Being large and thus heavy this helps the stability of the system. The platform is slotted so that the header can be slid out of position, and also to allow some horizontal adjustment for alignment purposes.

For the low temperature work, the specimen tube used was made of a non-magnetic cupro-nickel alloy. To ensure that the specimen tube remained central and did not vibrate in the dewar, a tufnol and perspex 'spider' was made to slide over the end. Into the lower end of the specimen tube was soldered a double electrical lead through.

4. Temperature Measurement and the Vacuum System

A copper-constantan thermocouple was made by threading the wire through P.T.F.E. sleeving. The junctions were formed by welding the ends of the wire in a hot gas flame. The electrical lead through mentioned above enabled one of the junctions to be mounted inside the specimen tube. The thermocouple wires were also soldered into lead throughs in the brass header. This allowed the reference junction to be placed in an external nitrogen dewar. This method of temperature measurement is not really satisfactory for two main reasons. Firstly, spurious temperature differences inside and outside the brass header produce a thermal gradient across the lead throughs. This can result in larger e.m.f.s. being observed. The second and most important reason is the fact that the thermocouple junction is not in direct contact with the sample. This leads to a difference between the observed temperature and the true temperature of the specimen. Since the thermocouple junction is lower than the sample it would be expected that the observed temperature would be on the low side. It may however be

necessary to consider such factors as the relative heating and cooling rates, and also the heat capacities of the materials used. For the present, a simplified approach has been adopted. Observed transition temperatures for different rare earth materials were compared with the true temperatures. This enabled a plot of observed temperature against true temperature to be made. (Figure 4.19)

The vacuum system allowed separate evacuation of the syphons, dewar walls, balance and specimen tube, and the inner dewar. It was also possible to flush with helium gas. A block diagram of the vacuum system is shown in figure 4.15. It should be noted that the balance head and specimen tube could be isolated from the inner dewar. This enabled either to be let up to air independently.

5. Specimen holders and suspensions

The basic specimen holder used in the Faraday balance was a small fused silica bucket. This was light in weight and small enough to fit inside the specimen tube. The bucket was suspended by a fine fused silica fibre. The top of the fibre was connected to the balance via a light chain of stainless steel fibres.

For investigations on loose particles the plain bucket was used. In the case where fixed particles were studied, secondary specimen holders were made. These were fabricated from perspex rod into one end of which a small hole was drilled. The particles were introduced into the hole, and fixed in place using wax. (Wax was used since this would not produce too much strain on the particles). The small perspex holder then fitted easily into the silica bucket.

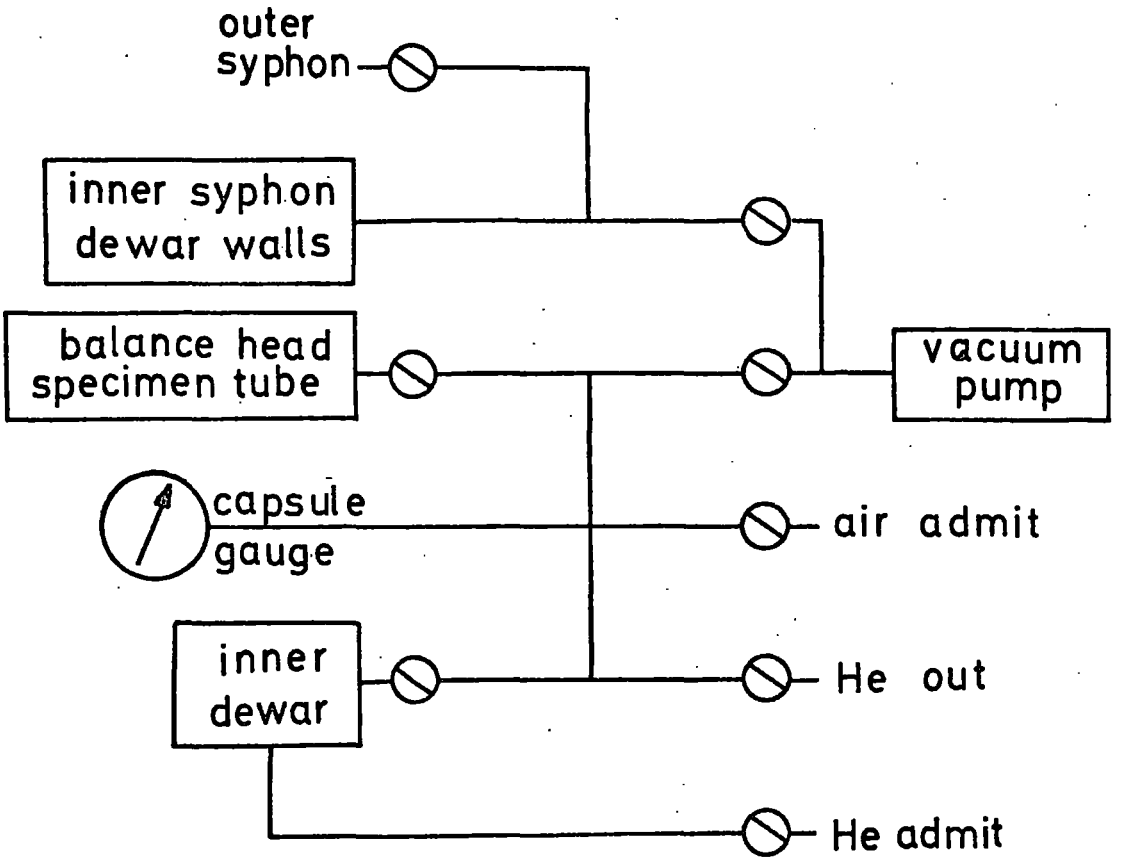

FIG. 4.15

VACUUM SYSTEM

6. Consideration of Undesirable Effects

In setting up the magnetometer the effect of external influences had to be considered. It was required that the balance be as sensitive as possible. To retain maximum speed of response the electrical damping was reduced to a minimum. Therefore any effects contributing 'noise' had to be eliminated or at least reduced to an acceptable level.

The framework supporting the balance was fairly heavy and stable. This was bolted to the floor to help the rigidity. The siting of the magnetometer was in a part of the laboratory fairly free from vibration from generators. The vacuum pump was placed well away from the balance head. The temperature of the laboratory was fairly constant over a particular run of the experiments. In order to avoid draughts, windows in the neighbourhood were kept closed. Since the balance depended on light to function, changes in background illumination had to be avoided. This was achieved by covering the balance head with a sheet of semi-opaque mylor. Loading the balance could produce noise. It had to be loaded gently to avoid shock and reduce pendulum effects. Air currents can cause beam motion due to buoyancy changes. For this reason evacuation and flushing of the system had to be done with the utmost care. With practice it was possible to reduce appreciably noise from most sources. However the pumping of the coolant through the solenoid still produced some noise. It is envisaged that this will be eliminated by the use of a super-conducting solenoid.

4.7.2. Setting up and Operating Procedure

It can be said that the Faraday Balance Magnetometer was designed to work in two principal modes of operation. Firstly

to measure magnetization versus field at constant temperature, and secondly to measure susceptibility versus temperature at constant field. Initially though, the system had to be set up and calibrated.

By the use of spirit levels and plumb-bobs, the balance and magnet were aligned during the construction. The solenoid was calibrated and these results are given in APPENDIX A. Before taking measurements the balance had to be zeroed and calibrated. Also the optimum position for the sample in the solenoid had to be determined.

An empty specimen pan and counterweight pan were attached to the balance beam, and the head sealed up. This was then evacuated. The balance was switched on and allowed to warm up for about twenty minutes. The zero adjustment controls were turned fully anticlockwise, and then the fine control advanced about five turns clockwise. By advancing the coarse and medium controls about four or five turns clockwise, the balance was zeroed first on the least sensitive range, and then successively on the more sensitive ranges. The most 'accurate' zero was obtained on the most sensitive range, and this was then valid for each of the other ranges. Once the balance had been zeroed, it could be calibrated. This entailed placing standard weights (2, 5, 20, 50 and 100 mgms) in the specimen pan. Depending upon the range, the observed weight could be matched with the true weight by altering the calibration controls on the side of the cabinet. Between calibrating each range, when a different weight was in the pan, the vacuum in the head was allowed to 'settle'. This ensured a reduction in the noise level. It was important that once a range had been calibrated,

the corresponding control associated with that range was not touched again except when re-calibrating. The balance was found to remain calibrated over long periods of time.

The effect of the zero control is not quite so critical. Once calibrated, the balance need not remain zeroed. It is the difference in weight due to the action of the magnetic field which is important. In fact the zero control can be used for electrical taring.

With the balance calibrated, it was ready for use in the magnetization measurements.

The position of the sample in the solenoid for magnetization measurements was different to that for susceptibility measurements. In each case, the position of the sample for maximum signal strength was found. The relevant suspension lengths and position of the solenoid are shown in figures 4.16a and 4.16b.

1. Magnetization vs Field

For magnetization versus field measurements, the solenoid was jacked into the upper position and bolted in place. The position of the sample was chosen such that the field gradient due to the solenoid at that point was a minimum, and the field a maximum. The constant field gradient was obtained from the supplementary coil which was inserted in the solenoid.

With the power to the solenoid and coil switched off, a sample was suspended from the balance and the specimen tube fastened in place. For the purpose of calibration, an iron sample, whose mass and magnetization were known, was used. The beam was approximately balanced by carefully loading weights into the counterweight pan and observing the meter needle

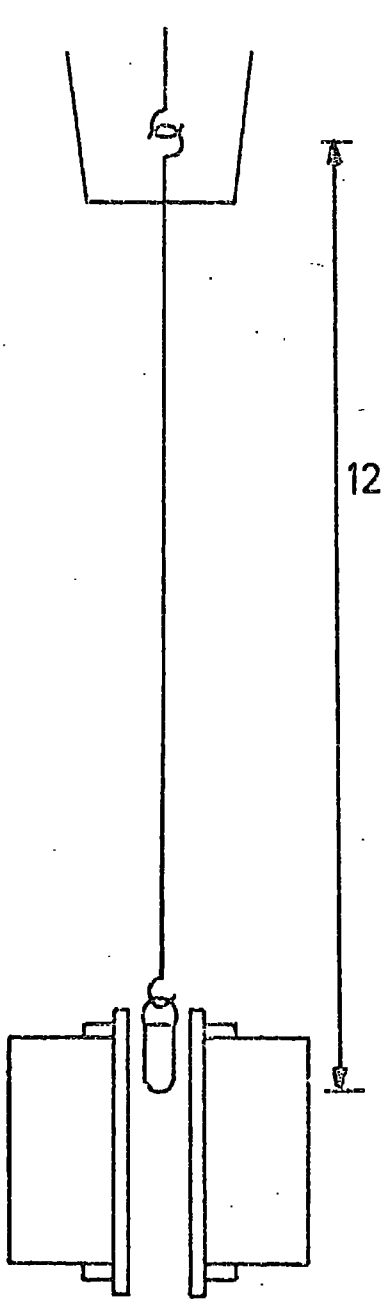

(a)
Susceptibility
Versus
Temperature
Measurements

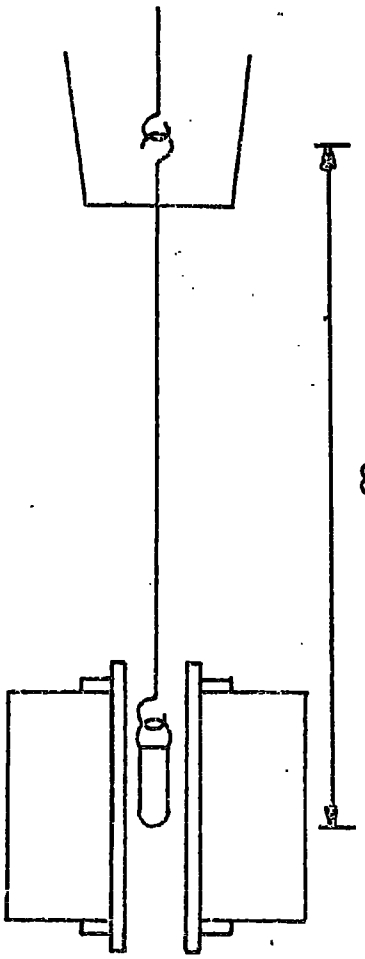

(b)
Room Temperature
Magnetization
Measurements

FIG. 4.16

SUSPENSION LENGTHS

deflection. If it had been necessary, absolute zeroing could have been accomplished by electrical taring. The balance head was then sealed up and evacuated. Power was applied to the main solenoid only and the current increased to give a field of about 2kOe. This produced a deflection on the pen recorder implying the presence of a field gradient. The signal was reduced by finely adjusting the height of the solenoid so as to give a minimum reading. The supplementary gradient coil was switched on and a new deflection obtained. This was maximised by carefully adjusting the position of the coil inside the solenoid. The system was thus adjusted to give maximum output. A plot of the force acting on the specimen as a function of field was thus produced with and without the effect of the gradient coil. It was found that to reduce unwanted hysteresis effects, the gradient coil should be switched in and out during one field sweep. This is shown in figure 4.17. Of course the force acting on a sample could be increased by increasing the current through the gradient coil, but this would mean re-calibration at the new value of current. Plots were also made with no sample. These zero runs produced no background signal.

It was thus possible to produce magnetization versus field curves in the first quadrant. In order to obtain information in the second quadrant it was necessary to reverse the polarity of the main field, and leave the gradient field as it was. Coercivity values could therefore be determined for the particles. In the third and fourth quadrants the magnetization becomes negative. To observe the resulting 'negative' force, it was necessary to 'back off' the balance. As a result it was possible to produce a complete hysteresis loop for a particular sample and also to measure remanences

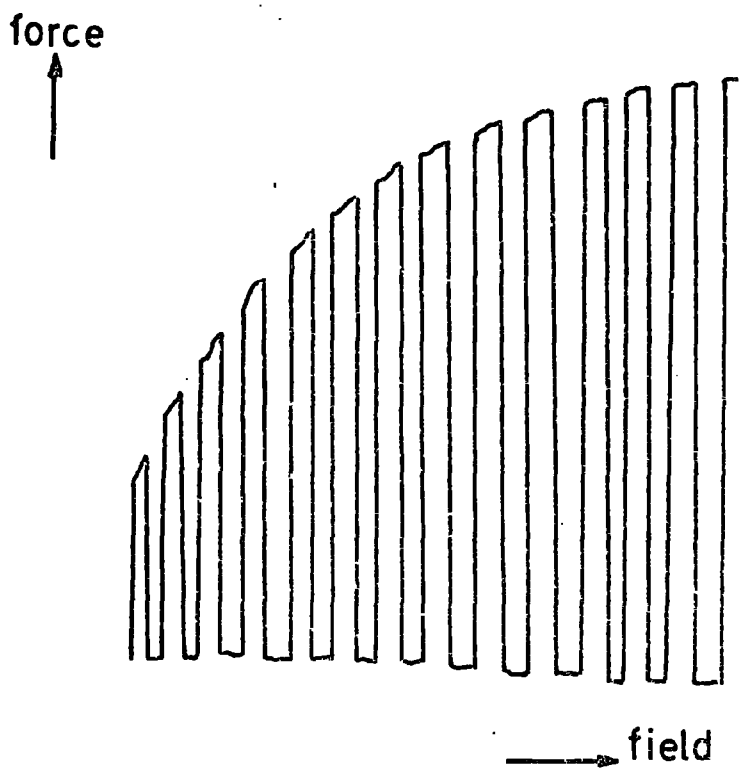

FIG. 4.17

TYPICAL FIELD FORCE TRACE

due to different magnetic histories.

2. Susceptibility vs Temperature

For measurements of susceptibility against temperature the dewars and brass header have to be incorporated into the system. This makes it possible to operate the magnetometer in the temperature range $4.2^{o}K$ - $300^{o}K$. The assembling procedure for this system is outlined in APPENDIX C. This time the sample is placed in a different position. The field is kept constant and hence the field gradient is constant. Therefore there is no need for a supplementary gradient coil. The position of the sample is chosen such that the product of field and field gradient is a maximum. The reason for this can be seen from section 4.7.3. A graph of $H_z \frac{dH_z}{dz}$ is shown in figure 4.18. Fine adjustment of the specimen position is more difficult in this case. Firstly there is a maximum height to which the solenoid can be raised due to the dewars, and secondly there is a limit as to how far the specimen tube can be lowered into the inner dewar. It is possible however to locate the sample in the operating position, taking care not to allow the silica bucket to touch the thermocouple junction. In fact it was found that the graph in figure 4.19 holds very well whether the bucket is close to the thermocouple or up to 4 cm from it. The additional error in the observed temperature only being about 2 degrees.

4.7.3. INTERPRETATION OF MEASUREMENT

It was stated earlier that a specimen magnetized in a field H_z of gradient dH_z/dz, experiences a force F_z.

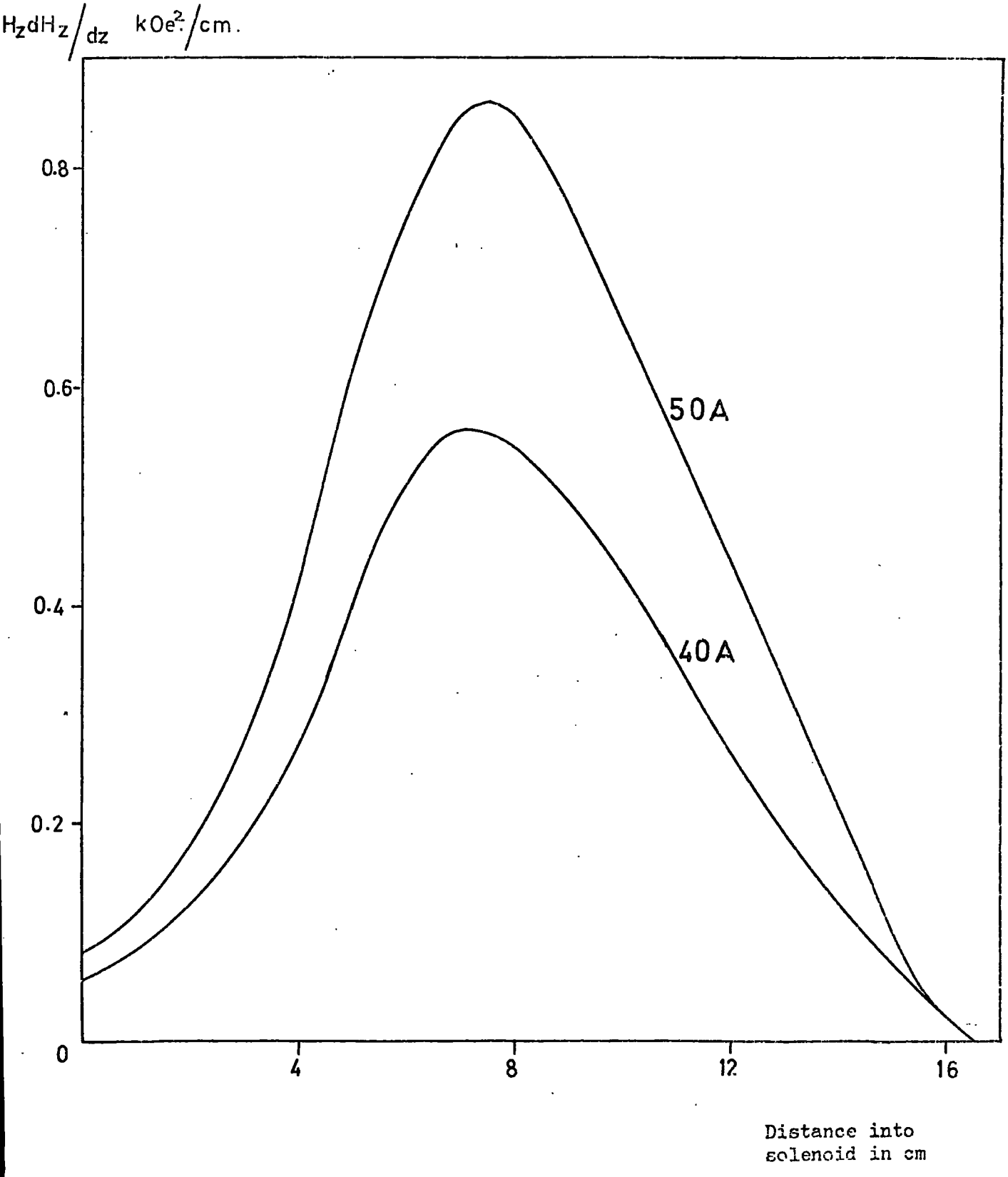

FIG. 4.18

VARIATION OF $H_z dh_z/dz$ INSIDE SOLENOID

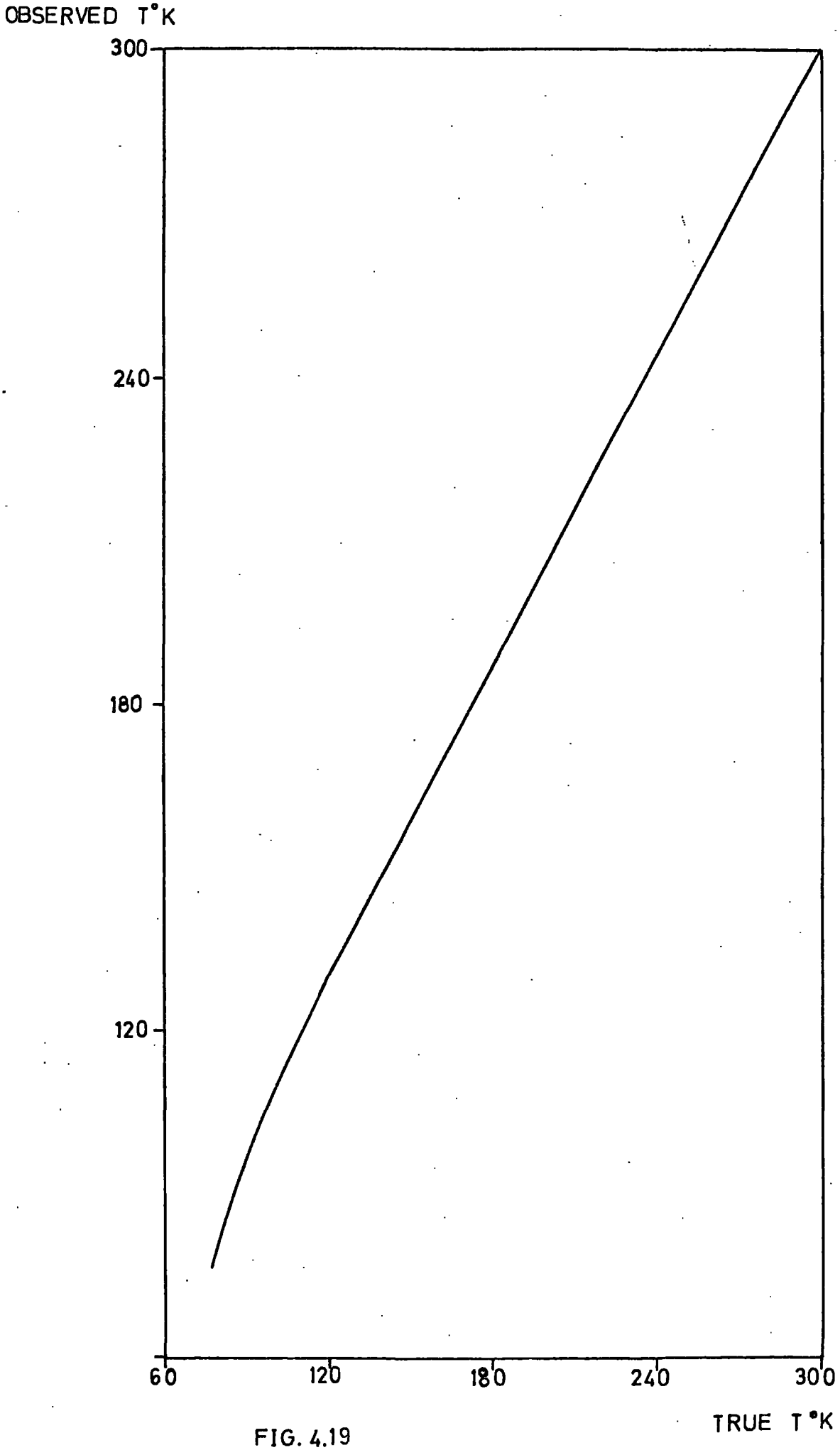

FIG. 4.19

TEMPERATURE CALIBRATION

This force is given by

$$F_z = Q_z \frac{dH_z}{dz} \qquad \ldots\ldots\ldots\ldots\ldots\ldots \quad (4.7.1)$$

where Q_z is the dipole moment in the z direction (4).

For a paramagnetic sample,

$$Q_z = m\chi H_z \qquad \ldots\ldots\ldots\ldots\ldots\ldots \quad (4.7.2)$$

where m is the mass of the sample, and χ is the susceptibility per unit mass.

$$\therefore \quad F_z = m\chi H_z \frac{dH_z}{dz} \qquad \ldots\ldots\ldots\ldots\ldots\ldots \quad (4.7.3)$$

Now the electronic balance produces an output which is proportional to the force. If the balance is calibrated, then the force can be simply expressed in terms of the deflection D of the X-Y recorder.

$$\text{i.e.} \quad F_z = A.D. \qquad \ldots\ldots\ldots\ldots\ldots\ldots \quad (4.7.4)$$

where A is a constant.

Combining expressions (4.7.3) and (4.7.4) and rearranging gives

$$\chi = \frac{D}{mH_z} \quad \frac{A}{\frac{dH_z}{dz}} \qquad \ldots\ldots\ldots\ldots\ldots\ldots \quad (4.7.5)$$

For susceptibility measurements H_z is kept constant. This means that $\frac{dH_z}{dz}$ will remain constant. H_z can be found from the calibration of the solenoid. By using a suitable specimen, it is possible to find the constant

$$C = \frac{A}{\frac{dH_z}{dz}}$$

It is therefore possible to determine the

susceptibilities of different samples. The method can also be used to obtain the variation against temperature of the initial susceptibility of ferromagnetic materials.

Expression (4.7.5) can be rearranged to give

$$D = \frac{m\chi H_z}{A} \frac{dH_z}{dz} \quad \text{..... (4.7.6)}$$

This shows that the signal will be a maximum when the product $H_z\, dH_z/dz$ is a maximum. (Since m, χ, and A are constant for a particular sample).

For a ferromagnetic sample the dipole moment is expressed by

$$Q_z = m\sigma \quad \text{..... (4.7.7)}$$

where σ is the specific magnetization. That is the magnetization per unit mass. For ferromagnetic substances one of the most important characteristics is the saturation magnetization. This means sweeping the field until the material saturates. Varying H_z however, causes dH_z/dz to change. For this reason the supplementary gradient coil is utilized. The field gradient due to this coil is $\frac{dh_z}{dz}$ and this remains constant even as the main field is swept.
A measure of the magnetization can be found by sweeping the field with and without the additional gradient. The difference between the two signals gives a true indication of the magnetization.

Taking expressions (4.7.1), (4.7.4) and (4.7.7) gives

$$\sigma = \frac{A\ D}{m\ \frac{dH_z}{dz}} \quad \text{..... (4.7.8)}$$

In the presence of the additional field gradient this becomes modified to

$$\sigma = \frac{A\,D'}{m}\left\{\frac{dH_z}{dz} + \frac{dh_z}{dz}\right\} \qquad \ldots\ldots\ldots\ldots\ldots \quad (4.7.9)$$

where D' is the new pen recorder deflection. Rearranging and subtracting these two expressions gives,

$$(D' - D) = \frac{\sigma m}{A}\left\{\frac{dH_z}{dz} + \frac{dh_z}{dz} - \frac{dH_z}{dz}\right\}$$

$$= \frac{\sigma m}{A}\,\frac{dh_z}{dz}$$

$$\therefore \quad \sigma = \frac{(D' - D)}{m}\left\{\frac{A}{dh_z/dz}\right\} \qquad \ldots\ldots\ldots\ldots\ldots \quad (4.7.10)$$

Again by using a suitable calibration specimen it is possible to find the constant

$$k = \frac{A}{\left\{\frac{dh_z}{dz}\right\}}$$

For this purpose a powdered pure iron sample was used.

$$\therefore \quad k = \frac{m(Fe)\ \sigma(Fe)}{\Delta D(Fe)}$$

where $\Delta D = D' - D$ (in mV)

using a gradient coil current of 5 amps and

$$m = 15.20 \pm 0.05 \text{ mgm}$$

$$\sigma = 218 \text{ e.m.u/gm}$$

$$\Delta D = 10.4 \pm 0.2 \text{ mV}$$

then $k = 320$ e.m.u/V.

Estimation of errors

Let the error in k be Δk, then

$$\left\{\frac{\Delta k}{k}\right\}^2 = \left\{\frac{\Delta m}{m}\right\}^2 + \left\{\frac{\Delta \sigma}{\sigma}\right\}^2 + \left\{\frac{\Delta \Delta D}{\Delta D}\right\}^2$$

For a standard calibration

$$\left\{\frac{\Delta k}{k}\right\}^2 \sim \left\{\frac{0.05}{15}\right\}^2 + \left\{\frac{1}{200}\right\}^2 + \left\{\frac{0.2}{10}\right\}^2$$

This gives $\frac{\Delta k}{k} \sim 2.5\%$

For other samples the mass and signal are different therefore the errors will be different.

At worst, $\frac{\Delta m}{m} = \frac{0.05}{10}$

$$\frac{\Delta \Delta D}{\Delta D} = \frac{0.2}{4}$$

$$\therefore \quad \left\{\frac{\Delta \sigma}{\sigma}\right\}^2 \sim \left\{\frac{0.05}{10}\right\}^2 + \left\{\frac{2.5}{100}\right\}^2 + \left\{\frac{0.2}{4}\right\}^2$$

This gives $\frac{\Delta \sigma}{\sigma} \sim 5.5\%$

CHAPTER 5

RESULTS AND DISCUSSION - 1

PHYSICAL CHARACTERISTICS

Micropowders of iron, cobalt, iron-cobalt alloys and nickel were prepared by the evaporation technique at pressures of Argon between 3 and 20 Torr. At these pressures the material evaporated from the filament as a grey smoke which circulated in the bell jar due to the gas flow. This 'smoke' settled on the substrates in the chamber and appeared to consist of a black 'soot'. For iron, cobalt and their alloys the particles formed into strands which settled like 'cobwebs'. The structure, morphology, and size of the particles were then investigated by X-ray diffraction and electron microscopy.

5.1 CRYSTAL STRUCTURE

In order to establish the crystal structures of the particles, X-ray powder photographs were obtained for several fibre deposits. The 'd' values were then computed. The results for iron, cobalt and nickel are shown in Tables 5.1, 5.2, and 5.3 respectively. It can be seen that the measured 'd' values agree very well with those of the powder file index.

Oxides do appear to be present but to a lesser extent in cobalt and nickel. It is difficult to say when the oxidation took place. It happened either during the evaporation or later when the particles were exposed to the air. The material was photographed again after several months, but no further

oxidation was observed. The reason for this may be that only the surface of the particles oxidised. This would then act as a protective shell, preventing any further oxidation.

An interesting result is that of cobalt. The f.c.c. to h.c.p. transformation has been suppressed. This confirms the findings of Kitchen (1) and Wada et al (2). Sebilleau and Bibring (3) have proposed a dislocation model to account for the f.c.c. to h.c.p. transformation. The suppression of this transformation in small particles may then be due to there being no suitable dislocation centres. The transformation is in fact a Martensitic one which occurs at 388°C. An attempt has been made to induce the h.c.p. phase by annealing and quenching (4) but subsequent analysis has shown this to be unsuccessful. As far as the magnetic properties are concerned it would have been desirable to have both phases of the material. This would have enabled a comparison to be made between the effects of cubic and uniaxial anisotropy.

All the iron and iron-cobalt alloy particles investigated, exhibited the b.c.c. lattice. Therefore somewhere between $Fe_{30}Co_{70}$ and pure cobalt there is a discontinuity of crystal structure. The nickel particles produced all showed the normal room temperature f.c.c. structure. Lattice parameters have been calculated for all the metals and alloys, and these are shown in Table 5.4. The observed values are in good agreement with the standard values. Broadening of the X-ray lines was observed, but this is thought to be due to strain rather than alloy inhomogeneity.

In addition to the particles produced in argon, iron particles were produced in air at 15 Torr. The results are

shown in Table 5.5. This time the particles show a much greater degree of oxidation. The two oxides Fe_3O_4 and $\gamma - Fe_2O_3$ both appear to be present. How this affects the magnetic properties will be discussed in Chapter 6.

5.2 PARTICLE MORPHOLOGY

To investigate the shape and size variation of the particles, several samples were studied with the aid of the electron microscope. Electron micrographs were obtained, and these show the particle morphologies in Fig. 5.1. All the photographs are for particles produced at a pressure of 15 Torr. Three things are immediately apparent in the micrographs. Firstly the particles appear to be almost perfectly spherical. Secondly they form necklace like chains, and thirdly the size of the particles is not constant. Instead they have a particle size distribution.

The effects of particle size and shape upon the magnetic properties will be discussed in Chapter 6. For the present it is reasonable to suggest that the origin of the particle chains is due to magnetic attraction. This chaining effect would itself be expected to affect the magnetic properties of an assembly of particles.

5.3 PARTICLE SIZE DISTRIBUTION

From enlarged micrographs particle diameter distributions were obtained for cobalt powders prepared at 5 and 10 Torr; and for Co, $Fe_{30}Co_{70}$, $Fe_{60}Co_{40}$, Fe, and Ni powders all prepared at 15 Torr. These distributions are shown in Figs. 5.2, 5.3, and 5.4. It was attempted to fit a known distribution to the observed ones. Without going into the details of a χ^2 fit, it seemed that a normal distribution gave the best fit to the

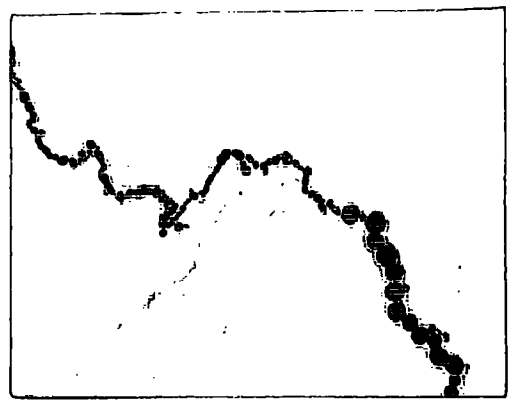

a) Co

b) $Fe_{30}Co_{70}$

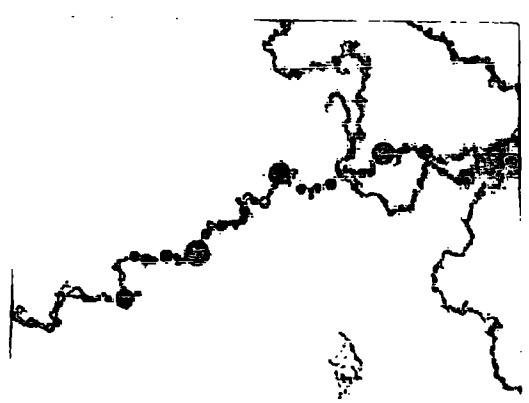

c) $Fe_{60}Co_{40}$

1μm.

FIG. 5.1

ELECTRON MICROGRAPHS

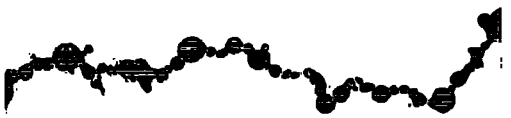

d) Fe

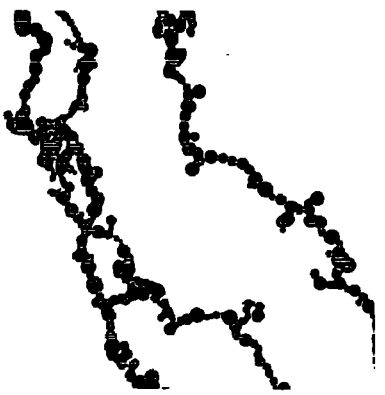

e) Ni

1μm.

FIG. 5.1 (CONT'D)

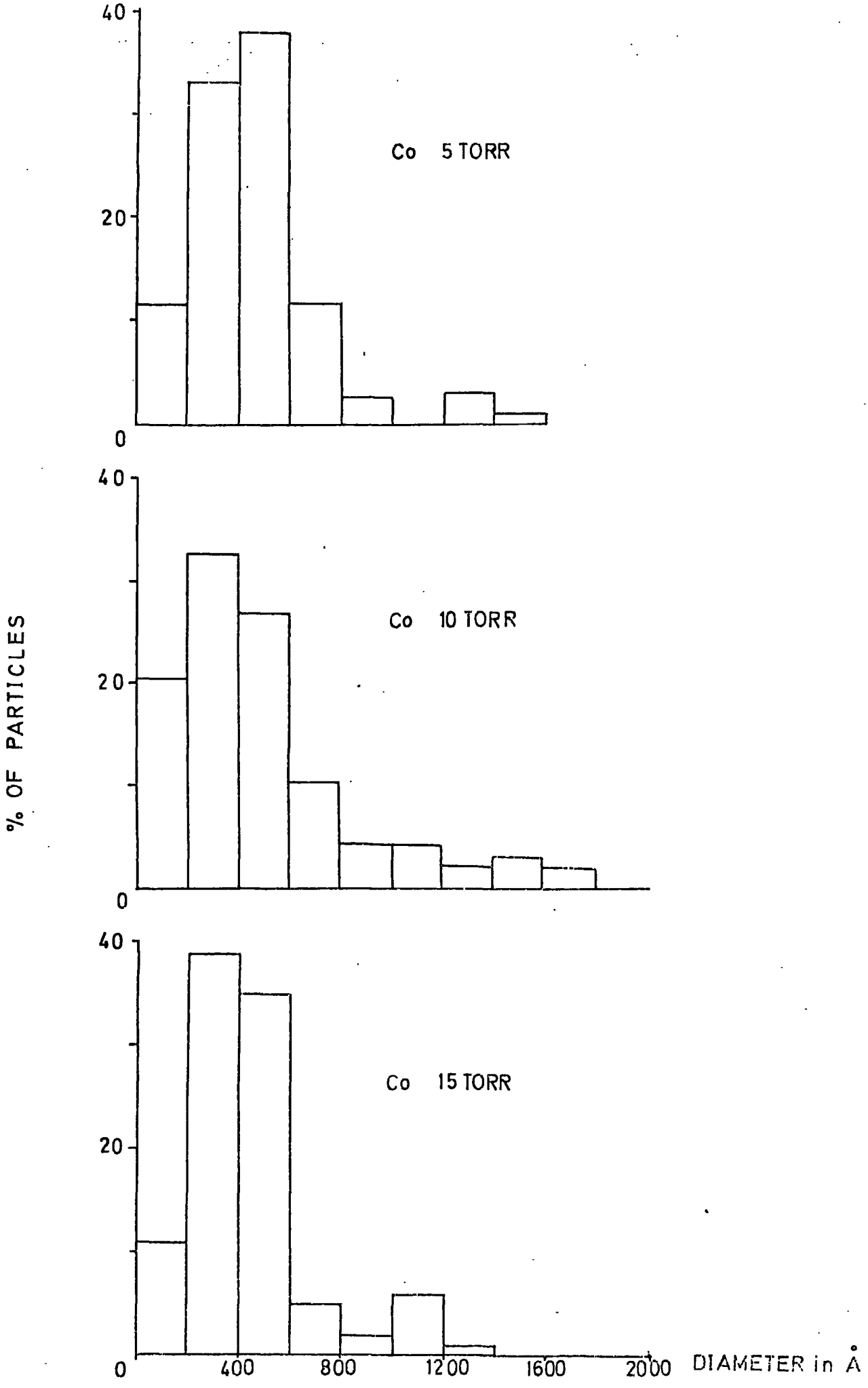

FIG. 5.2 PARTICLE SIZE DISTRIBUTIONS

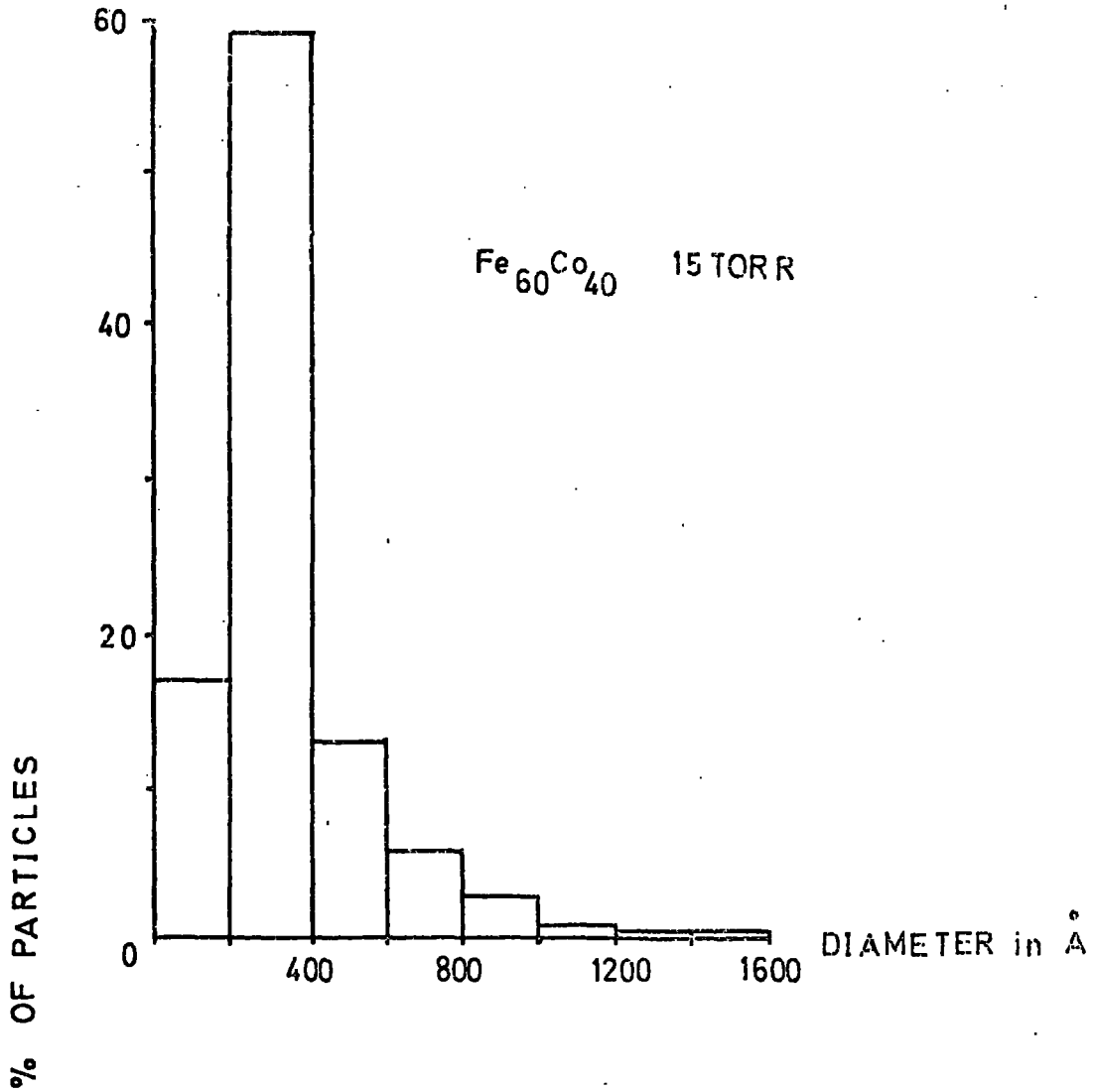

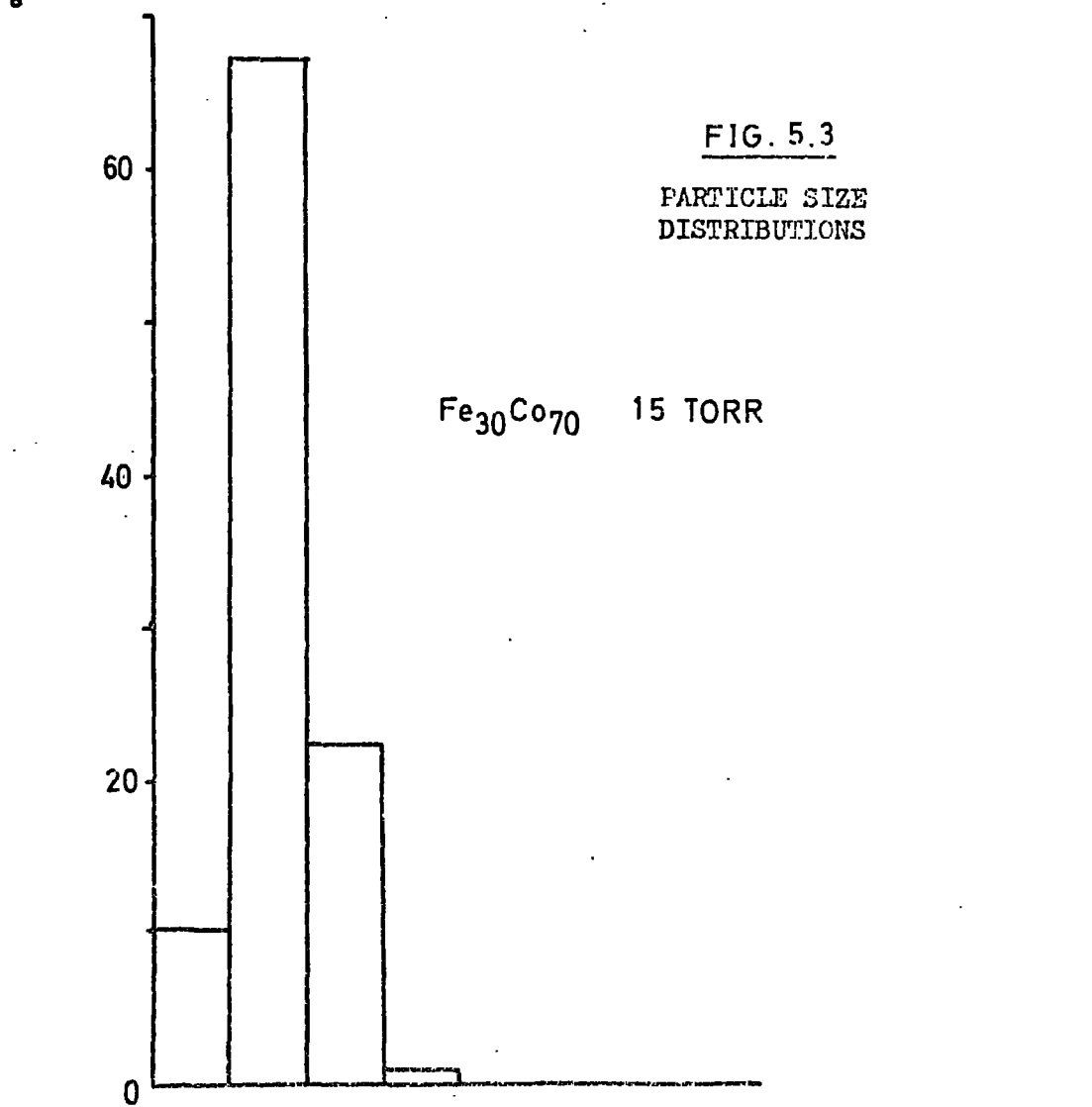

FIG. 5.3

PARTICLE SIZE DISTRIBUTIONS

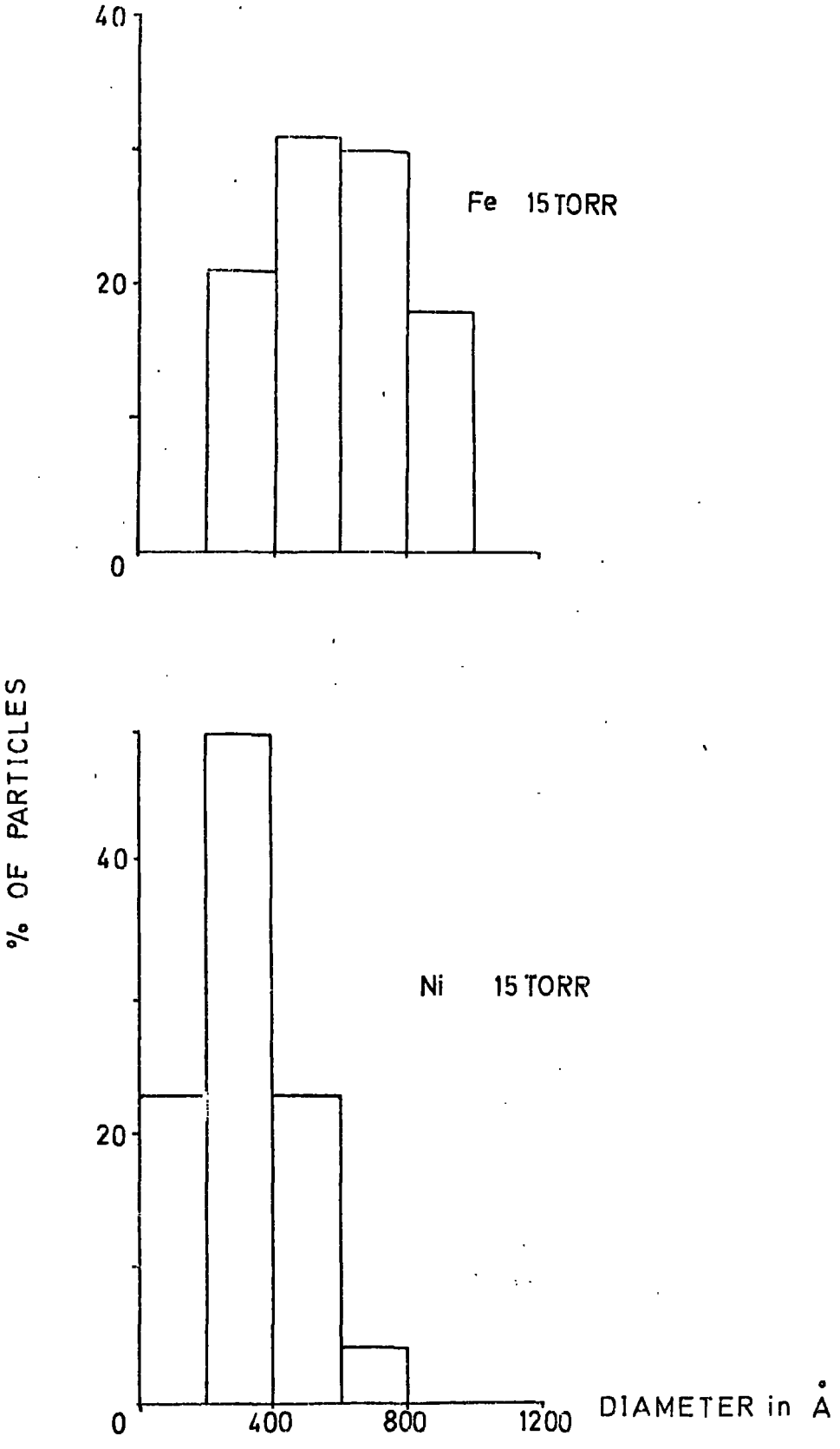

FIG. 5.4

PARTICLE SIZE DISTRIBUTIONS

observed data.

Table 5.6 gives further information concerning the maximum and minimum diameters in addition to the mean diameter for each particle. It would seem that as far as cobalt is concerned, evaporation pressures between 5 and 15 Torr have little effect on the particle size. For all the particles produced at 15 Torr, the maximum observed diameter is not more than 1500Å and the minimum not less than about 80Å. For each sample, approximately 200 particles were measured. This gives a standard error of the mean of about 5% at the most.

The magnetic implications of the above results are discussed in the next Chapter.

IRON 'd' VALUES IN Å

THIS WORK		FROM ASTM POWDER FILE INDEX			
Sample	Intensity	Fe	I/I_o	γFe_2O_3	Fe_3O_4
2.928	V.V.W.			2.950	2.966
2.508	V.W.			2.521	2.530
2.367	V.V.W.				2.419
2.017	V.S.	2.027	100	2.089	2.096
				1.702	1.712
				1.608	1.614
1.432	W.	1.433	19		1.483
1.168	M.	1.170	30		
1.013	M/W	1.013	9		
0.906	M.	0.906	12		
		0.827	6		

V = VERY, W = WEAK, M = MEDIUM, S = STRONG

TABLE 5.1

COBALT 'd' VALUES IN Å

THIS WORK		FROM ASTM POWDER FILE INDEX				
Sample	Intensity	f.c.c.Co	I/I_o	h.c.p.Co	I/I_o	CoO
						2.460
				2.165	20	2.130
2.041	S.	2.047	100	2.023	60	
				1.910	100	
1.767	M.	1.772	40			
						1.506
						1.285
1.250	M.	1.253	25	1.252	80	
				1.149	80	
				1.083	20	
1.068	M.	1.069	30	1.066	80	1.065
				1.047	60	
1.022	M/W	1.023	12	1.015	20	
						0.977
						0.953

W - WEAK, M - MEDIUM, S = STRONG

TABLE 5.2

NICKEL 'd' VALUES IN Å

THIS WORK		FROM ASTM POWDER FILE INDEX		
Sample	Intensity	Ni	I/I_o	Ni_2O_3
				3.23
				2.80
				2.30
2.033	V.V.S.	2.031	100	
2.014	V.W.			2.02
1.753	M/S	1.762	42	1.77
				1.62
				1.40
1.241	M/S	1.246	21	
1.115	V.V.W.			1.11
1.0609	M/S	1.0624	20	
1.0140	M.	1.0172	7	
		0.8810		
		0.8084		
		0.7880		

V = VERY, W = WEAK, M = MEDIUM, S = STRONG

TABLE 5.3

SAMPLE	STRUCTURE	OBSERVED a_o IN Å $\pm$ 0.002	STANDARD a_o IN Å *
Fe	B.C.C.	2.861	2.8601
$Fe_{80}Co_{20}$	B.C.C.	2.858	2.8607
$Fe_{60}Co_{40}$	B.C.C.	2.859	2.8542
$Fe_{30}Co_{70}$	B.C.C.	2.836	2.8384
Co	F.C.C.	3.537	3.5370
Ni	F.C.C.	3.514	3.5166

* VALUES TAKEN FROM "HANDBOOK OF LATTICE SPACINGS" (5)

TABLE 5.4

LATTICE PARAMETER FOR DIFFERENT SAMPLES

IRON + OXIDE 'd' VALUES IN Å

THIS WORK		FROM ASTM POWDER FILE INDEX			
Sample	Intensity	Fe	I/I_o	γ-Fe_2O_3	Fe_3O_4
2.931	M.			2.950	2.966
2.509	M.			2.521	2.530
2.368	V.W.				2.419
2.027	V.S.	2.027	100	2.089	2.096
1.705	M/W			1.702	1.712
1.621	V.W.			1.608	1.614
1.480	M/W				1.483
1.433	M.	1.433	19		
1.170	S.	1.170	30		
1.015	M.	1.013	9		
		0.906	12		
		0.827	6		

V = VERY, W = WEAK, M = MEDIUM, S = STRONG

TABLE 5.5

PARTICLE SIZES

SAMPLE	PRESSURE IN TORR	MAX. DIA. IN Å	MIN. DIA. IN Å	MEAN DIA. IN Å
Co	5	1420	140	466
Co	10	1810	90	486
Co	15	1300	90	444
$Fe_{30}Co_{70}$	15	610	90	328
$Fe_{60}Co_{40}$	15	1430	150	353
Fe	15	1000	220	590
Ni	15	720	130	306

TABLE 5.6

CHAPTER 6

RESULTS AND DISCUSSIONS - 2

In this chapter, the magnetic measurements will be presented first together with comments when appropriate. In the latter half of the chapter, the overall implications will be discussed, and an attempt will be made to fit these results to a satisfactory model.

Using both the Faraday Balance Magnetometer and the Pulsed Field Magnetometer, such measurements as magnetization, coercivity and remanence have been made. Hysteresis loops have also been investigated.

6.1. SATURATION MAGNETIZATION

Initially, unfixed particulate samples were magnetized in fields of up to 10kOe. The resulting magnetization was measured using the Faraday Balance. Even in these fields, it was sometimes found impossible to saturate samples. In these cases though, the magnetization was starting to "level off". The saturation value was then found by plotting the magnetization σ, at applied field H, against $(1/H^2)$, and extrapolating to $(1/H^2 = 0)$ (1). The saturation magnetization was found for a number of samples produced at different pressures. The results are shown for four compositions in figure 6.1. The full lines represent mean values. This shows that the saturation magnetization is fairly constant over the range of evaporation pressures. The scatter about the mean is greatest for Fe and least for Co and Ni. This is thought to be due to the fact that more variable amounts of oxide are present in Fe than in Co and Ni.

The saturation magnetization of large samples of iron-cobalt

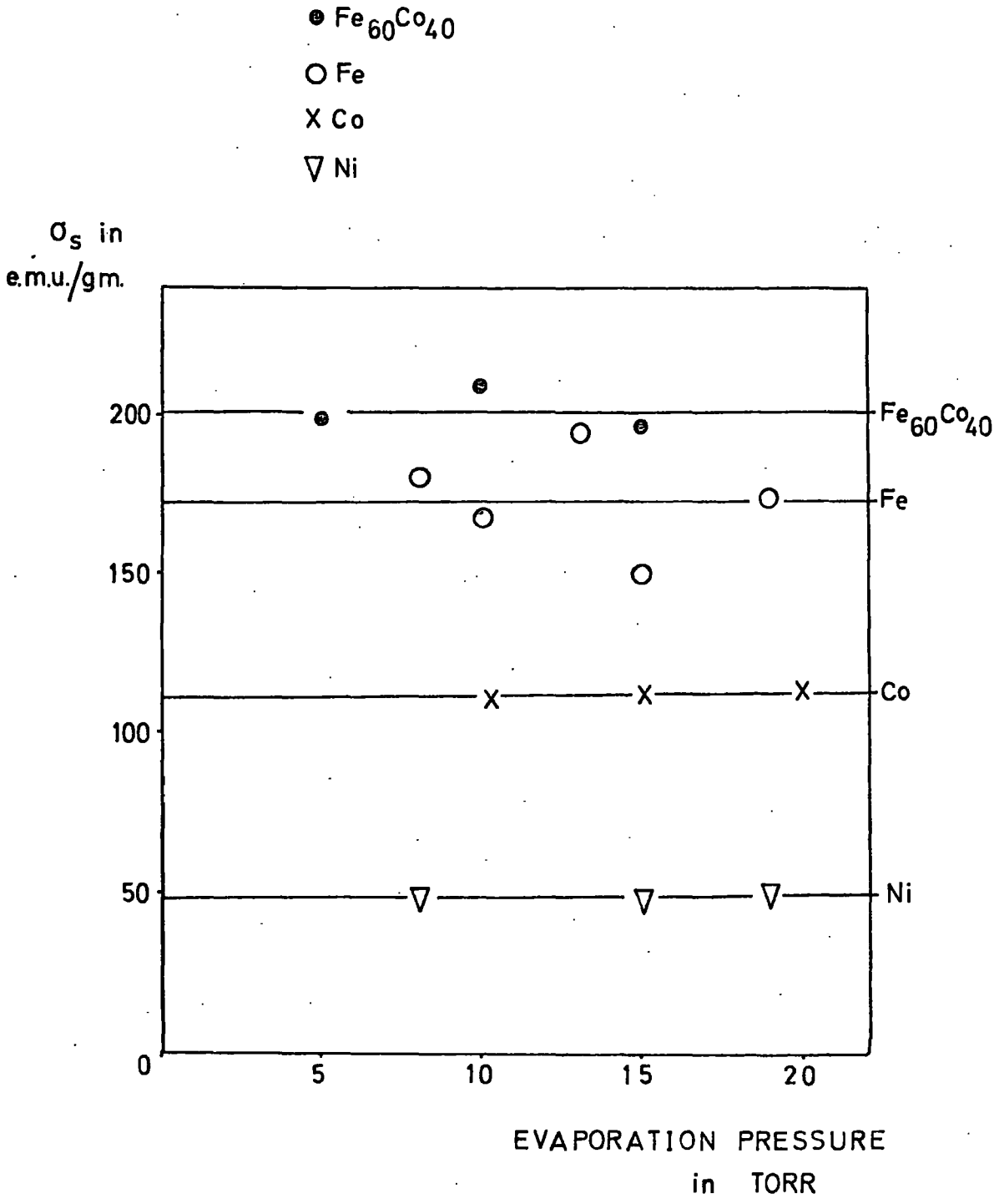

FIG. 6.1

SATURATION MAGNETIZATION AS A FUNCTION OF PRESSURE

alloys were also measured. These are compared with the mean values for the particles in figure 6.2. The results from the Faraday Balance and the Pulsed system are shown separately. The observed saturation magnetization of fine particles is somewhat lower than for large samples, although the trend with composition is similar. The values obtained by the Faraday Balance are higher than those by the Pulsed Field system. The reliability of the latter is expected to be lower, for the reasons outlined in section 4.6.6. The uncertainty in the Faraday Balance results is about 6% compared with 12% for those using the Pulsed Field System.

The decrease in the saturation moment of fine particles compared to large samples is believed to be due to the partial oxidation of their surfaces. Iron appeared to oxidise the most, and was expected to suffer the most. However, the mean saturation value of Co is 70% whilst that of Fe is 80% of the bulk values. On reflection this does not seem unreasonable. Consider a particle consisting of a ferromagnetic core surrounded by an oxide layer. If the oxide surrounding the core is antiferromagnetic it will not contribute any additional magnetization whereas if it is ferrimagnetic it will.

In the case of cobalt, the oxide is antiferromagnetic. It can then be shown that the depth of the oxide layer is approximately 10% of the radius of the particle. In the case of iron, it was shown in the last chapter that both Fe_3O_4 and Fe_2O_3 are present. These are both ferrimagnetic at room temperature. On this basis it can be shown that the Fe results can be explained by a mixed oxide layer, the depth of which is again approximately 10% of the radius of the particle. (see APPENDIX D).

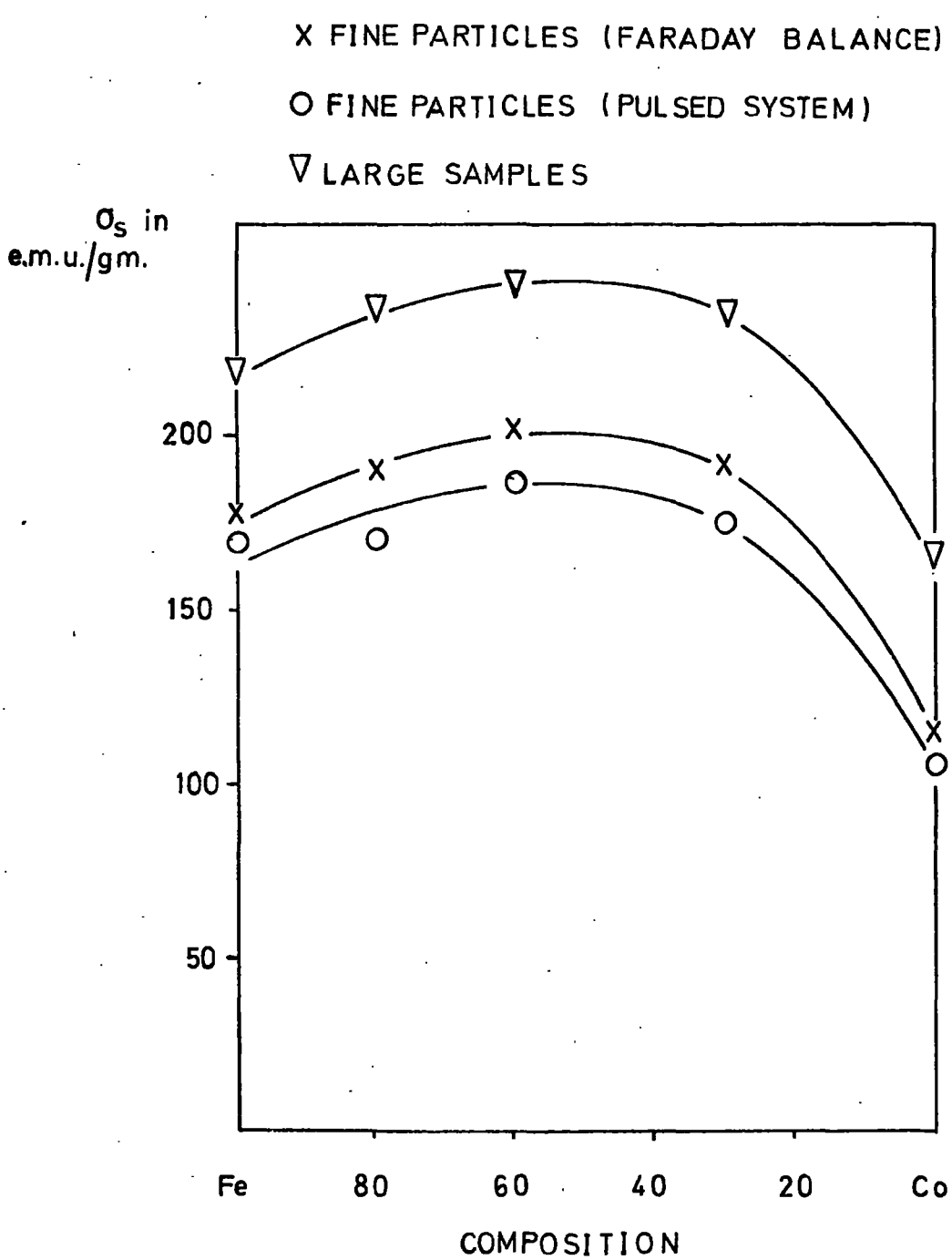

FIG. 6.2.

VARIATION OF σ_s WITH COMPOSITION

Nickel which is the least reactive with oxygen has a mean saturation value 90% of that of the bulk value. These values agree very well with those of Wada et al (2).

The magnetization of the heavily oxidised iron sample was also measured. The value obtained was in between that for γFe_2O_3 and Fe_3O_4.

For coercivity, remanence and hysteresis studies, unoriented particles were fixed in wax. Attempts were also made to align the particles before the wax had time to solidify. Subsequent results showed that this was unsuccessful, even in aligning fields of 4kOe. It is believed that this inability to saturate or align the particles is due to demagnetizing fields. Even so it was expected that chains of particles would align so that their axes lay in the field direction. If the chains are approximated to infinite cylinders, the axes are easy directions. If, however, the particles are treated as isolated spheres, the demagnetizing fields can be as high as 7kOe. These fields have no effect on the coercivity although they do affect the remanence.

6.2. COERCIVITY MEASUREMENTS

Using the Faraday Balance, coercivities of random assemblies were measured after the application of a field of 10kOe. As a check that this was in fact the maximum coercive force, use was made of the following expression (3)

$$\frac{H_{APP}}{H_c} = a_1 + a_2 H_{APP} \quad \ldots\ldots\ldots\ldots\ldots\ldots \quad (6.1)$$

where H_{APP} = Applied Field

H_c = Coercive force at field H_{APP}

a_2 = Reciprocal coercivity

a_1 = Constant

Rearranging (6.1) gives

$$a_2 = \frac{1}{H_c} - \frac{a_1}{H_{APP}}$$

Therefore as H_{APP} tends towards infinity $H_c = {}^1/a_2$

This function was plotted for different samples in figure 6.3. The values obtained were the same as those for a field of 10kOe.

The coercivity was also measured using the Pulsed Field Magnetometer, after applied fields of 38kOe. The results from both pieces of apparatus are shown in figure 6.4. It can be seen that the observed coercivities are in good agreement although the values produced by the Pulsed Field method are slightly higher than those for the Faraday Balance. This may be due to the former measurements being performed at liquid nitrogen temperature. It is difficult to assess the errors for the Pulsed system although those for the Faraday Balance are about 6%.

The coercivities of the nickel and iron oxide samples were also measured using the Faraday Balance. Nickel was found to have a coercivity of 260 Oe and the oxide coercivity of 360 Oe.

6.3. REMANENCE CURVES

The different forms of remanence that may be acquired have been explained in section 2.5. In the present work, the static remanence and the d.c. demagnetization remanence have been measured using the Faraday Balance. So that samples could be saturated, fields of 14kOe were used.

In measuring the static remanence, it was curious to find that the ratio of remanence to saturation magnetization was seldom greater than 0.25. Actual values of $I_r(\infty)/I_s$ are given

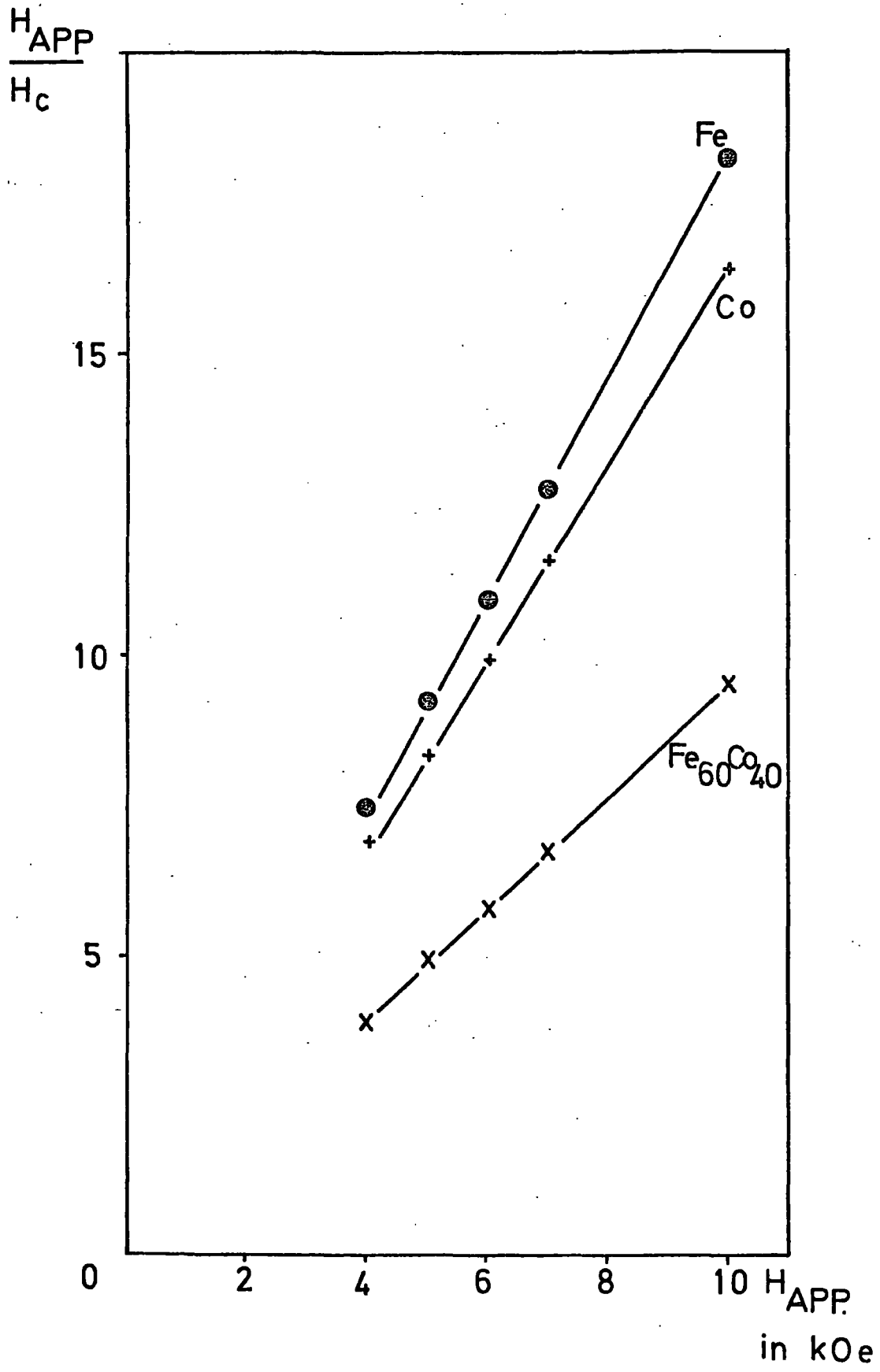

FIG. 6.3

$\frac{H_{APP}}{H_c}$ versus H_{APP}

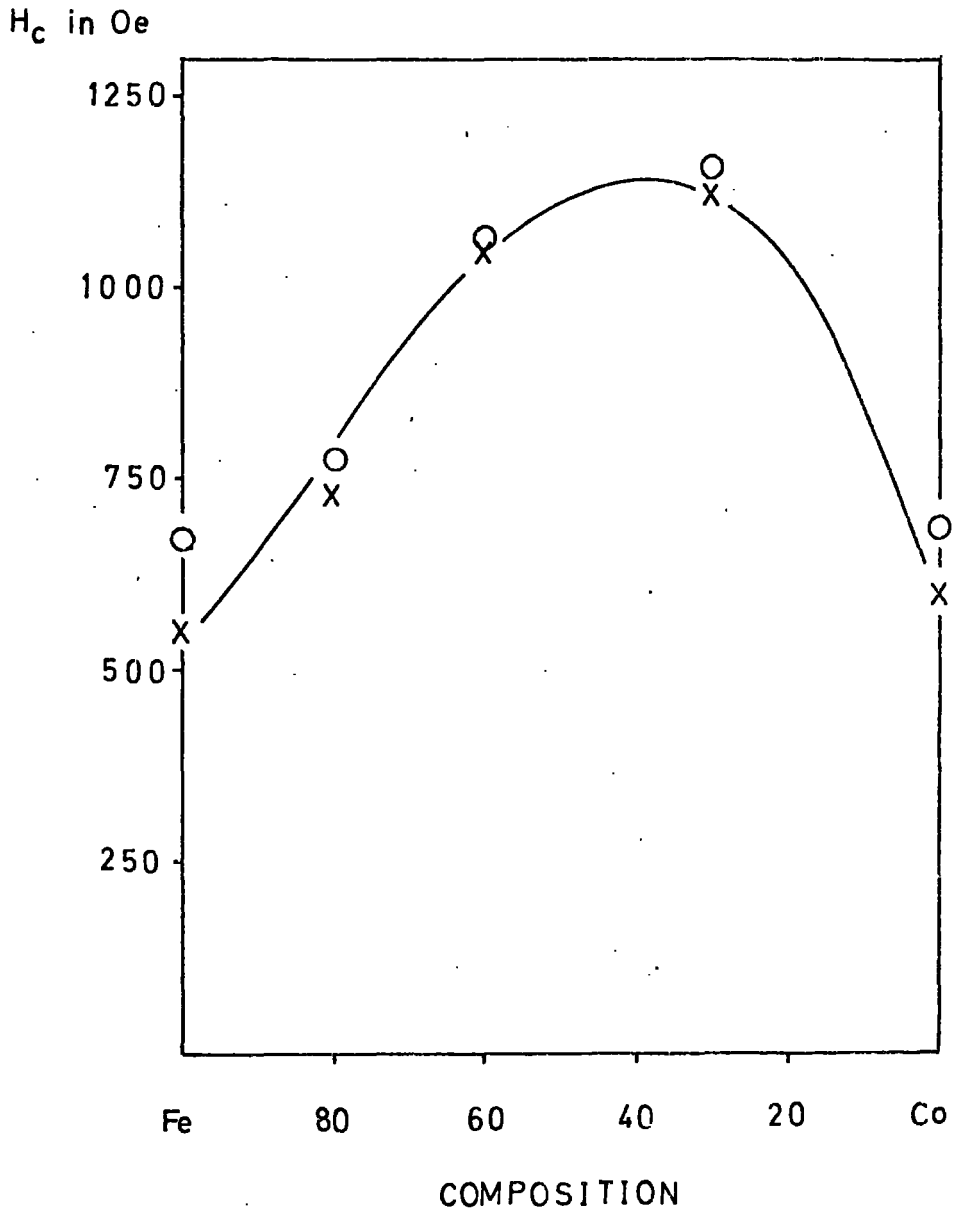

FIG. 6.4

VARIATION OF COERCIVITY
WITH COMPOSITION

later in the chapter. The results were surprising since the theoretical value for a random assembly is 0.5 (4). These values cannot be due to incoherent reversals. They may however be due to demagnetization effects or to the presence of superparamagnetic or multidomain particles.

In practice, $\sigma_r(H)$, $\sigma_D(H)$ and σ_s were measured, and not $I_r(H)$, $I_D(H)$ and I_s. This presented no problems because

$$\frac{\sigma_r(H)}{\sigma_s} = \frac{I_r(H)}{I_s}$$

also $$\frac{\sigma_r(H)}{\sigma_r(\infty)} = \frac{I_r(H)}{I_r(\infty)}$$

and $$\frac{\sigma_D(H)}{\sigma_r(\infty)} = \frac{I_D(H)}{I_r(\infty)}$$

Therefore values of σ can be transformed quite readily to fit expressions for I.

Recalling expression (2.27)

$$I_D(H) = I_r(\infty) - 2I_r(H)$$

and rearranging we obtain

$$\frac{I_r(H)}{I_r(\infty)} = \frac{1}{2}\left\{1 - \frac{I_D(H)}{I_r(\infty)}\right\} \quad \text{.....(6.2)}$$

This function is valuable because it eliminates absolute values, and permits remanence curves of different samples to be plotted simultaneously.

Figures 6.5, 6.6, and 6.7 show the remanence curves for different samples. $\frac{I_r(H)}{I_r(\infty)}$ and $\frac{I_D(H)}{I_r(\infty)}$ are plotted as functions of $|H|$. It can be seen that in most cases, fields greater than

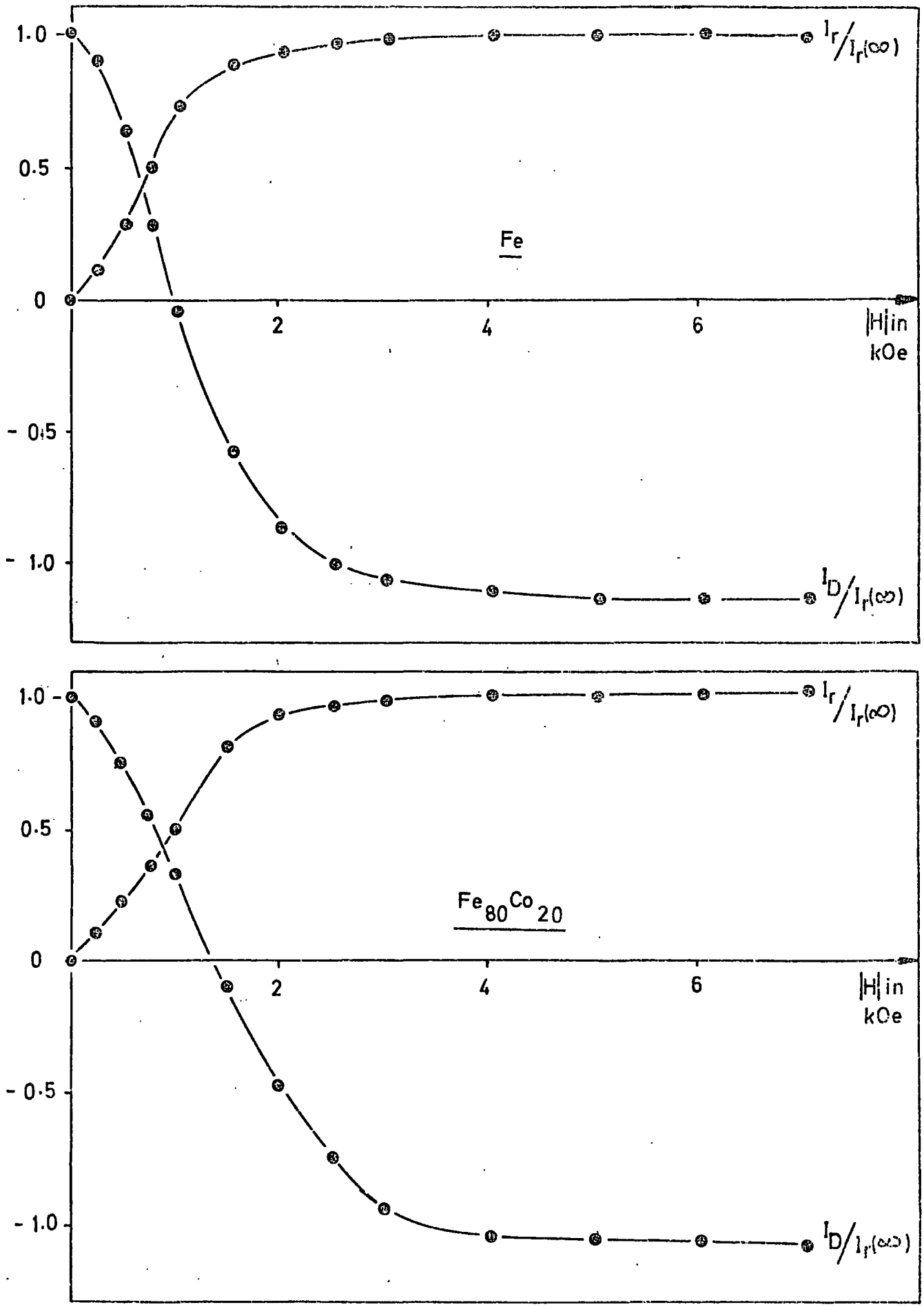

FIG. 6.5

REMANENCE CURVES FOR Fe AND $Fe_{80}Co_{20}$

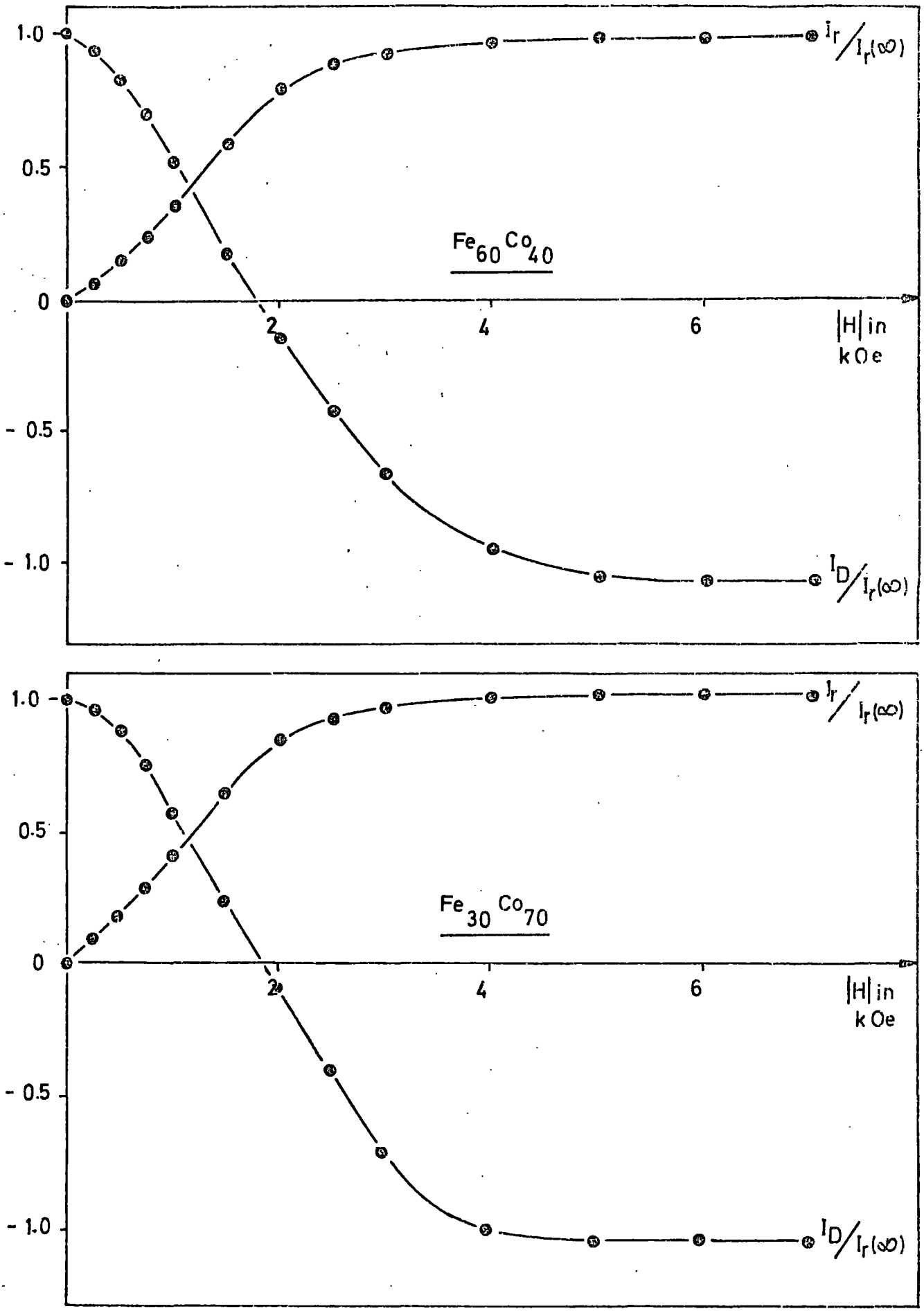

FIG. 6.6

REMANENCE CURVES FOR
$Fe_{60}Co_{40}$ AND $Fe_{30}Co_{70}$

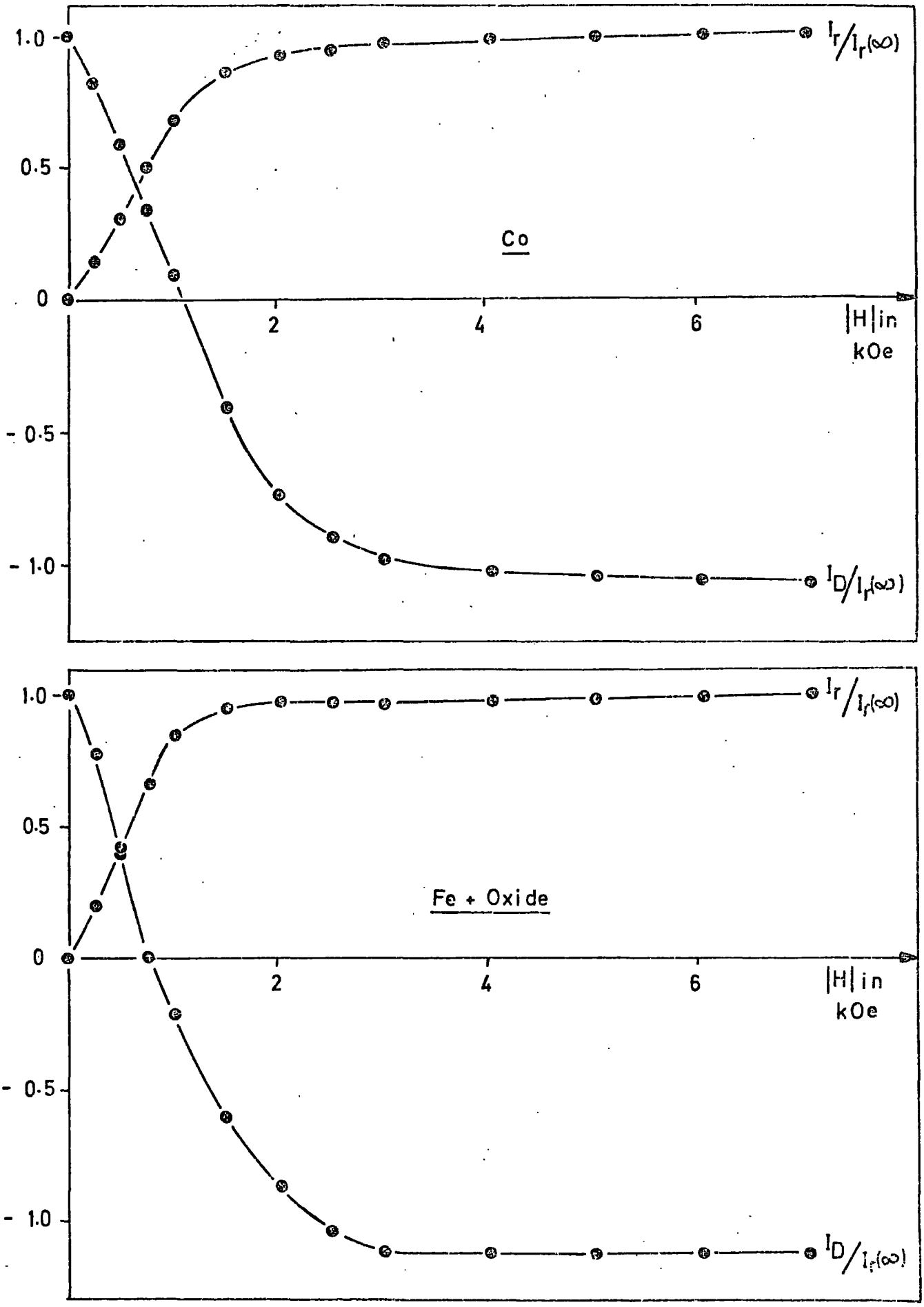

FIG. 6.7

REMANENCE CURVES FOR
Co AND Fe + Oxide

7000 Oe were required to produce saturation remanence, indicating that the samples contained particles with intrinsic coercivities as high as 7000 Oe. (Intrinsic coercivity of a particle is that coercivity the particle would exhibit if the direction of lowest magnetic anisotropy energy were parallel to the field).

From these results, the remanence coercivity can be measured, and expression (6.2) may be plotted. H_r was estimated, and plotted as a function of composition in figure 6.8. The trend is the same as for the coercivity (see fig. 6.4). For a random assembly of uniaxial single domain particles of uniform anisotropy the ratio H_r/H_c should be 1.09 (5). Observed values are plotted against composition in figure 6.9. It can be seen that the values are fairly constant with a mean value of 1.75. These increased values are attributed to anisotropy variations of the compacts and also possibly to particle interactions. Gaunt (6) found for a simple distribution of anisotropies a ratio of 2.02. Higher values still may be due to superparamagnetism.

Expression (6.2) is plotted in figure 6.10. It would appear that there are two linear portions to the graph. Originally this was thought to be due to the effects of cubic magnetocrystalline anisotropy. To find the extent of this anisotropy, the initial susceptibility of iron and cobalt was measured as suggested by Wohlfarth (7). This was found to be temperature independent, showing that shape anisotropy must be dominant. The shape anisotropy arises mainly from the chaining of the particles, and to a lesser extent from the particles themselves since these are almost spherical. If the chains have formed as a result of dipole-dipole attraction, then they will exhibit a uniaxial

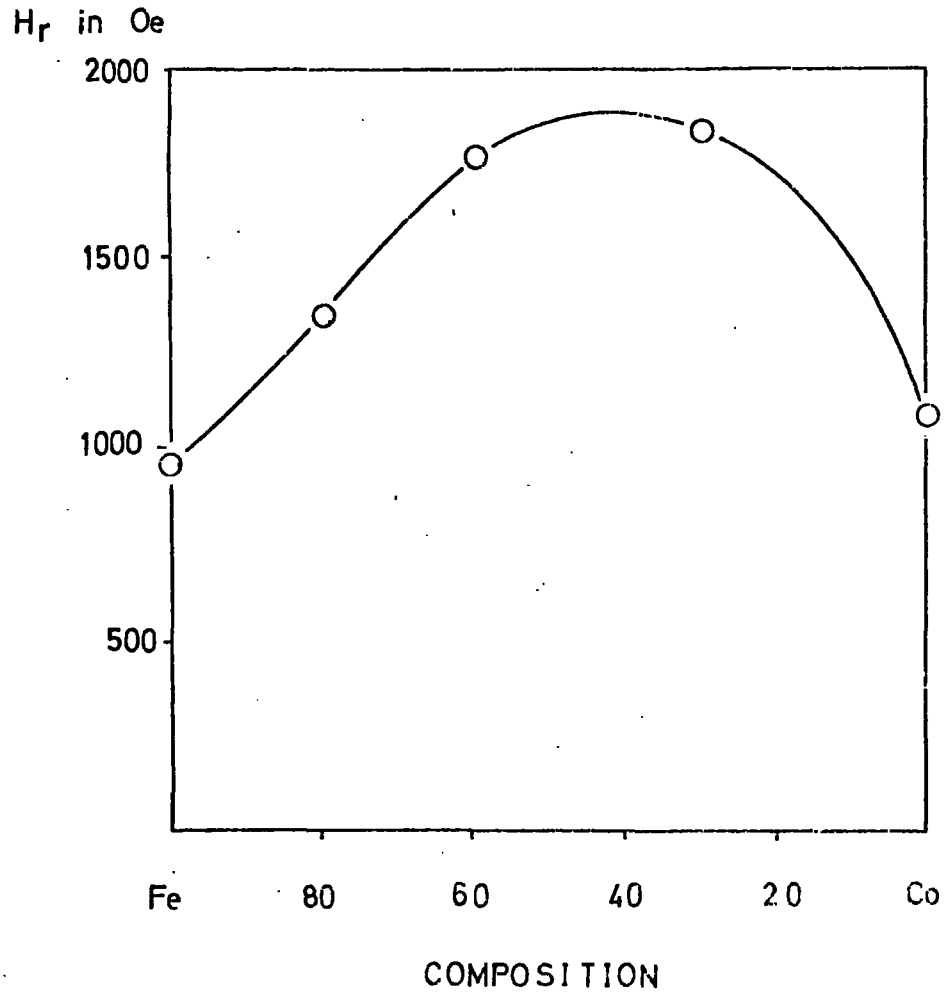

FIG. 6.8

VARIATION OF THE REMANENCE
COERCIVITY WITH COMPOSITION

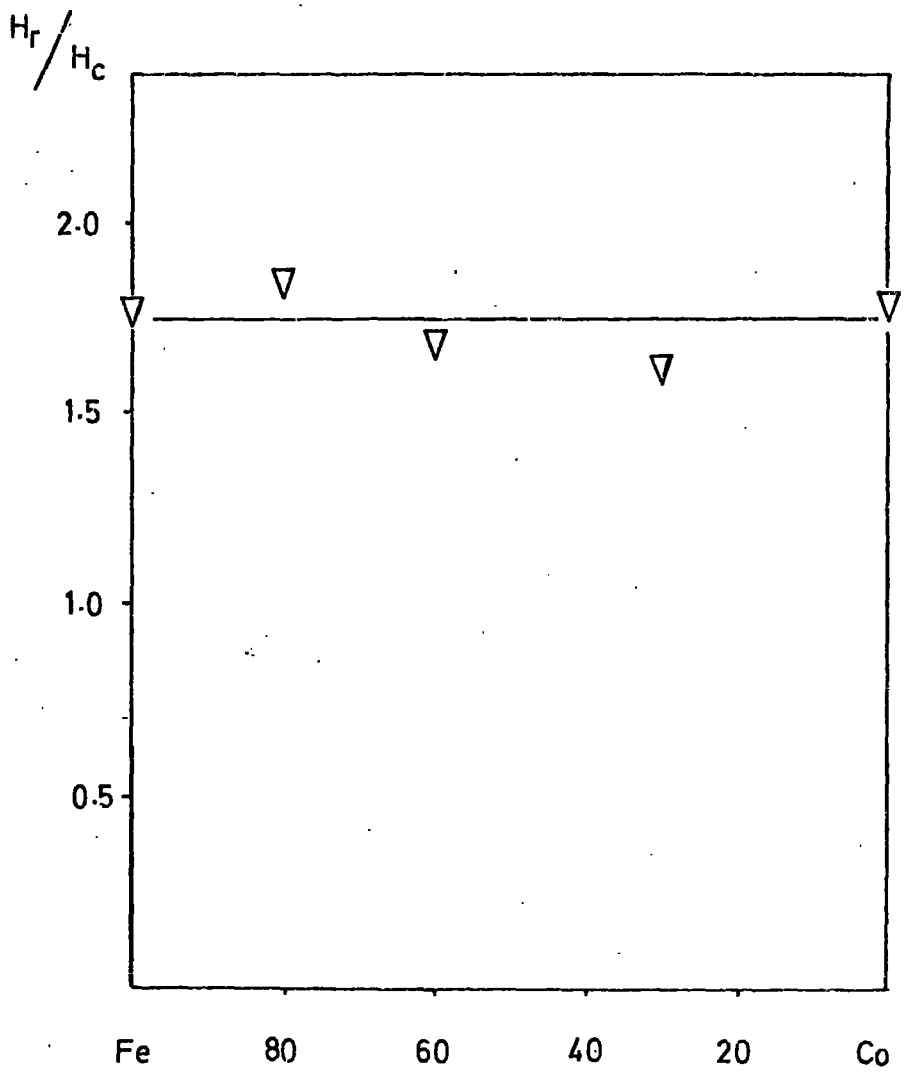

FIG. 6.9

VARIATION OF H_r/H_c WITH COMPOSITION

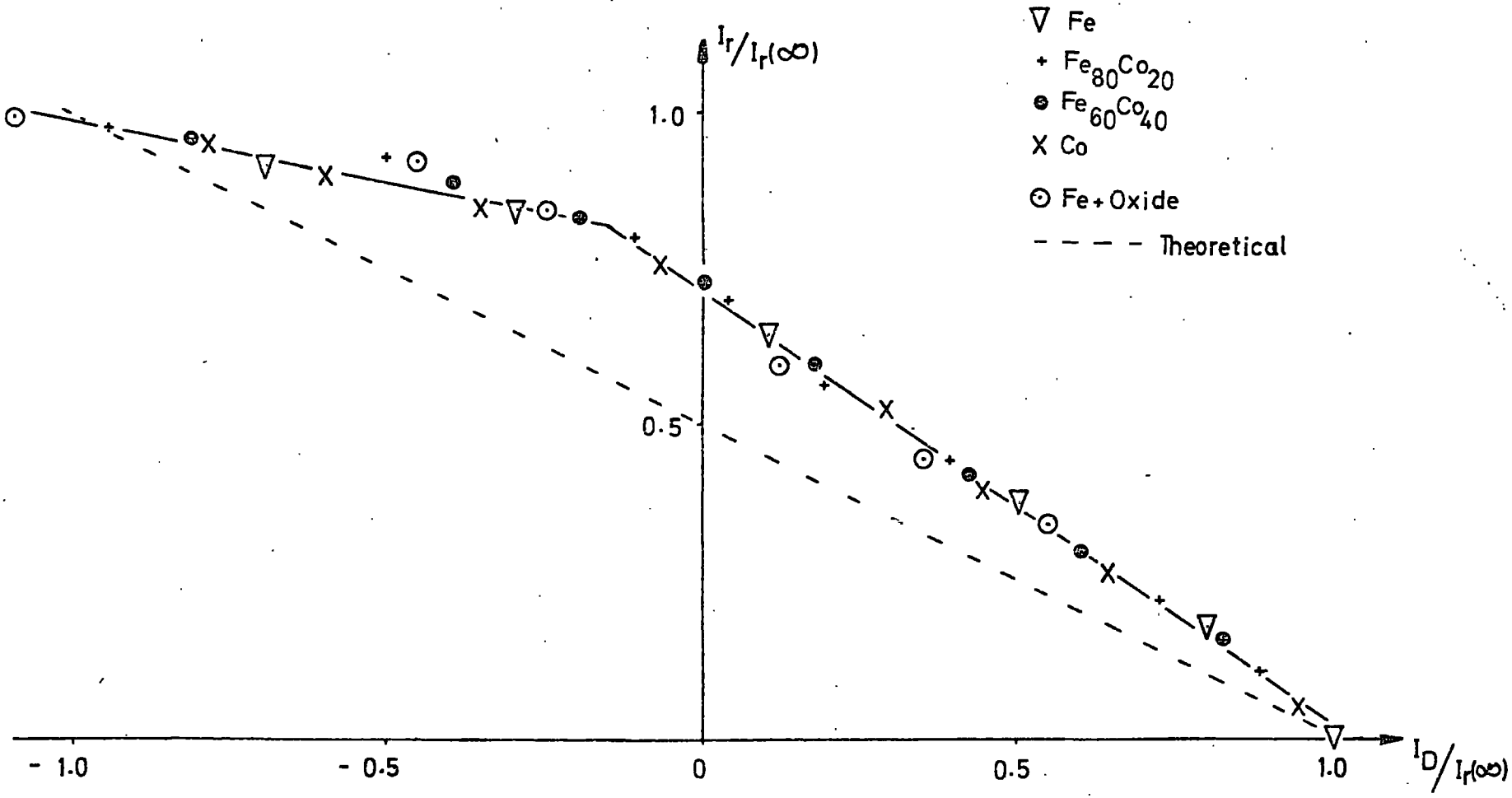

FIG. 6.10

STATIC REMANENCE VERSUS D.C. DEMAGNETIZATION REMANENCE FOR DIFFERENT SAMPLES

shape anisotropy along the axis of the chain.

However the two linear portions may not be genuine. This has been suggested by Wohlfarth (8) who thinks the deviation from the theoretical line may be due wholly to interactions. If this is so, it is most probably due to interactions between particles in a chain rather than interactions between chains, because the volumetric packing fraction has been estimated as 0.06 ≡ 6%.

6.4. HYSTERESIS LOOPS

The theoretical hysteresis loop for a random assembly of particles was first predicted by Stoner and Wohlfarth. This is shown in figure 6.11. The remanence to saturation ratio is 0.5 and the coercivity has a value of h = 0.479 where

$$h = \frac{HI_s}{2K}$$

In the present work, samples were not taken to saturation with the Faraday Balance, and so only minor loops were obtained. Using the Pulsed Field system, much higher fields could be generated, thus saturating the samples. For Co, a field of about 13.5 kOe was required to attain saturation. Hysteresis loops for different samples are shown in figures 6.12 to 6.16 inclusive. For the Pulsed Field loops, only the low field magnetization is shown. All the loops show the difficulty to saturate in low fields. They also show that the remanence is much lower than is to be expected for a random assembly of particles.

6.5. DISCUSSION

These results can be used in an attempt to explain the magnetization changes taking place in the particles. Before doing so, the results of the last chapter will be reconsidered.

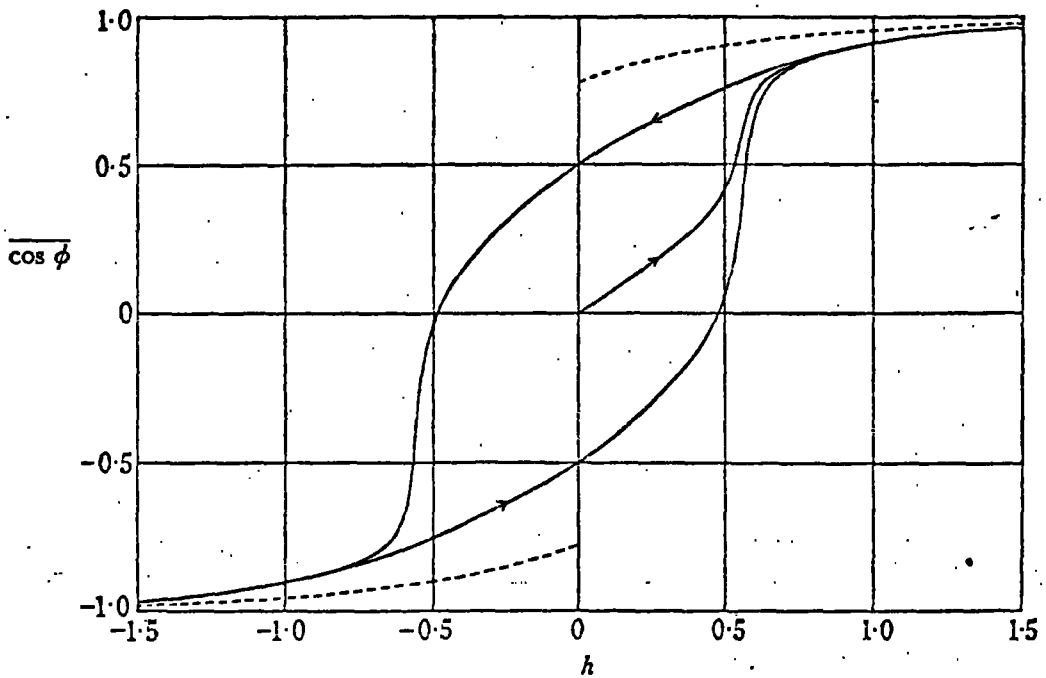

FIGURE 6.11 Magnetization curves for prolate (full curves) and oblate (broken curves) spheroids orientated at random. The curves refer to similar prolate (or oblate) spheroids orientated at random. $\overline{\cos\phi}$ is proportional to the mean resolved magnetization per spheroid in the positive field direction, or to the resultant magnetization in this direction of the assembly. $H = (|D_a - D_b|)\, I_0 h$.

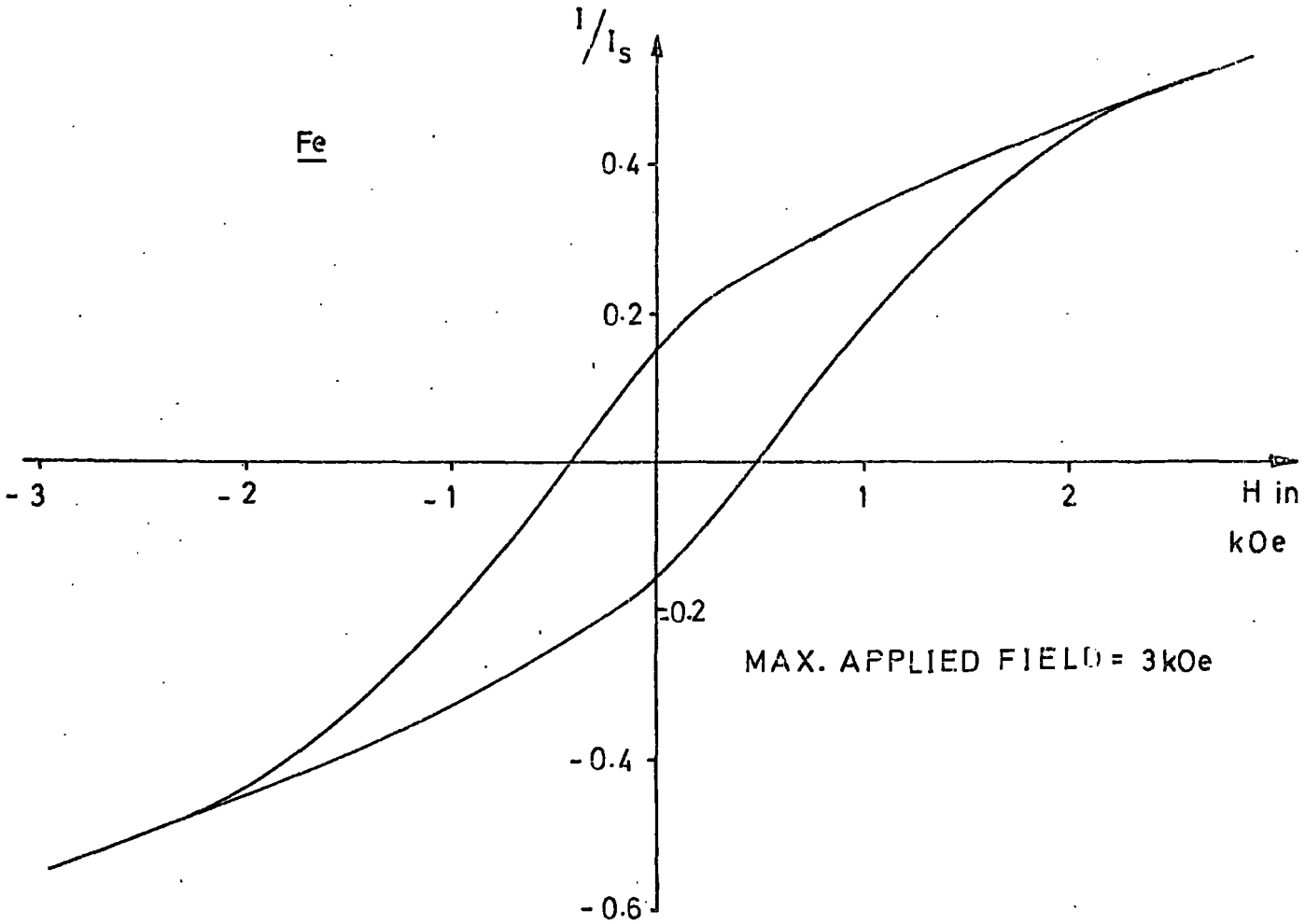

FIG. 6.12

HYSTERESIS LOOP FOR IRON

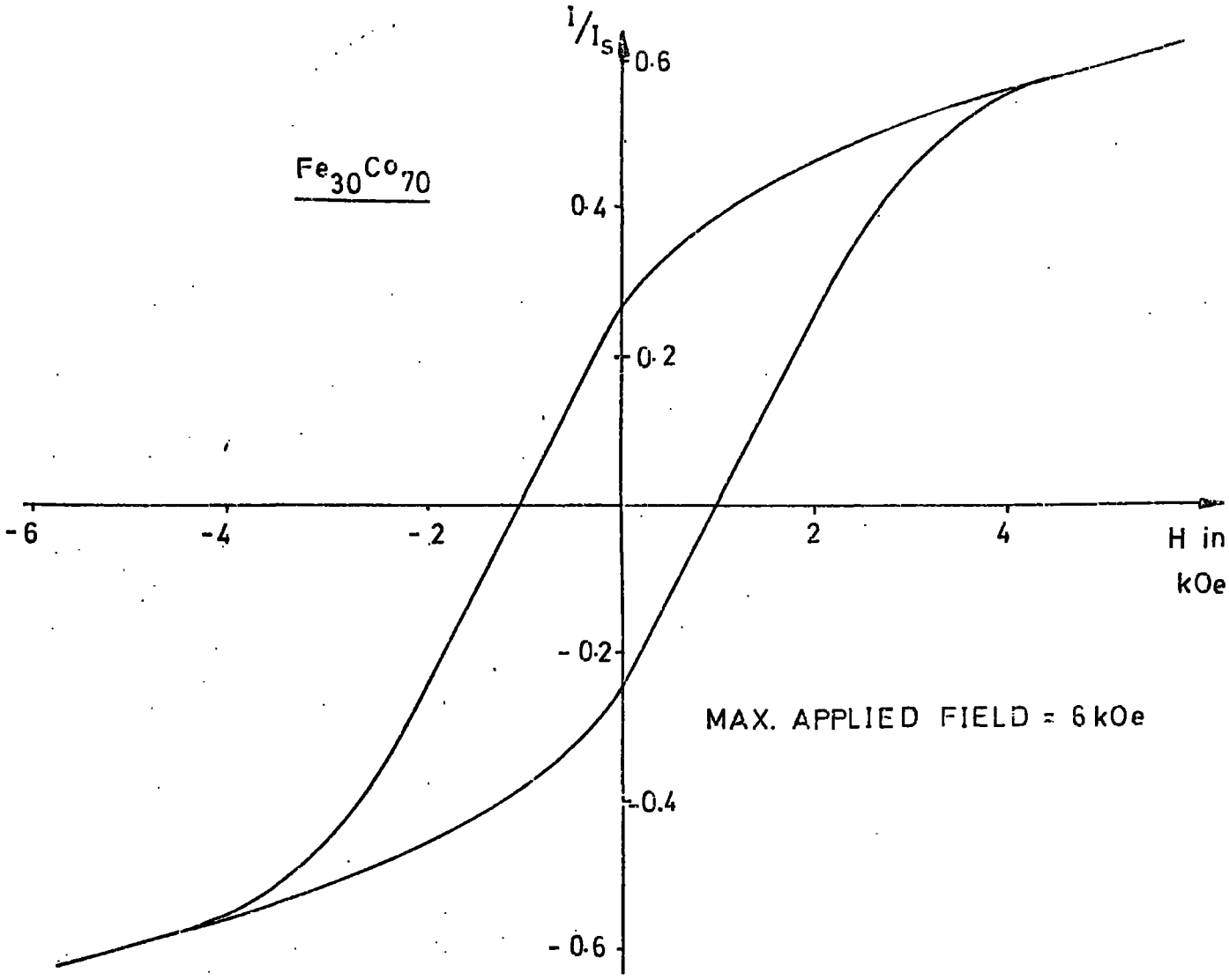

FIG. 6.13

HYSTERESIS LOOP FOR $Fe_{30}Co_{70}$

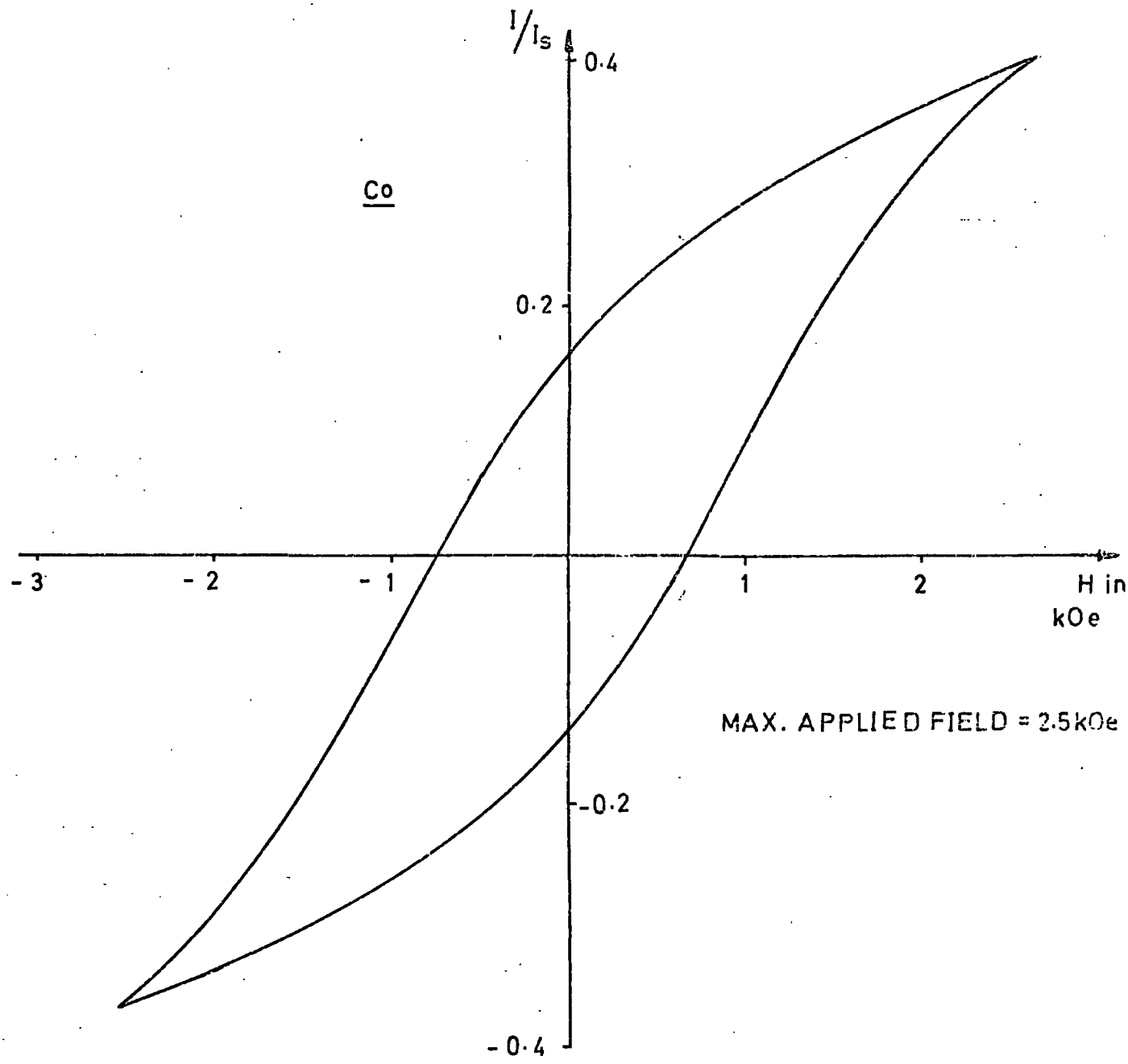

FIG. 6.14

HYSTERESIS LOOP FOR COBALT

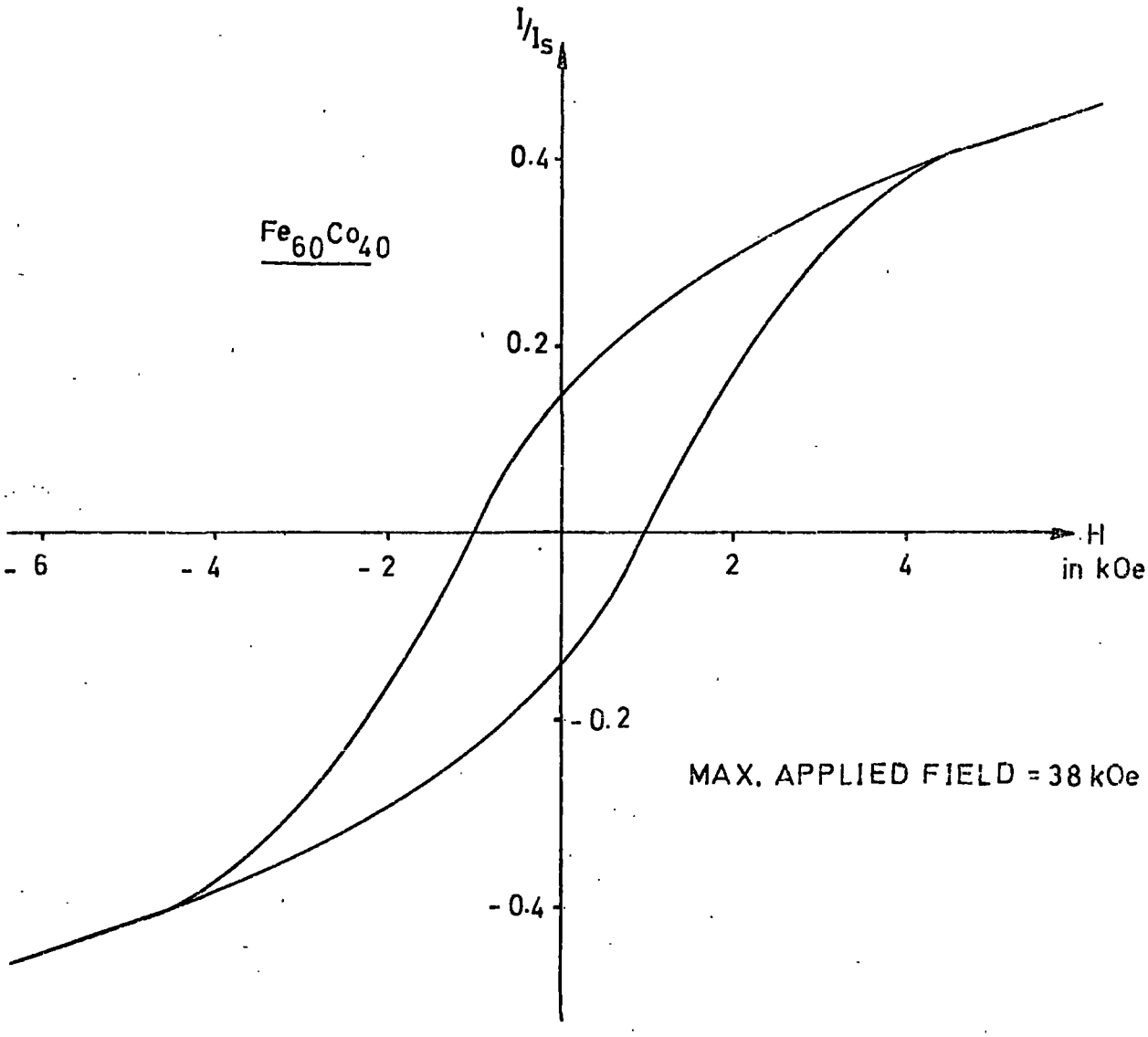

FIG. 6.15

HYSTERESIS LOOP FOR $Fe_{60}Co_{40}$

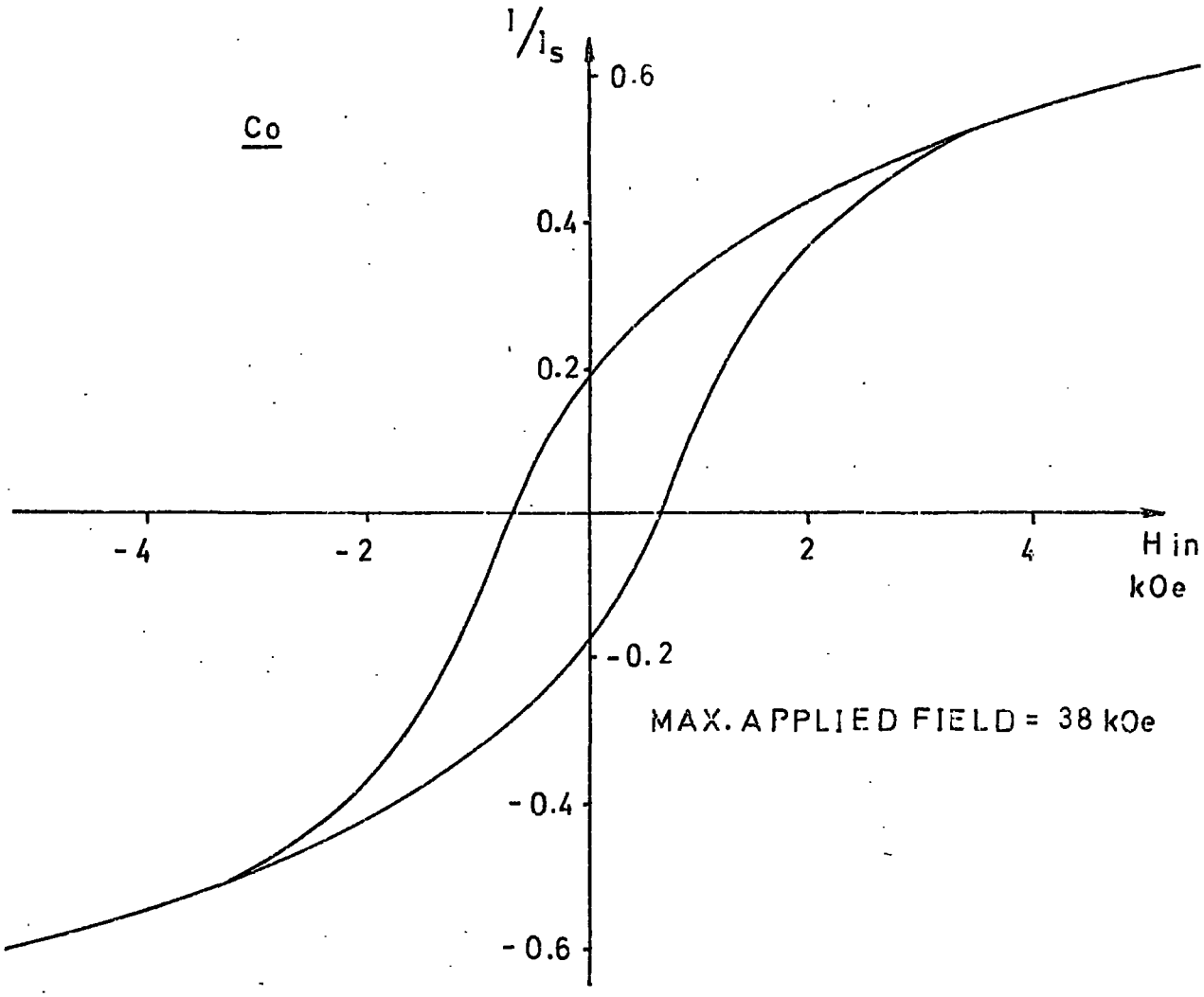

FIG. 6.16

HYSTERESIS LOOP FOR COBALT

All the particles produced have a cubic structure of one form or another. These particles are believed to be single crystals. Since the individual particles are spherical, it may be expected that only magnetocrystalline anisotropy should be present. However, because the particles chain together, a uniaxial shape anisotropy will be present. This is believed to be the dominant anisotropy. The formation of chains is thought to be due to the magnetic attraction of the particles. If the particles are considered as dipoles, opposite poles will attract thus forming a chain, the easy direction of which will be along the axis of the chain.

As far as the reversal mechanism is concerned, there would appear to be three possibilities.

1) Coherent rotation
2) Fanning in a chain of spheres
3) Curling.

For curling, a chain of spheres is approximated to an infinite cylinder. This seems unlikely since the spheres in a chain are not uniform in size, and the chain goes to zero diameter at the point of interparticle contact.

Although coherent reversals may be present, the visual evidence of the electron micrographs would seem to point towards the fanning mechanism.

Perhaps the most important factor governing the reversal processes is the particle size range. That is whether or not all the particles are within the single domain range. It will be recalled that for a mixture of shape and magnetocrystalline anisotropies, the upper limit for the radius of a single domain particle is given by expression (2.22).

$$b_c = \left\{ \frac{2\pi kA}{D_b I_s^2} \right\}^{\frac{1}{2}}$$

Values of b_c are only approximate since A can vary by a factor of 4. Assuming $A = 5 \times 10^{-6}$ estimates of the critical diameter are given in Table 6.1.

At the lower end of the scale,

$$b_s = \left\{ \frac{75kT}{4\pi K} \right\}^{\frac{1}{3}}$$

This time k is Boltzmann's constant and T the temperature. As a rough estimate T was taken as $300^{o}K$ and $K_1 = 4 \times 10^6$ erg/c.c. The size differs little from sample to sample, and is approximately 150A^{o} for an infinite cylinder and 120A^{o} for a sphere. (These values are for the diameter, not the radius).

Although not all the particles lie in this range, a large proportion do so. Therefore many of the particles should be single domain in nature. Few of the particles are small enough to be superparamagnetic, therefore this type of behaviour is expected to be "swamped". It will be shown later that the controlling factor is the volume of particles of a particular kind and not the number which influences the magnetic properties.

A summary of the magnetic results is given in Table 6.2. It can be seen that the attempt to align the particles had little effect on the remanence to saturation ratio or on the coercivity. Also shown are the results for the nickel and the heavily oxidised iron samples. For the latter, both the coercivity and the magnetization are much lower than for pure iron. This is to be expected if the sample is composed primarily of γFe_2O_3 and Fe_3O_4.

Assuming different mechanisms to be present, values of

Sample	Upper Critical Diameter in Å	Lower Critical Diameter in Å for a sphere	Lower Critical Diameter in Å for a cylinder
Fe	470	160	70
$Fe_{80}Co_{20}$	420	160	70
$Fe_{60}Co_{40}$	390	∞	60
$Fe_{30}Co_{70}$	400	170	60
Co	660	280	90
Ni	1460	340	150

TABLE 6.1

CRITICAL SIZE RANGE

Sample	σ_s Particles	σ_s Bulk	I_s Particles	I_s Bulk	σ_r/σ_s F.B.M.	σ_r/σ_s P.F.M.	H_c in Oe F.B.M.	H_c in Oe P.F.M.	H_r in Oe	H_r/H_c	σ_r/σ_s Aligned F.B.M.	H_c Aligned F.B.M.
Fe	175	218	1370	1719	0.17	0.15	550	670	975	1.78	0.18	550
$Fe_{80}Co_{20}$	189	236	1520	1900	0.17	0.15	730	780	1350	1.85	0.17	740
$Fe_{60}Co_{40}$	201	244	1670	2030	0.23	0.16	1050	1070	1780	1.70	-	-
$Fe_{30}Co_{70}$	190	235	1610	2000	0.26	0.18	1120	1160	1830	1.63	-	-
Co	112	161	980	1400	0.20	0.18	610	690	1100	1.80	0.23	640
Ni	49	54	440	489	0.27	-	260	-	-	-	0.32	270
Mixed Oxide	77	-	-	-	0.16	0.19	360	670	750	2.08	0.17	370

σ_s is measured in e.m.u/gm.

I_s is measured in erg Oe^{-1} cm^{-3}.

F.B.M. = Faraday Balance Magnetometer.

P.F.M. = Pulsed Field Magnetometer.

TABLE 6.2

MAGNETIC MEASUREMENTS

coercivity due to each process have been calculated. These are shown for different samples in Table 6.3. In each case the assembly of particles has been assumed to be random. No single model satisfies the observed values, although in some cases, the trends over the composition range are similar. It would seem therefore that a hybrid model is required to explain the experimental results.

Bean has investigated the hysteresis loops of mixtures of ferromagnetic micropowders (9). He calculated the resulting loops by adding the magnetizations of the components for a given field, weighting them in proportion to their volume fraction of the total. The magnetization I of a mixture of N types of particles in a field H can be expressed by

$$I(H) = \sum_{n=1}^{N} I_n(H)\, f_n \Big/ \sum_{n=1}^{N} f_n$$

where f_n is the volume fraction of the nth constituent and $I_n(H)$ is its magnetization in field H. Bean used this method for non-interacting particles, assuming that the constituents were superparamagnetic, single domain and multidomain particles.

A similar method has been adopted in the present work, to try to explain the hysteresis loops for Co and $Fe_{60}Co_{40}$. These have been chosen because the samples were saturated in each case. In calculating the loops, various assumptions were made based upon earlier results. Since there are a small number of superparamagnetic particles, the volume contribution of these is assumed to be negligible. In addition to the single domain and possibly multidomain particles, it is assumed that particles with an incoherent reversal mechanism are also present. From the electron micrographs, it would seem likely that fanning would be such a

Sample	Coherent		Incoherent		Observed Coercivity in Oe
	Cubic Crystalline Anisotropy $0.64K_1/I_s$	Uniaxial Shape Anisotropy $0.958\pi I_s$	Rotation in a Chain $0.72\pi I_s$	Symmetric Fanning $0.54\pi I_s$	
Fe	224	4120	3100	2320	550
$Fe_{80}Co_{20}$	185	4580	3460	2580	730
$Fe_{60}Co_{40}$	0	5020	3780	2830	1050
$Fe_{30}Co_{70}$	171	4840	3640	2730	1120
Co	555	2940	2200	1660	610
Ni	66	1330	985	750	260
Mixed Oxide	-	1270-1450	950-1090	710-810	360

TABLE 6.3

THEORETICAL AND OBSERVED VALUES OF COERCIVITY

process. In particular, the symmetric fanning mechanism in randomly oriented infinite chains has been assumed to be operative. Magnetization values for this process have been taken from Table II of Jacobs and Bean's paper on fanning in a chain of spheres (10). The magnetization values of coherent rotation have been taken from Table 6 of Stoner and Wohlfarth's paper (4). In each case though the field parameter is different. For this reason a new field parameter H' has been introduced where

$$H' = \frac{Ha^3}{\mu 2K_n} \sim \frac{2.5H}{\pi I_s}$$ for an infinite chain of touching particles

and $$H' = \frac{5Kh}{\pi I_s^2}$$

To simplify the multidomain contribution, it has been assumed that the magnetization of such a particle varies linearly between two field values $\pm H'_A$ as shown in figure 6.17. At other field values the magnetization is saturated. This is somewhat oversimplified as there will be some rounding near saturation. It is believed that the difficulty to saturate samples is due to this multidomain component saturating only at high fields. From the Pulsed Field experiments, the samples were found to saturate at about 13kOe. This then gives the multidomain magnetization in a given field.

The magnetization due to the fanning process can be readily found since this depends only on the saturation magnetization (10). The coherent contribution depends on the anisotropy constant as well as the saturation magnetization. Therefore a value for K must be chosen to start with. By taking

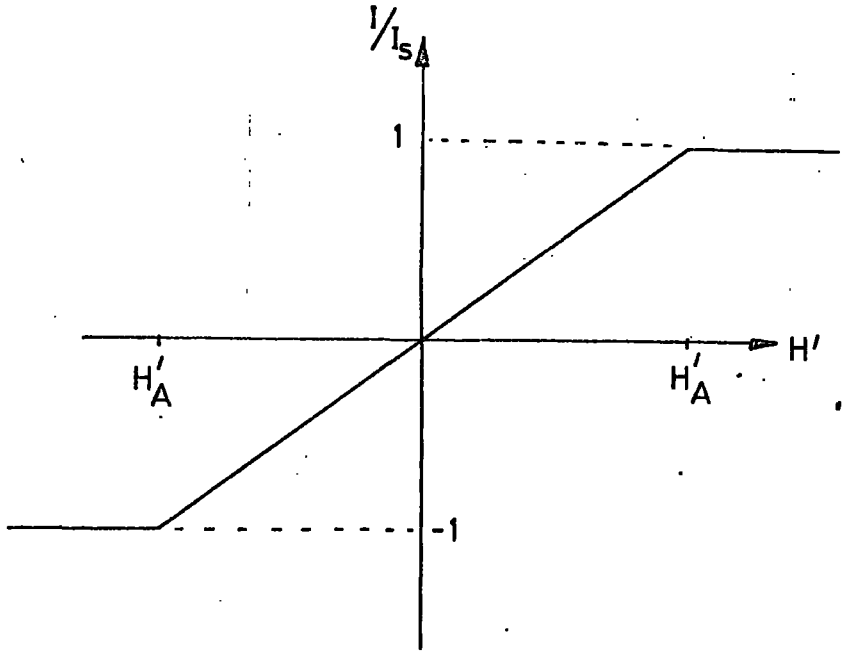

FIG. 6.17

MAGNETIZATION VARIATION FOR MULTIDOMAIN PARTICLES

different values for the volume fractions, hysteresis loops may be derived. The task is made easier knowing that at zero field, only the coherent and incoherent mechanisms are contributing to the remanence. Therefore the multidomain component can be found immediately.

If a satisfactory fit is not found between the derived loops and the experimental one, another value must be chosen for K and the process repeated. The present calculations were done by hand, but it is envisaged that a computer program could be used to speed the analysis.

Figure 6.18 shows two experimental loops together with sets of derived points. It must be emphasized that the method is only approximate because of the various assumptions. In general, K will not be single valued but will itself have a distribution of values. Superparamagnetic effects were neglected, and the multidomain magnetization is only an estimate. Interactions were also neglected. The points shown in figure

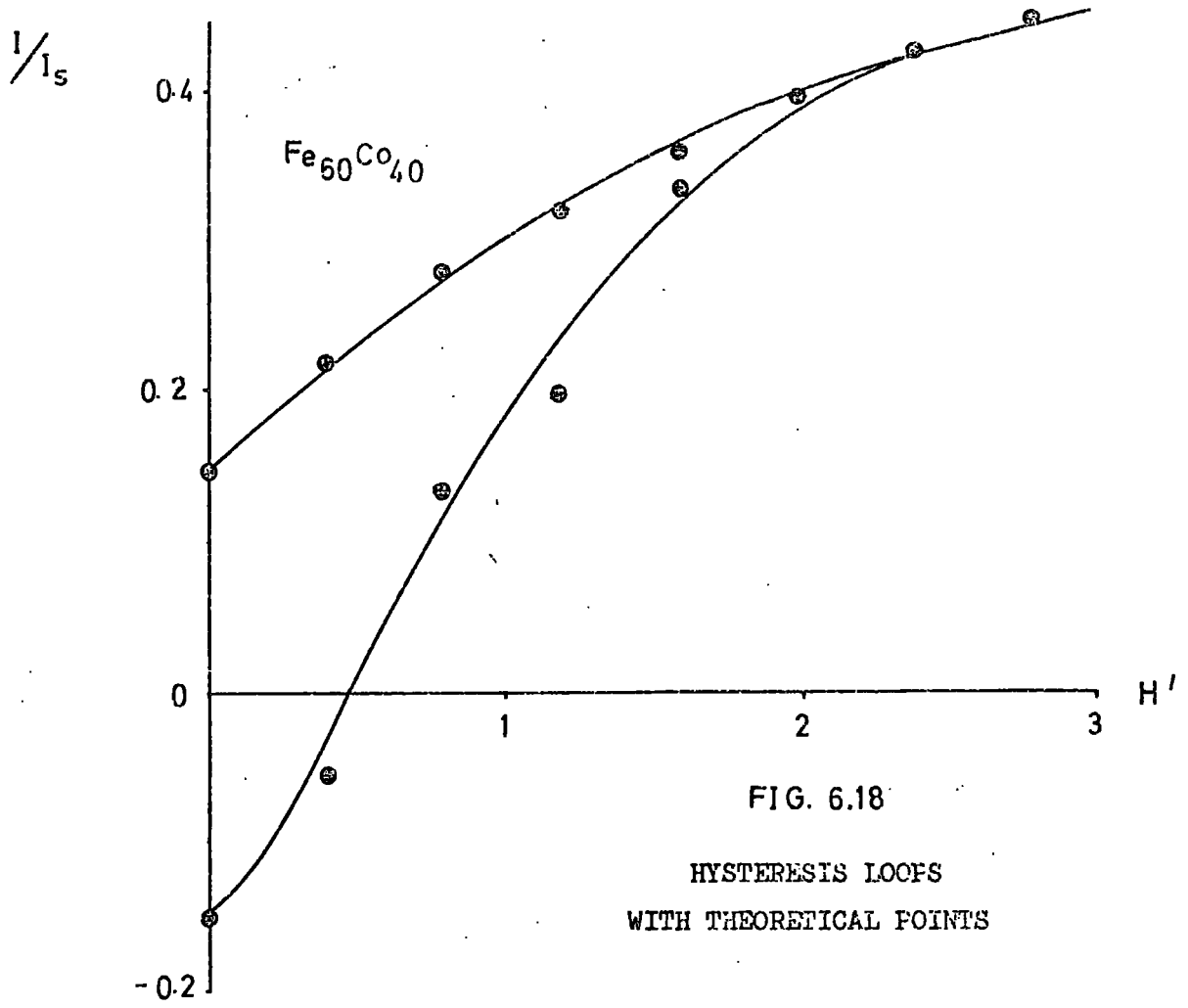

FIG. 6.18

HYSTERESIS LOOPS
WITH THEORETICAL POINTS

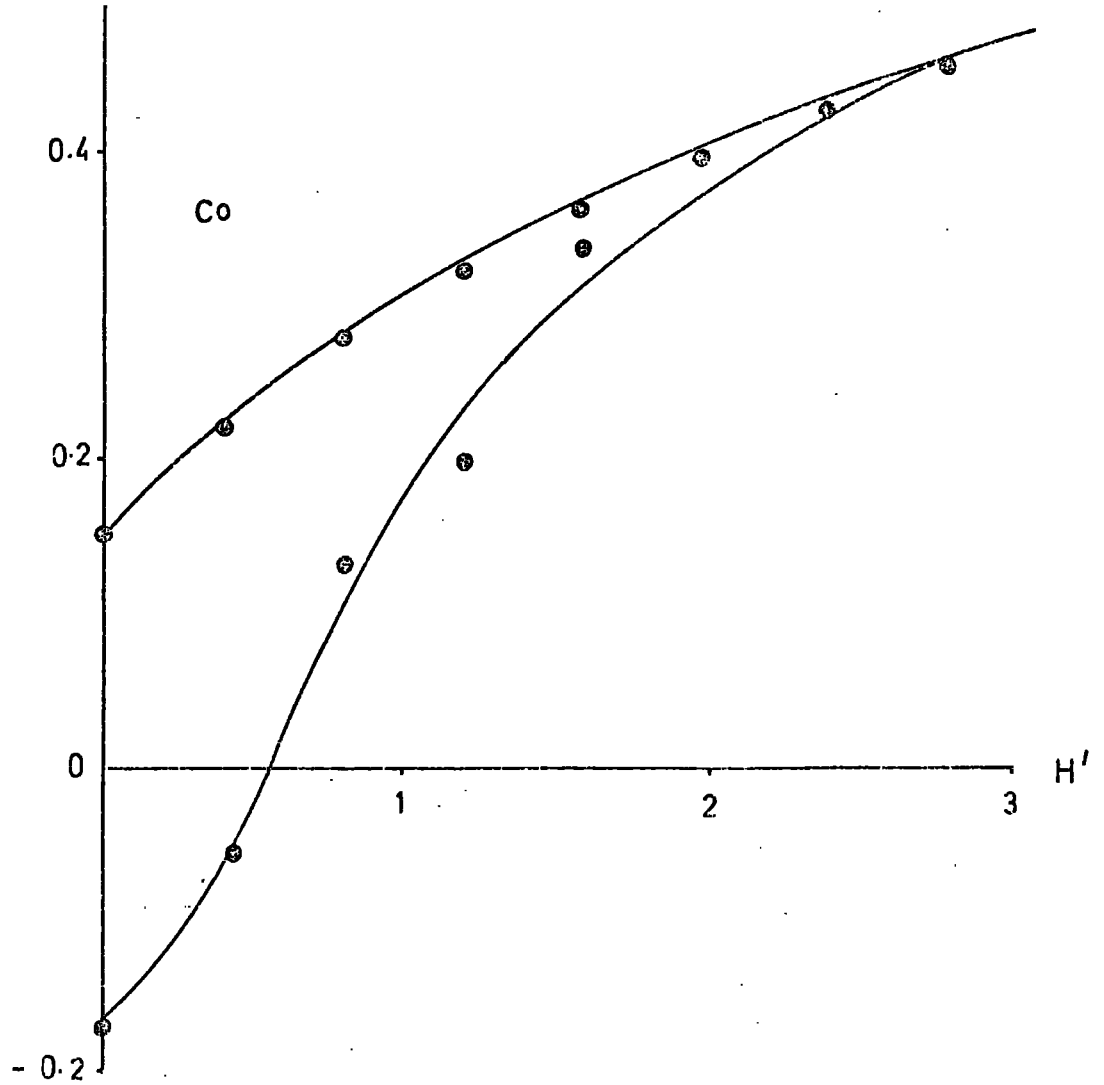

6.18 were obtained by taking approximately 15% fanning, 15% coherent rotation and 70% by volume of multidomain behaviour. The "average" value of K was found to be 6.00×10^5 erg/cc. Again it must be emphasized that these values are only approximate.

It is interesting to note that the fanning process leads to a higher coercivity than that of the coherent process. The former mechanism gives a value of 1660 Oe for cobalt, and the latter a value of 590 Oe. This can be explained if the coherent reversals are taking place in the individual particles rather than in chains of particles. Since the particles are nearly spherical, the associated shape anisotropy may not be much greater than the magnetocrystalline anisotropy.

The demagnetizing factors may be found from K.

$$K = K_1 + \frac{1}{2} I_s^2 (D_b - D_a)$$

For $Fe_{60}Co_{40}$, $K_1 = 0$. If the particles are assumed to be prolate ellipsoids,

$$2D_b + D_a = 4\pi$$

This gives $D_b \sim 4.3$ and $D_a \sim 3.9$, which is fairly consistent with a particle which is almost spherical.

In the case of cubic cobalt however, where $K_1 = -8.5 \times 10^5$ erg/cc, $D_b \sim 5.2$ and $D_a \sim 2.3$. This is more consistent with an elongated single domain particle. The electron micrographs do not provide any evidence of such particles being present.

The similarity between the two loops obtained for cobalt in different fields would appear to support the belief that the difficulty to saturate is due to the non-hysteretic component,

DURHAM UNIVERSITY
SCIENCE
- 6 APR 1976
SCIENCE
LIBRARY

i.e. the multidomain process.

There is however, a rather discomforting dilemma. The field required to accomplish total saturation is approximately 13kOe. This is too high to be explained by simple demagnetizing effects of multidomain particles. At the most this would amount to about 6kOe for cylindrical cobalt particles. For spherical particles it would only be about 4kOe. The need for such a high saturating field is puzzling.

It may however be linked with the field required to remove a spike domain of reverse magnetization. This field has been investigated experimentally in $SmCo_5$ by Searle and Garrett (11) and found to be several factors higher than the demagnetizing field.

CHAPTER 7

CONCLUSION AND SUGGESTIONS FOR FURTHER WORK

Conclusion

To conclude this thesis, it may be best to summarize the results. Perhaps the most general statement that can be made is to say that the evaporation-condensation technique can be used successfully to produce ultrafine particles of ferromagnetic material. However, the nature and properties of these particles cannot be expressed quite so generally.

All the particles produced appear to be nearly spherical, but are not the same size. Instead, there is a distribution of sizes. This in itself, complicates the magnetic processes involved. Visual evidence from electron microscopy shows that the particles join together to form necklace like chains. The magnetization changes in an assembly of particles produced by this technique would seem to be best explained by a mixture of three different processes.

The first of these is coherent reversal. This is believed to take place in individual particles rather than in chains. The former mechanism leads to a lower coercivity. Since the particles are almost spherical, the magnetocrystalline anisotropy may contribute significantly to the toal anisotropy. Depending upon the extent of the coherent process, it may be possible that the effects of magnetocrystalline anisotropy would not be observed in experiment. (For example the temperature dependence of the initial susceptibility).

The second process is that of fanning in an infinite chain of spheres. This model was originally proposed to explain incoherent reversals in elongated single domain particles.

Even so, it would seem to apply equally well to actual chains of spheres. The coercivity arising from this process depends upon the number of particles in a chain, and the saturation magnetization. For an infinite chain, this was found to be higher than the coercivity produced by coherent rotation. (In the present work that is).

The third magnetization process is that of multidomain behaviour. This is the least understood of the three. Extremely high fields are required to saturate the multidomain particles. This may be due to the presence of spike domains of reverse magnetization. However, for the present, a simplified multidomain model has been assumed.

It may be possible to obtain a larger proportion of single domain particles by reducing the evaporation pressure to the submillimetre range. This however will probably increase the proportion of superparamagnetic particles. Even so, the volumetric fraction may still be small.

On a laboratory scale, the amount of powder that can be collected from one evaporation is small (at most 50mgm). In its present form it is not therefore a commercial proposition. It may be possible to overcome the problem by adopting some sort of continuous feed process.

Even if this were so, it seems unlikely that these particles would find any widespread commercial applications either in the permanent magnet industry or in the magnetic tape industry. To be successful in these fields, the particles should fulfil the general requirements for magnetic hardness. That is, high coercivity and high remanence. For the recording applications, the material should also exhibit as square a hysteresis loop as possible.

The present investigation may however, provide useful information for workers using the evaporation method to observe domains.

Suggestions for further work

It is perhaps easier to suggest things that other people might do than those which one might attempt oneself. The work which has composed this thesis has only touched at the tip of the iceberg. There are many more experiments which could be carried out in the future.

Perhaps one of the most important of these is to try to produce hexagonal cobalt particles. This may be possible by using an alloy of cobalt with some other hexagonal non-magnetic metal. The particles may then adopt an hexagonal structure.

Measurements of coercivity over a range of temperatures are important in that they give a better indication of the presence and extent of magnetocrystalline anisotropy.

Anisotropy may also be measured using a torque magnetometer. This requires the fixing in place of aligned particles. When set, the assembly can be formed into a disc to account for shape anisotropy. The problems encountered here are in the alignment and collection of the particles. Also, the binder used in fixing must prevent movement but at the same time must not introduce stress. The alignment problem may be overcome by using a strong aligning field during the evaporation process.

Besides trying to align chains, it may be informative to try to break them up completely so that the fanning mechanism is inhibited. This may be possible using an ultrasonic agitator.

Measurement of the other remanence curves would provide invaluable information for comparison with Wohlfarth's expressions, and possible evaluation of interaction effects.

Particles should also be produced at very high pressures to try to obtain an assembly composed wholly of multidomain particles.

Finally attempts should be made to produce fine particles of other permanent magnet materials such as Alnico. The magnetic hardness of this is due to isolated islands of ferromagnetic material within a non-magnetic matrix. These islands are believed to consist of single domain particles. Fine particles of Alnico would then have totally different magnetic properties.

APPENDIX A

CALIBRATION OF THE OIL COOLED SOLENOID

In order that the field be known at a particular point on the axis of the solenoid for any given current, the following method of calibration was adopted.

Using a fluxmeter and probe, the maximum field produced in the solenoid was found for various values of current. The results are shown in Figure A.1. Next, a Hall probe which had been zeroed, was placed at different points in the solenoid. The Hall voltage was measured whilst the magnet current was kept constant. This was repeated for a range of currents. The results are shown graphically in Figure A.2. From these latter results, the maximum field position can be estimated. The Hall probe was fixed at this position, and the voltage recorded for different solenoid currents. The results are shown in Figure A.3. It was assumed that the field at this position would correspond to the maximum field obtained from the fluxmeter. Therefore using Figures A.1 and A.3, the graph of Hall voltage versus field was plotted (see Figure A.4).

Using Figures A.2 and A.4 it was thus possible to map the field inside the solenoid for different values of magnet current (see Figure A.5). Finally, it was possible to derive one more graph. That is, a plot of field versus magnet current, for any position inside the solenoid. This is shown in Figure A.6.

SOLENOID CALIBRATION
MAGNET CURRENT VS MAXIMUM FIELD(FLUXMETER)

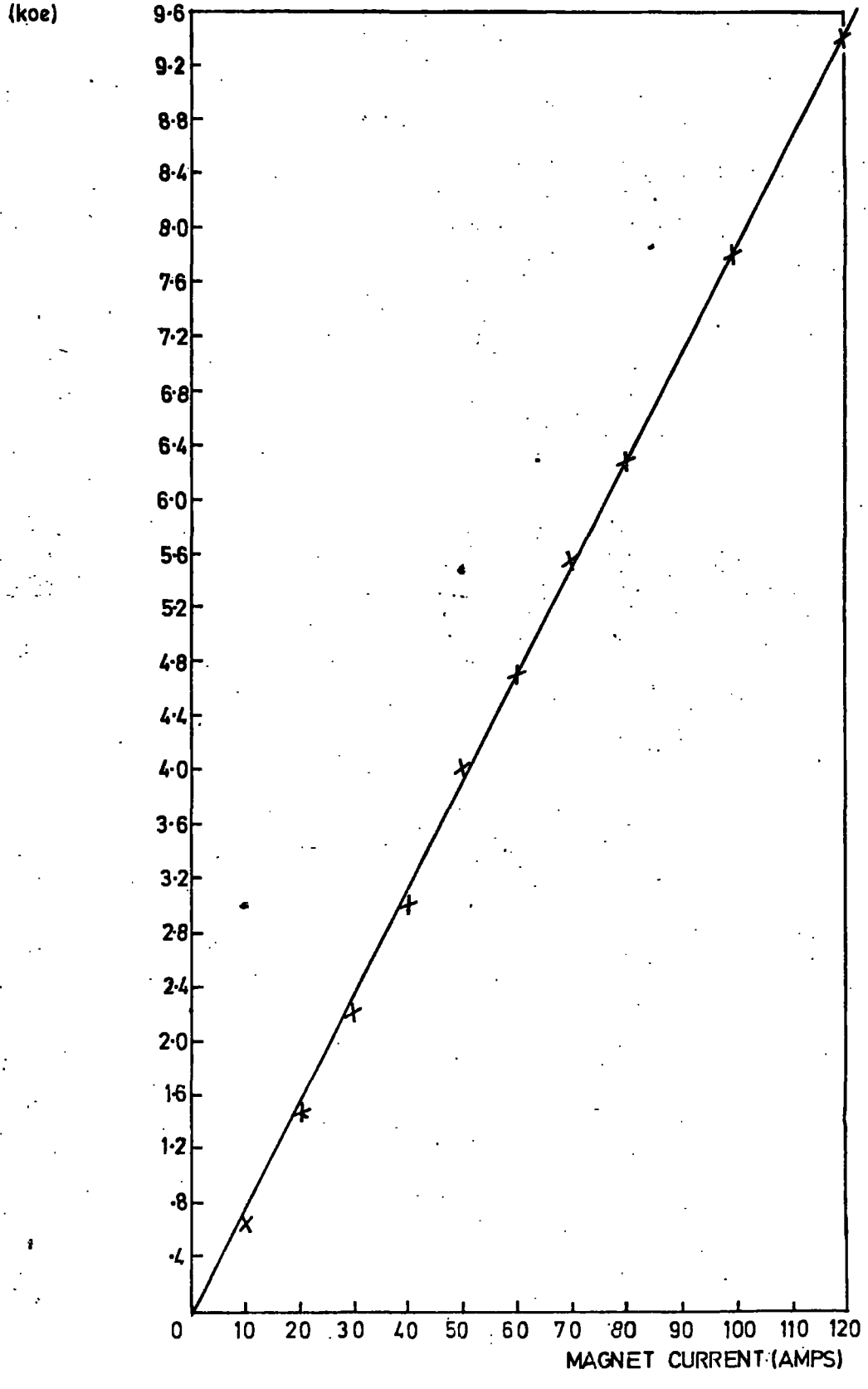

FIG A1

POSITION OF HALL PROBE VS HALL VOLTAGE
FOR DIFFERENT VALUES OF CURRENT.

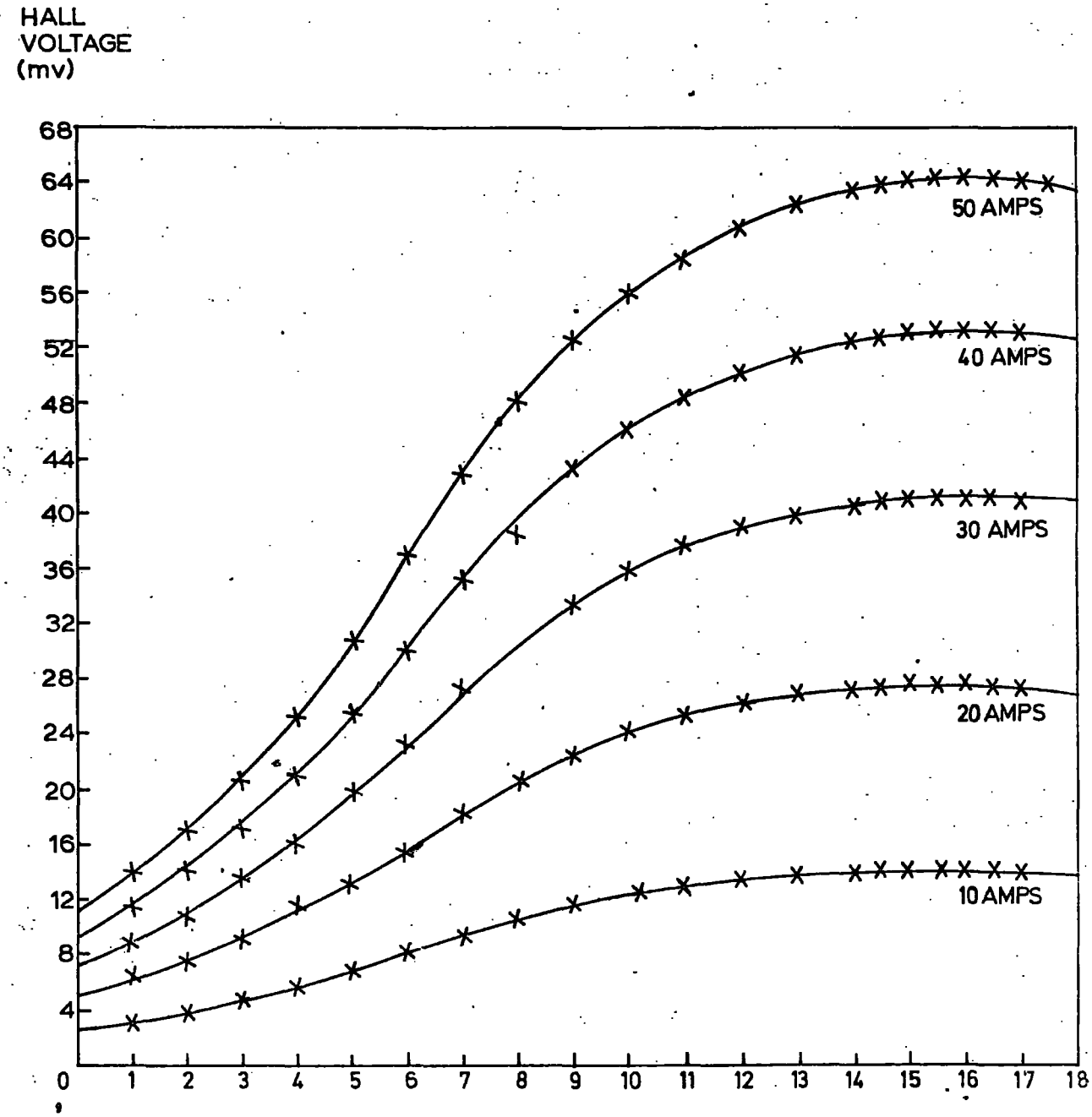

FIG A2 POSITION OF HALL PROBE IN MAGNET RELATIVE TO TOP OF INNERTUBE (cm).

MAGNET CURRENT VS HALL VOLTAGE AT MAXIMUM FIELD POSITION.

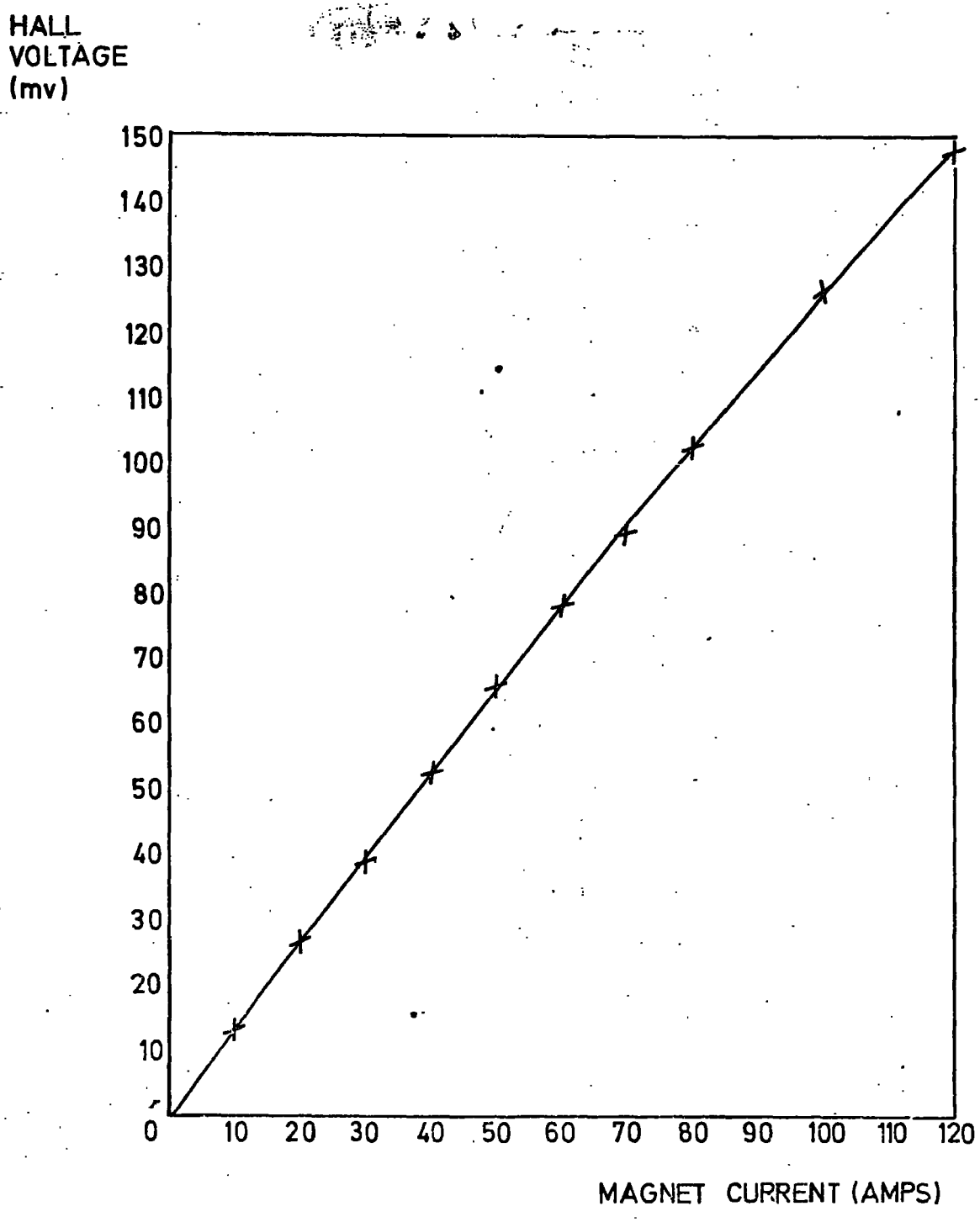

FIG A3

CALIBRATION CURVE.
HALL VOLTAGE VS FIELD.

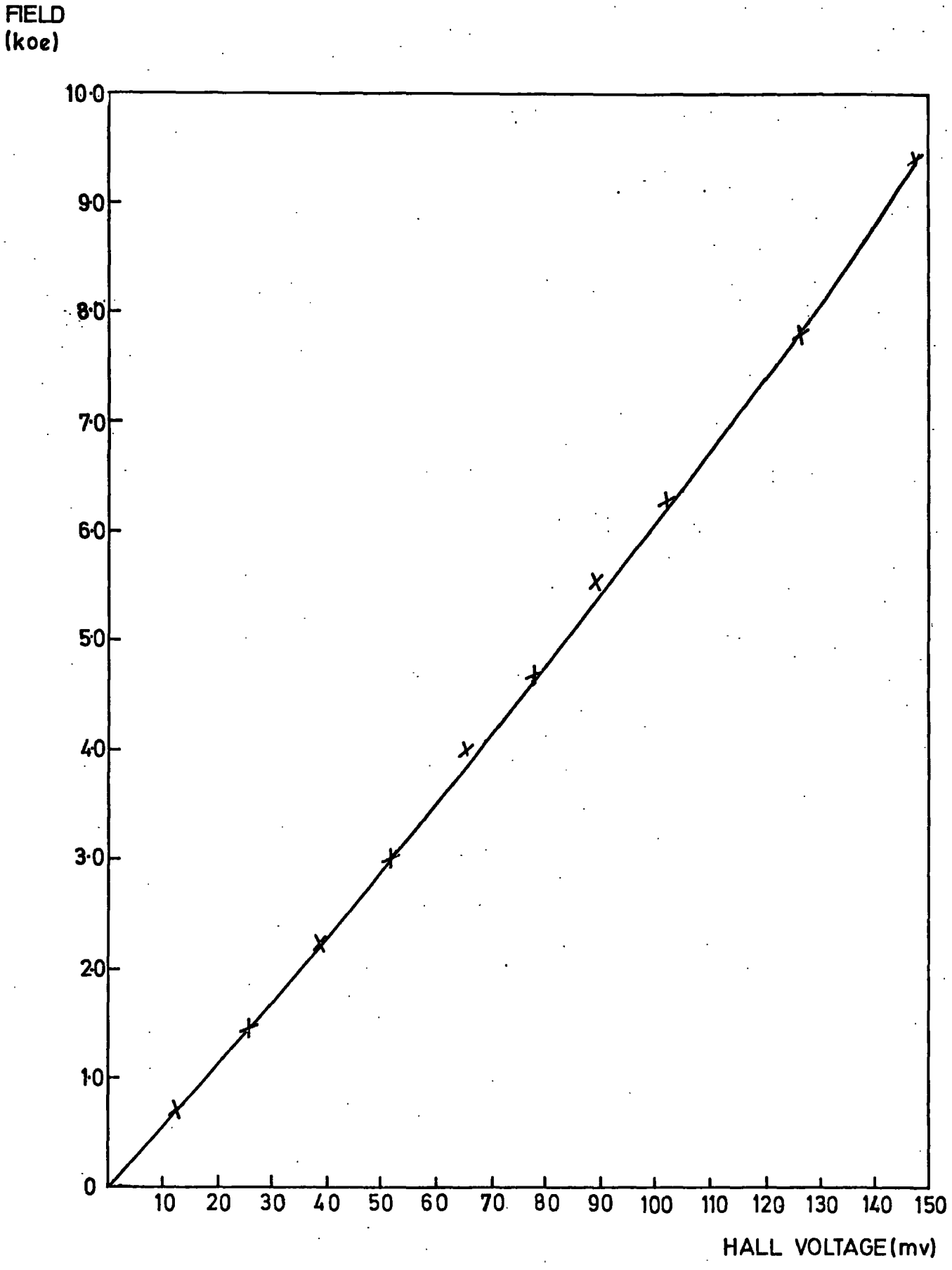

FIG A4

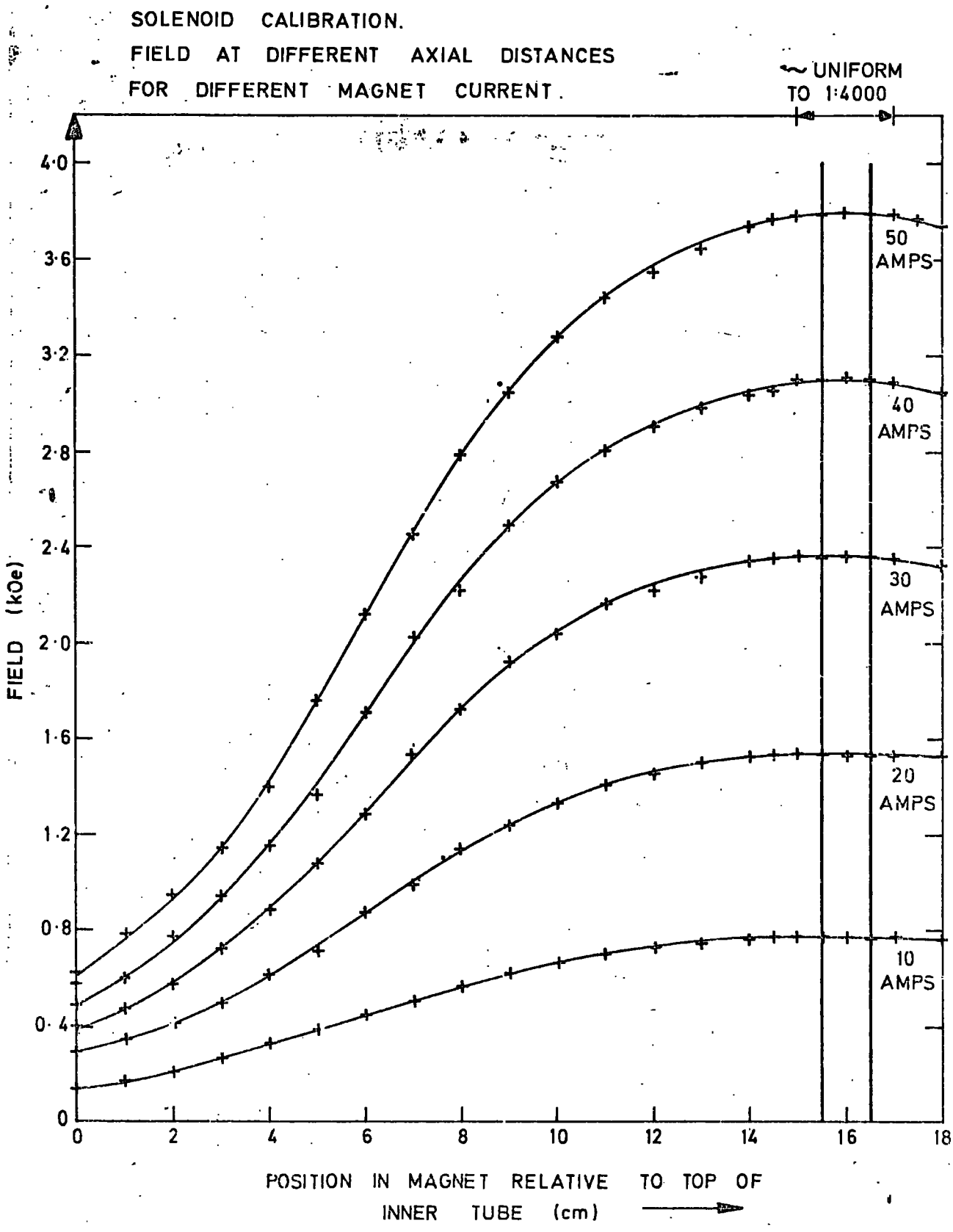
SOLENOID CALIBRATION.
FIELD AT DIFFERENT AXIAL DISTANCES
FOR DIFFERENT MAGNET CURRENT.
~ UNIFORM
TO 1:4000
50
AMPS
40
AMPS
30
AMPS
20
AMPS
10
AMPS
FIELD (kOe)
4·0
3·6
3·2
2·8
2·4
2·0
1·6
1·2
0·8
0·4
0
0
2
4
6
8
10
12
14
16
18
POSITION IN MAGNET RELATIVE TO TOP OF
INNER TUBE (cm)

FIG. A 5

SOLENOID CALIBRATION.
MAGNET CURRENT VS FIELD AT A
PARTICULAR POINT IN THE SOLENOID.

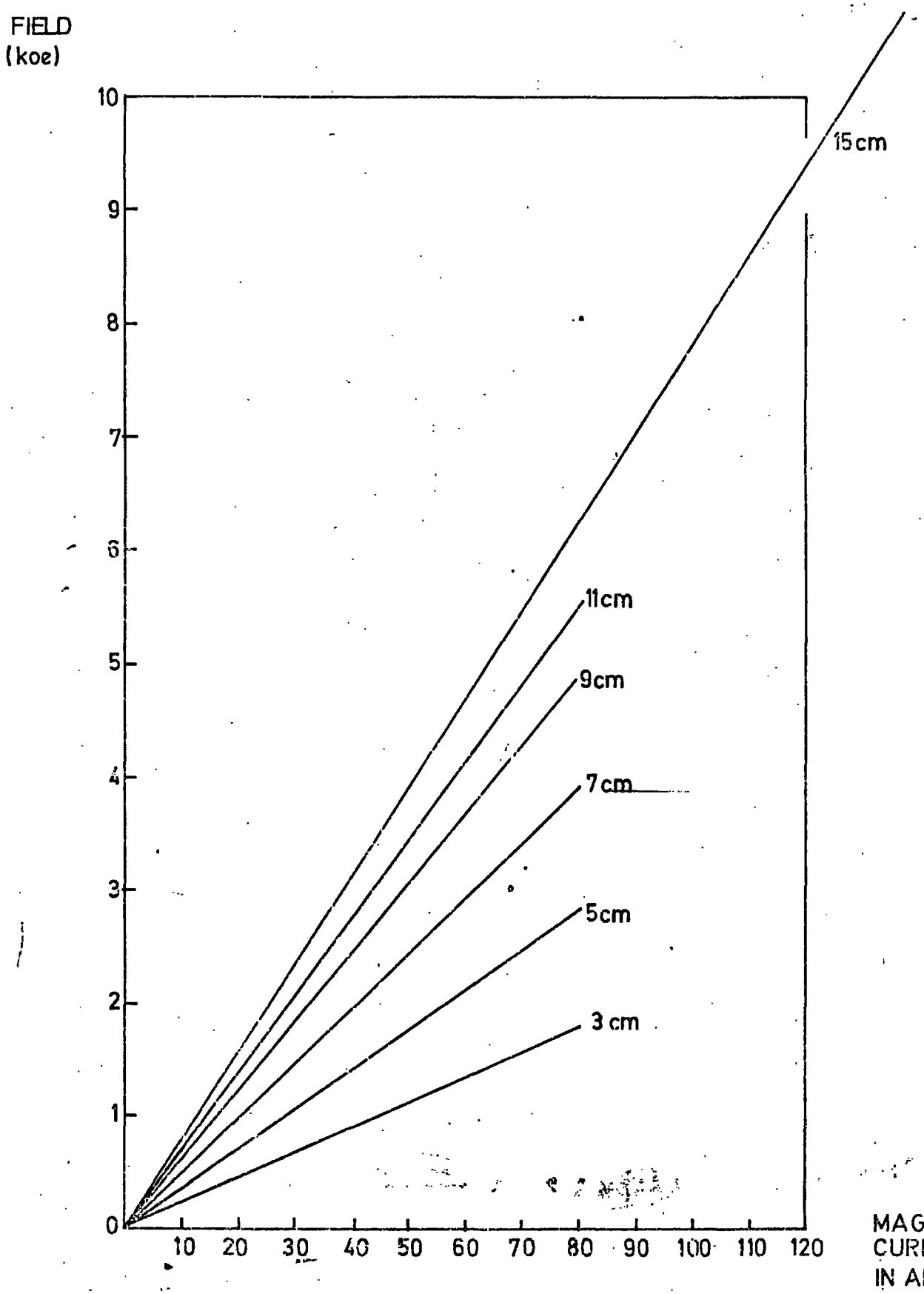

FIG A6

APPENDIX B

```
JLV:PROC OPTIONS(MAIN);
 DCL P,L1,L2,P1,P2,X2,X1,S,TH,DHKL,Q(M,K) FLOAT;
 GET LIST(P,L1,L2,P1,P2);
   /*P IS HOLE SEPARATION
   L1 IS WAVELENGTH OF KALPHA1
   L2 IS WAVELENGTH OF KALPHA1
   P1 IS PERCENTAGE TRANSMISSION OF L1
  P2 IS PERCENTAGE TRANSMISSION OF L2*/
  L=(P1*L1)+(P2*L2);
  PUT EDIT('LINE NO.','DHKL','LOGD','Q')
     (PAGE,SKIP(2),X(15),A,X(12),A,X(12),A,X(12),A);
      DO M=1 TO 2;
  GET LIST(N);
  DO K=1 TO N;
  GET LIST(X2,X1);
  /*X2,X1 ARE SCALE POSITIONS OF CORRESPONDING ARCS*/
  S=X2-X1;
  /*S IS THE ARC LENGTH*/
  PY=3.141629 ;
   TH=(PY*S)/(4*P);
  /*TH IS THE ANGLE THETA IN RADIANS*/
  IF M=1 THEN DO;
  DHKL=L/(2*SIN(TH));
  /*THIS IS THE CONDITION FOR BRAGG REFLECTION AT LOW THETA*/
           END;
     IF M=2 THEN DO;
  DHKL=L/(2*COS(TH));
  /*THIS IS THE CONDITION FOR BRAGG REFLECTION AT HIGH THETA*/
             END;
          Q(M,K)=1/(DHKL*DHKL);
  /*Q IS DEFINED AS 1/DHKL SQUARED*/
  PUT EDIT(M,K,DHKL,LOG(D),Q(M,K))
        (SKIP(3),X(18),F(1),F(1),X(12),F(12,10),X(4),F(8,5),X(8),F(8,7));
        END;
        END;
        END;
```

ASSEMBLING THE FARADAY BALANCE FOR LOW TEMPERATURE EXPERIMENTS

Refer to figures 4.9a and 4.14.

1. With the solenoid as low as possible insert the inner and outer dewars together with the seating ring.
2. Lower the specimen tube and spider through the top plate into the dewars.
3. Place the brass header over the top of the specimen tube and through the top plate. Make sure that the sealing ring and sleeve are on the header.
4. Connect the thermocouple wires to the lead throughs in the brass header.
5. Lower the top part of the header carefully over the specimen tube so that it passes through the gland nut and 'O' ring.
6. Bolt both parts of the header to the platform by means of the clamping ring.
7. Tighten the gland nut on the specimen tube so that the reference marker is just visible.
8. Carefully raise the solenoid and lead the inner dewar into the brass header.
9. Fasten the inner dewar in position by attaching the springs from the platform of the dewar cradle.
10. Ensure that a small gap exists between the dewars to allow liquid nitrogen down into the tail.
11. Chock the solenoid in position.
12. Insert and lower the half transfer syphon into the header and seal in position with the 'O' ring and gland nut.

The system is now ready for use, and the same method applies for loading a specimen as for the room temperature system.

APPENDIX D

ESTIMATION OF THE OXIDE DEPTH

Imagine a particle to consist of a metallic core of volume V_m, surrounded by a uniform oxide layer of volume V_o.

If I_m is the magnetization of the metal and I_o that of the oxide, then the observed magnetization of the particle is given by

$$I = \frac{I_m V_m + I_o V_o}{V_m + V_o}$$

This assumes that the field due to the metal is adequate to align the magnetization in the oxide.

In the case of cobalt $I = 980$, $I_m = 1400$, and $I_o = 0$

$$\therefore \quad V_m / (V_m + V_o) = 98/140 = 0.7$$

This is the volume fraction of the metal core. The ratio of the radius of the core to the total is simply

$$r_m / r_T = \sqrt[3]{0.7} \sim 0.89$$

Therefore the depth of the oxide layer is approximately 11% of the radius of the particle.

In the case of iron, a mixed oxide layer surrounds the core. Suppose that Fe_3O_4 contributes all of the oxide magnetization. Then $I = 1370$, $I_m = 1720$, and $I_o = 480$

$$\therefore \quad V_m / (V_m + V_o) = 89/124 = 0.72$$

Again the depth of the oxide layer is approximately 11% of the radius of the particle.

Actually, if Fe_2O_3 had been assumed to contribute all the oxide magnetization, $I_o = 420$, and the depth of the oxide layer would still have been about 10% of the total particle radius.

REFERENCES

CHAPTER 1

1. Kneller E., "Magnetism and Metallurgy", Vol.1.
2. Wohlfarth E.P., "Magnetism", Vol.III.
3. Beeck O. et al, Proc. Roy. Soc. A177,62 (1940)
4. Kimoto K., and Nishida I., Jap. J. App. Phys.6, 1047 (1967)
5. Kimoto K. et al, Jap. J. App. Phys.2, 702 (1963)
6. Tasaki A. et al, Jap. J. App. Phys.13, 271 (1974)
7. Wada A. et al, Jap. J. App. Phys.8, 599 (1969)
8. Hutchinson R.I. et al, J. Sci. Inst. 42, 885 (1965)
9. Sarma N.V., and Moon J.R., Phil. Mag.16, 433 (1967)
10. Lavin P.A., Cobalt 43, 87 (1969)
11. Allen L.R. et al, U.S. Patent Office No.3,049,421 (1962)
12. Al-Bassam T., Ph.D. Thesis, Durham (1969)
13. Al-Bassam T., and Corner W.D., J.Phys.C (GB) 4, 47 (1971)
14. Herring, et al, J.Phys.F (GB) 3, 157 (1973)
15. Lucretius Carus, "On the Nature of The Universe", (Penguin Classics)
16. Mattis, "The Theory of Magnetism" 1965
17. Vonsovskii S.V., "Magnetism" Vol.1.
18. Stoner E.C., "Magnetism" 1948
19. Bozorth R.M., "Ferromagnetism" 1951
20. Kittel C., "Introduction to Solid State Physics"
21. Tebble and Craik, "Magnetic Materials"
22. Chikazumi S., "Physics of Magnetism"
23. Weiss P., J. Phys.6, 667 (1907)
24. Heisenberg W., Z. Physik. 49, 619 (1928)
25. Slater J.C., Phys. Rev.49, 537 (1936)
26. Stoner E.C., Repts. Prog. Phys.11, 43 (1947)
27. Bitter, "Introduction to Ferromagnetism"
28. Bates L.F., "Modern Magnetism"

CHAPTER 2

1. Néel L., J. Phys. Rad. 15, 225 (1954)
2. Bean C.P. et al, J.App.Phys. 30, 318S (1959)
3. Jacobs I.S., and Bean C.P., "Magnetism" Vol.III
4. Wohlfarth E.P., Advances in Physics 8, 87 (1957)
5. Frei E.H., Shtrikman S., and Treves D. Phys. Rev. 106, 446 (1957)
6. Stoner E.C., and Wohlfarth E.P., Phil. Trans. Roy. Soc. London A240, 599 (1948)
7. Néel L., Compt. Rend 224, 1488 (1947)
8. As 7 above
9. Johnson C.E., and Brown W.F., J. App. Phys. 32, 243S (1961)
10. As 5 above
11. Jacobs I.S., and Bean C.P., Phys. Rev. 100, 1060 (1955)
12. Shtrikman S., and Treves D., "Magnetism" Vol. III
13. Aharoni A., J. App. Phys. 30, 70S (1959)
14. Brown W.F., J. App. Phys. 30, 62S (1959); Phys. Rev 58, 736 (1940); 59, 528 (1941); 60, 139 (1941)
15. Aharoni A., and Shtrikman S., Phys. Rev. 109, 1522 (1958)
16. Shtrikman S., and Treves, D., J. Phys. Rad. 20, 286 (1959)
17. Aharoni A., J. App. Phys. 30, 70S (1959)
18. Wohlfarth E.P., "Magnetism" Vol. III
19. Morrish A.H., "The Physical Principles of Magnetism"
20. Kneller E., "Magnetism and Metallurgy" Vol. 1
21. Rado G.T., and Suhl H., "Magnetism" Vol. III
22. Meiklejohn W.H., Rev. Mod. Phys. 25,302 (1953)
23. Luborsky F.E. et al, J. App. Phys. 35, 2055 (1964)
24. Tasaki A. et al, Jap. J. App. Phys. 4, 707 (1965)
25. Petrov A.E. et al, Sov. Phys. Sol. Stat. 13, 1318 (1971)
26. Jacobs I.S., and Luborsky F.E., J. App. Phys. 28, 467 (1957)
27. Tanaka T., and Tamagawa N. Jap. J. App. Phys. 6, 1096 (1967)

CHAPTER 2

28. Tasaki A, et al, Jap. J. App. Phys.12, 940 (1973); 13, 271 (1974)

29. Wohlfarth E.P., J. App. Phys. 29, 595 (1958)

30. Wohlfarth E.P., Research (London) 8, S42 (1955)

31. Gaunt P., Phil. Mag. 8, 1127 (1960)

32. Johnson C.E., and Brown W.F., J. App. Phys. 29, 313 (1958); 29, 1699 (1958)

CHAPTER 3

1. Kittel C., Rev. Mod. Phys. 21, 541 (1949)

2. Stoner E.C., "Magnetism and Matter" Methuen (1934)

3. Weiss P., and Forrer, Ann. Phys. 5, 153 (1926)

4. Tanaka T., and Tamagawa N., Jap. J. App. Phys. 6, 1096 (1967)

5. Weiss P., and Forrer Ann. Phys. 5, 153 (1926)

6. Kittel C., Rev. Mod. Phys. 21, 541 (1949)

7. Hall, J. App. Phys. 31, 157S (1960)

8. Sucksmith W., and Thompson, Proc. Roy. Soc. A225, 362 (1954)

9. Rodbell D.S., J. Phys. Soc. Japan 17, B313 (1962)

10. Sato and Chandrasekhar, Phys. Chem. Solids 1, 228 (1957)

CHAPTER 4

1. Beeck O., et al, Proc. Roy. Soc. A177, 62 (1940)

2. Kitchen P., private communication

3. Kusaka K, et al, Jap. J. App. Phys. 8, 599 (1969)

4. Zijlstra H., "Experimental Methods in Magnetism" Vol. IX

5. Poldy C., Ph.D. Thesis, Durham 1972

6. Primavesi G., Ph.D. Thesis, Durham 1972

7. Crangle J., et al, Proc. Roy. Soc. A321, 477 (1971)

CHAPTER 4

8. Hunter J., Ph.D. Thesis, Durham 1973

9. Castrol Ltd., private communication

CHAPTER 5

1. Kitchen P., I.R.D. Technical Memorandum 1969

2. Wada N., et al, Jap. J. App. Phys. 7, 1287 (1968); 8, 599 (1969)

3. Sebilleau F., and Bibring H., Inst. Met. Mono. and Rep. Series 18, 209 (1956)

4. Lavin P., I.R.D. Technical Memorandum 1968

5. Pearson, "Handbook of Lattice Spacings and Structure of Metals"

CHAPTER 6

1. Johnson C.E., and Brown W.F., J. App. Phys. 29, 313 (1958)

2. Wada N., et al, Jap. J. App. Phys. 8, 599 (1969)

3. Lavin P.A., Cobalt 43, 87 (1969)

4. Stoner E.C., and Wohlfarth E.P., Phil. Trans. Roy. Soc. (London) A240, 599 (1948)

5. Wohlfarth E.P., J. App. Phys. 29, 595 (1958)

6. Gaunt P., Phil. Mag. 5, 1127 (1960)

7. Wohlfarth E.P., Comm. Sol. State Phys. 3, 168 (1971)

8. Wohlfarth E.P., private communication to Corner W.D.

9. Bean C.P., J. App. Phys. 26, 1381 (1955)

10. Jacobs I.S., and Bean C.P., Phys. Rev. 100, 1060 (1955)

11. Searle and Garrett, J. App. Phys. 45, 5037 (1974)

UNIVERSITY APR 1976 LIBRARY